Dissertation zur Erlangung des Doktorgrades der Fakultät für Chemie und Pharmazie der Ludwig-Maximilians-Universität München

Structural and Functional Analysis of Translationally Inactive Eukaryotic Ribosomes:

Regulation of Hibernation with Lso2/CCDC124 and Stalling on the Fungal Arginine Attenuator Peptide

Jennifer Nicole Wells
aus
Rhode Island, USA

München, 2020

Dissertation zur Erlangung des Doktorgrades der Fakultät für Chemie und Pharmazie der Ludwig-Maximilians-Universität München

Structural and Functional Analysis of Translationally Inactive Eukaryotic Ribosomes:

Regulation of Hibernation with Lso2/CCDC124 and Stalling on the Fungal Arginine Attenuator Peptide

Jennifer Nicole Wells
aus
Rhode Island, USA

München, 2020

Erklärung

Diese Dissertation wurde im Sinne von § 7 der Promotionsordnung vom 28. November 2011 von Herrn Prof. Dr. Roland Beckmann betreut.

Eidesstattliche Versicherung

Diese Dissertation wurde eigenständig und ohne unerlaubte Hilfe erarbeitet.

München, 29.06.2020

_____

Jennifer N. Wells

Dissertation eingereicht am: 29.06.2020

1. Gutachter: Prof. Dr. Roland Beckmann

2. Gutachter: Prof. Dr. Klaus Förstemann

Mündliche Prüfung am: 28.07.2020

Parts of this thesis have been published or submitted to scientific journals:

"Structure and function of yeast Lso2 and human CCDC124 bound to hibernating ribosomes"

Jennifer N. Wells[#], Robert Buschauer[#], Timur Mackens-Kiani, Katharina Best, Hanna Kratzat, Otto Berninghausen, Thomas Becker, Wendy Gilbert, Jingdong Cheng*, and Roland Beckmann* (2020). PLOS bio. 18 (7): https://doi.org/10.1371/journal.pbio.3000780

[#]These Authors contributed equally

*Corresponding Author

In press at PLOS Biology, 2020

Parts of this thesis have been presented at international conferences:

Poster presented at the Protein Synthesis and Translational Control Meeting at the EMBL in Heidelberg, Germany, 2019

"Protection factors Lso2, CCDC124 and EBP1 bound to yeast and human 80S ribosomes"

Jennifer N. Wells, Robert Buschauer, Timur Mackens-Kiani, Katharina Best, Hanna Kratzat, Otto Berninghausen, Thomas Becker, Wendy Gilbert, Jingdong Cheng, and Roland Beckmann

Summary

Translational regulation is a complex and multifaceted process. The ribosome, mRNA, tRNAs, intercellular metabolites and protein complexes, and additional ribosome binding factors all contribute to modulating protein production in the cell. Each variable in their own right may govern activation, repression, or alteration to the cascade of events which dictate protein synthesis and ultimately, cell survival or death. Much of the current understanding of these processes comes from works carried out in prokaryotic systems, while less is known from the more complex and higher ordered eukaryotic species.

First, this investigation considers the contribution of mRNA to translational output. This work considers how translational stalling on non-optimally coded mRNAs is recognised, pursuing previous reports implicating the yeast helicase Dhh1 as a sensor for this type of translational stalling. With the hope of generating a high resolution cryo-EM structure of the Dhh1-ribosome complex, a biochemical analysis was carried out and attempts were made to isolate the complex by affinity purification of endogenous Dhh1 from yeast, as well as by *in vitro* reconstitution from purified components. Attempts to recapitulate Dhh1-ribosome binding under optimised conditions was unsuccessful, revealing there is no direct interaction between these two biomolecules.

Next, the study investigates how the recently identified ribosome binding and hibernation factor Lso2, and human homologue CCDC124, reversibly inhibit translation during extended periods in a nutrient depleted environment. Therefore, the molecular structure for Lso2/CCDC124 in complex with the ribosome was solved by single particle cryo-EM for native yeast and human hibernation complexes. Subsequently, the yeast Lso2-80S complex was reconstituted from purified components and assessed by cryo-EM. Agreement between the native and reconstituted Lso2-80S structures was confirmed, allowing utility of the reconstituted Lso2-80S for functional analysis. In all cases, the novel eukaryotic hibernation complex was observed with ribosomes adopting the distinct non-rotated, post-translocational state. As such, the significance of ribosome rotation was assessed in the context of ribosome recycling, by assembling enzymatic *in vitro* splitting assays with the recycling factors Dom34 and ABCE1 (Rli1 in yeast). Indeed,

this work was able to demonstrate that the Lso2-80S hibernation complex is almost quantitatively split 4 fold more than controls, while the Stm1-80S exhibits only 0.7 fold the splitting observed for controls. Taken together, this new data provides key insights into how the Lso2-80S hibernation complex contributes to regulation of translation, allowing eukaryotic cells to survive long term starvation.

Finally, this investigation concludes with an attempt to structurally characterise the fungal arginine attenuator peptide (AAP), a ribosome arrest peptide. Preliminary biochemical analysis identified the optimal conditions for arginine dependent stalling in *in vitro* translation using *S. cerevisiae* and *N. crassa* cell free translation systems. As such, high concentrations of ribosome-nascent chain complexes stalled on the AAP were purified for cryo-EM analysis. Unfortunately, though the study produced high resolution electron density maps from *N. crassa* ribosomes stalled on the AAP, poor local resolution at the critical areas of interest prevented deduction of the peptides stalling mechanism. Still, there is evidence to suggest that regulatory upstream open reading frames like AAP may serve more broadly as a means to regulate gene expression in eukaryotes. As such, structural derivation of these regulatory mechanisms remains an important goal in translational research. Having optimised a system for generating AAP stalled 80S samples for cryo-EM, this work has still managed to contribute to the ongoing progress within this vein of research.

Table of Contents

Abbreviations

A	adenine
A-site	aminoacyl-site
aa	amino acid
AAP	arginine attenuator peptide
ATP	adenosine triphosphate
C	cytosine
CCDC124	coil-coil domain containing protein 124
CMV	cytomegalovirus
CP	central protrusion
CTF	contrast transfer function
CV	column volumes
D.m.	Drosophila melanogaster
DCC	decoding centre
DNA	deoxyribonucleic acid
DTT	dithiothreitol
E-site	exit-site
E.c.	*Escherichia coli*
EBP1	ErbB3-binding protein 1
EDTA	Ethylenediaminetetraacetic acid
EF	elongation factor
ER	endoplasmic reticulum
G	guanine
GAC	GTPase associated centre
GCN2	general control non-derepressible 2
GO	gene ontology
GTP	guanosine triphosphate
h	hours
H.s.	Homo sapiens
HA	hemagglutinin
HRI	haeme-regulated eIF2 kinase
HRP	horseradish peroxidase
IC	initiation complex
IF	initiation factor
ISR	integrated stress response
IVT	in-vitro translation
kDa	kilo Dalton
L	liters
LB	Luria broth
LiAc	lithium acetate
Lso2	Long-annotated short open reading frame
LSU	large subunit

LUCA	last universal common ancestor
MAP	methionine aminopeptidase
MDa	Mega Dalton
mg	milligram
ml	milliliter
mM	millimolar
MOPS	3-(N-morpholino)propanesulfonic acid
mRNA	messenger ribonucleic acid
mRNP	messenger ribonucleoprotein
N.c.	Neurospora crassa
NAT	N-terminal acetyltransferase
NC	nascent chain
NGD	no-go decay
nm	nanometer
NMD	nonsense mediated decay
NSD	nonstop decay
NTD	N-terminal domain
OD	optical density
ORF	open reading frame
P-site	peptidyl-site
PABP	poly-(A) binding protein
PAGE	polyacrylamide gel electrophoresis
PAP	poly-a polymerase
PBS	phosphate buffered saline
PCR	polymerase chain reaction
PDB	protein databank
PEG	poly-ethylene glycol
PERK	PKR-like endoplasmic reticulum kinase
PIC	pre-initiation complex
PIP	EDTA-free protease inhibitor cocktail pill
PKR	protein kinase R
PMSF	phenylmethylsulfonyl fluoride
PTC	peptidyl transferase centre
PTM	post-translational modification
RAP	ribosome arrest peptide
RBF	ribosome binding factor
RF	release factor
RNA	ribonucleic acid
RNC	ribosome nascent-chain complexes
RNP	ribonucleoprotein
rpm	rotations per minute
RQC	ribosome-associated quality control
rRNA	ribosomal ribonucleic acid

RT	room temperature
S (unit)	Svedburg unit
S.c.	Saccharomyces cerevisiae
SA	splitting assay
SD	Shine-Dalgarno sequence
SDS	sodium dodecyl sulfate
SRP	signal recognition particle
ssDNA	single stranded DNA
SSU	small subunit
T	thymine
TBS	Tris buffered saline
TCA	Trichloroacetic acid
Tris	tris(hydroxymethyl)aminomethane
tRNA	transfer ribonucleic acid
U	uracil
uORF	upstream open reading frame
UPR	unfolded protein response
UV	ultraviolet
V	Volts
v/v	volume by volume
w/v	weight by volume
WT	wild type
YP	yeast extract peptone
YPD	yeast extract-peptone dextrose
β-ME	β-mercaptoethanol
µg	microgram
µl	microliter
µM	micromolar

List of Figures

List of Tables

Introduction

The code for life is stored in deoxyribonucleic acid (DNA), chains of pentose sugars linked together by phosphates. One of 4 alternate nucleobases adenine (A), thymine (T), guanine (G) and cytosine (C) conjugated to each sugar molecule. The bases are read out in groups of three, known as codons, for which 64 distinct possibilities exist. As each codon coincides with either one of the 20 amino acids, or for the 'stop' or 'start' codons, there is degeneracy of the genetic code. The central dogma of molecular biology defines the flow of information from DNA to protein, describing the processes of transcription and translation (Crick, 1970). First, small regions of DNA selected for protein production must be copied from the mass of genetic information stored in cellular genomic DNA. Next DNA is transcribed by an enzyme called RNA polymerase into ribonucleic acid (RNA). This is an archaic form of DNA, which exists in shorter stretches than DNA and utilizes uracil (U) in place of T bases. RNA contains an additional -OH (hydroxyl) group conjugated to the 2' carbon of the pentose sugar backbone. This modification created a distinction between the properties and overall structure of RNA and DNA. Most significantly, the RNA helix is expanded with larger groove regions, making RNA less resistant to harsh conditions, UV damage, and enzymatic attack than DNA, but gives RNA more conformational freedom to form complex secondary structures. Thereby, this simple hydroxyl modification allows the shorter RNA sequences significantly more versatility and even the capacity for catalysis in the broader biological context. As such, RNA can be found in the cell in many forms; ribosomal RNA (rRNA) folds and compacts to eventually form an impressive molecular machine of Megadalton (MDa) scale, capable of catalysis, and, at the center of this central dogma; messenger RNA (mRNA) serves to directly relay the information stored in DNA to the translational machinery; transfer RNA (tRNA) can be conjugated to individual amino acids, allowing for their delivery to the ribosome for synthesis of to a new polypeptide or protein, and more. Finally, the process of translation is carried out by the ribosome, a mix of proteins and RNA which assembles and coordinates with countless additional factors to simultaneously decode the genetic information for synthesis of new proteins.

Ribosomes manufacture proteins by reading genetic information from mature mRNA

transcripts and allocating the appropriate amino acid for each triplicate nucleotide codon. As the ribosome moves along the mRNA in the 5' to 3' direction, amino-acids are brought to the ribosome conjugated to the 3' end of tRNAs The anticodon stem loop of the tRNA probes the mRNA for proper Watson Crick base pairing, in the decoding center (DCC) of the ribosomal small subunit (SSU). Once correct mRNA-tRNA base pairing is read out by the rRNA of the SSU, the tRNA will be fully accommodated by the ribosome, as additional contacts form between the tRNA and the ribosomal large subunit (LSU). In the fully accommodated state, amino acids will be covalently linked in a condensation reaction within the peptidyl transferase center (PTC) within the ribosomal LSU. The processes of tRNA decoding, accommodation, and peptidyl transfer, is coupled with the dissociation of de-acetylated tRNAs off/out of the ribosome, and translocation of the ribosome along the mRNA. As such the process proceeds iteratively as the growing amino acid chain or nascent-chain (NC), passes through a tunnel in the core of the LSU before exiting to the cytoplasm, until a STOP codon is reached.

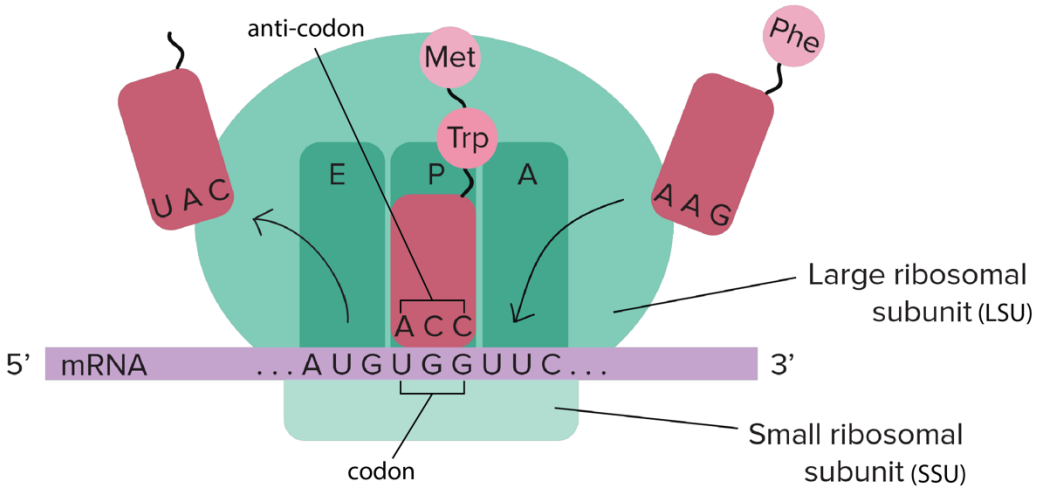

Figure 1: Translation
A ribosome carrying out the process of translation elongation. *Adapted from "Translation: Figure 3," (OpenStax, 2016)*

1.1. The Ribosome

While all ribosomes are large, multi MDa molecular machines composed of ribosomal proteins (r-proteins) and rRNA, variability in their composition and increased complexity among higher ordered species correlates with other evolutionary trends.

Fully assembled ribosomes as well as their components (SSU, LSU, rRNA) are annotated by Svedberg units (S), referring to their sedimentation coefficient (Svedberg, 1947). The r-proteins are annotated with either an uppercase (LSU) or lowercase (SSU) alphanumeric indicator, with rRNA helices being similarly annotated with either upper or lowercase 'h' and species-specific numbering. This system allows researchers to readily make the distinction between different ribosomal components from different ribosomal species (Ban et al., 2014).

In all cases, the core of the ribosome is predominantly populated by rRNA, with r-proteins located more towards the solvent surface corresponding with the evolution of the ribosome (Fox, 2010). The SSU/LSU interface is stabilized by a high concentration of Mg^{2+} and a number subunit-subunit interactions (Spahn et al., 2004). Both bacteria like *Escherichia coli* (*E.c.*) and archaea have 70S ribosomes of ~2.3 MDa. Here, 21 r-proteins and 16S rRNA make up the 30S SSU, while 33 r-proteins, 23S rRNA, and 5S rRNA form the 50S LSU (Melnikov et al., 2012). The ribosomes of lower eukaryotes, i.e. 80S ribosomes from *Saccharomyces cerevisiae (S.c.)* and *Neurospora crassa (N.c.)* are ~3.3 MDa with 33 r-proteins and 18S rRNA in the 40S SSU, and 46 r-proteins, 5.8S rRNA, 25S rRNA, and 5S rRNA in the 60S LSU (Melnikov et al., 2012). The largest and most complex ribosomes belong to higher eukaryotes, e.g. Rabbit or Human (*H.s.*), whose 80S is ~4.3 MDa and composed of 40S SSU with 33 r-proteins, and 18S rRNA, 47 r-proteins, 5.8s rRNA, 28S rRNA, and 5S rRNA in the 60S LSU (Figure 2) (Anger et al., 2013; Melnikov et al., 2012). Ribosomes are extremely large with complex quaternary structures which have made excellent targets for structural analysis(Beckmann et al., 1997; Beckmann et al., 2001; Ramakrishnan, 1986, 2002; Spahn et al., 2001; Yonath et al., 1982). Therefore, key features have been identified and assigned appropriate nomenclature to maintain consistency within the field of research (Ban et al., 2014).

Landmark features of the SSU are the head, body, platform, and beak regions. The SSU harbours the mRNA channel and DCC, as well as the 3 tRNA binding regions deemed the A, P, and E sites (Figure 2). The LSU has a number of key features and catalytic regions of interest. It can be oriented by the central protuberance (CP), with the L1-stalk near the E site. (Anger et al., 2013; Melnikov et al., 2012). On the other side of the CP, by the A site, is the ribosomal P stalk, made up of five P-proteins (Ballesta and Remacha, 1996). Below the P stalk, at the edge of the A site on the LSU, is the catalytic

GTPase-associated centre, composed of uL11, H43, H44 and the P stalk (Spahn et al., 2004). The most critical catalytic area of interest on the LSU is the peptidyl transferase centre (PTC), which is responsible for the catalytic activity of the ribosome in synthesis of new proteins and is composed entirely or rRNA. The 4 critical bases of the PTC are most often referred to using the *E.c.* base numbering U2585, A2602, U2506, A2451, C2063.

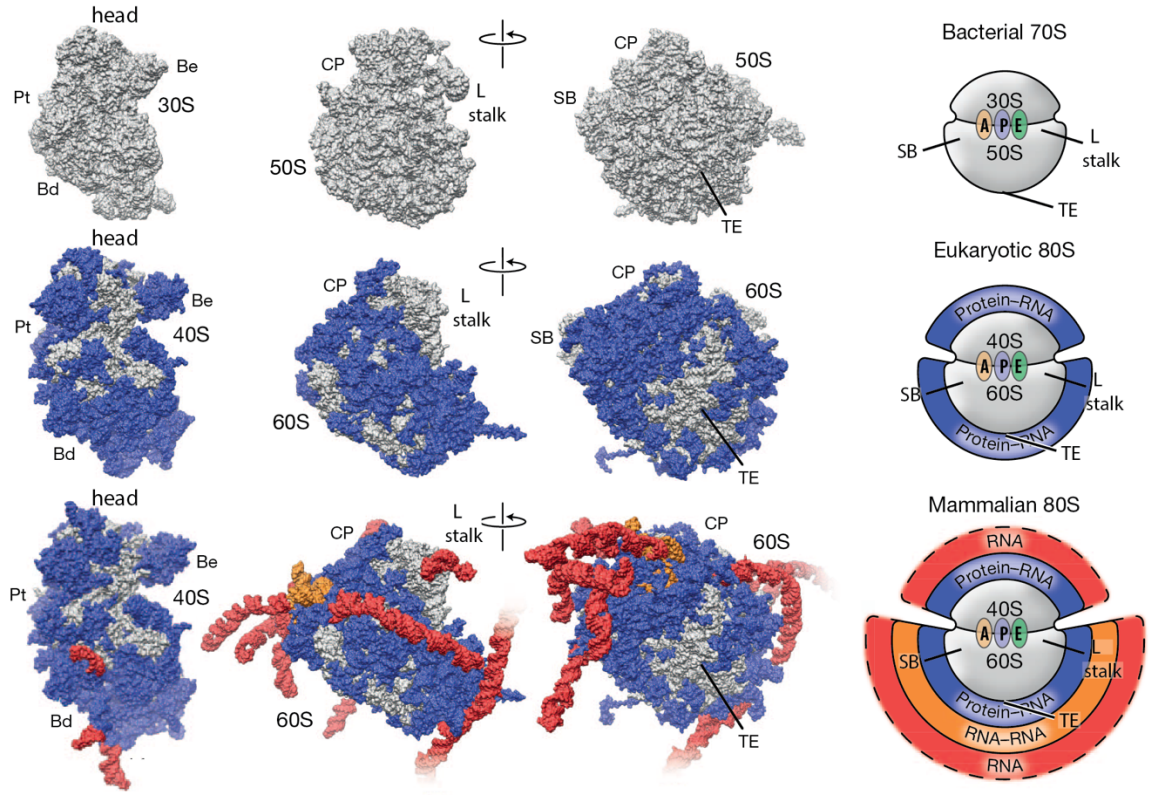

Figure 2: Ribosomal organisation and species differences
Bacterial ribosomes, displayed in grey, are composed of a 30S small subunit and 50S large subunit. Ribosomes from eukaryotes have a 40S small subunit and 60S large subunit, which vary from their bacterial counterparts by the addition of proteins and rRNA at the surface, displayed in blue. Ribosomes from metazoans and other higher eukaryotes, such as mammalian ribosomes, again possess a 40S small subunit and 60S large subunit, but further vary in their surface rRNA content upon comparison with ribosomes from lower eukaryotes. These additional rRNA helices, displayed in red, are known as expansion segments. (Pt-Platform, Bd-Body, Be-Beak, CP-central protuberance, SB-Stalk base (referring to the P stalk), TE-Tunnel exit) *(Adapted from (Anger et al., 2013)*

Eukaryotic mRNA modifications

In the case of mRNA, eukaryotes carry out a complex maturation process than in prokaryotes, whereby mRNA exported from the nucleus undergoes significant modification before being utilised by the ribosome for translation. mRNA often

undergoes splicing, or, removal of non-coding genetic intronic regions, though this does not occur in the budding yeast *S.c.*. Before translation, mRNA is also subjected to modification at both ends. At the 5'-end, a 7-methyl(guanine)-cap is added, referred to as the 5' cap, while the 3'-end is poly-adenylated. In the past, the length of the poly(A) tail is was thought to be associated with mRNA half-life and overall stability, akin to telomere lengths in ageing. However, recent work has revealed that poly(A) length may actually serve as a quality control mechanism and strategically shortening of these regions may occur throughout mRNA lifecycle (Lima et al., 2017). Both these modifications will serve as clients for binding factors which aid in circularisation of mRNA during eukaryotic translation initiation, as well as within the broader scope of translational regulation. Indeed, it is upon the ends of mRNA where a large degree of coupling between mRNA degradation, and initiation of translation on an mRNA is found.

1.2. The Translation Cycle

Translation is a highly coordinated cycle, which can be divided into four steps; initiation, elongation, termination, and recycling. In eukaryotes, termination and recycling are coupled and while elongation has been fairly well conserved throughout evolution, though divergence can be found in the other stages of translation between prokaryotic and eukaryotic systems, where a further increase in complexity is found in higher ordered species.

Initiation

Initiation represents a point of divergence between prokaryotic and eukaryotic translation (Sonenberg and Hinnebusch, 2009). In both systems, an initiation complex assembles on the ribosomal SSU. Translation will only begin once the mRNA is positioned at an AUG start codon with initiator methionine tRNA in the P site. In prokaryotes, this initiator tRNA is annotated as fMet-tRNA$_i^{fMet}$ while the eukaryotic counterpart is Met-tRNA$_i^{Met}$ (Jackson et al., 2010; Kaminishi et al., 2007). In prokaryotes, proper positioning of mRNA at the AUG start codon is modulated by the Shine-Dalgarno sequence (SD), positioned 7-10 nt upstream of the start codon (Shine and Dalgarno, 1974). The SD of the mRNA pairs with the anti-SD region of the SSU 16S rRNA, while three initiation factors (IFs) prepare the ribosome to begin translation (Kaminishi et al., 2007). Each IF plays a role in formation the initiation

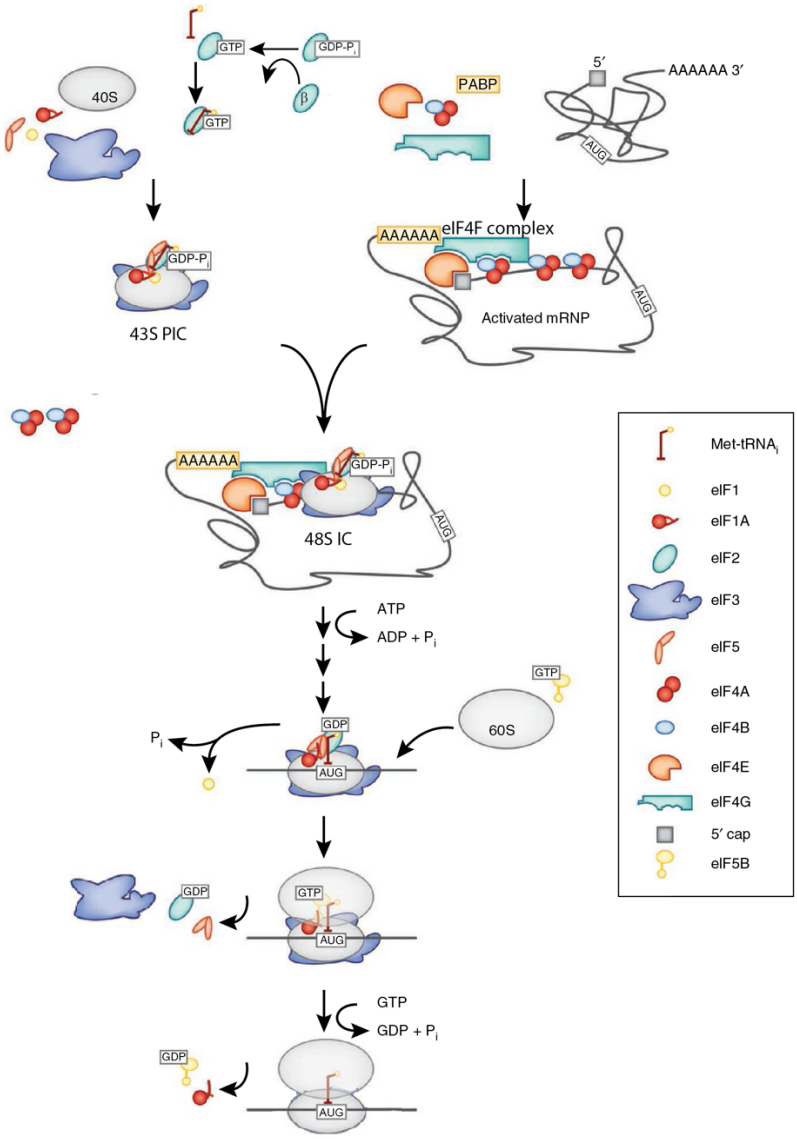

Figure 3: Eukaryotic translation initiation
The fully assembled 43S PIC is composed of the SSU, Met-tRNA$_i^{Met}$ in complex with eIF2 and GTP, and initiation factors eIF1, eIF1A, eIF3, and eIF5. Meanwhile, the eIF4F complex, composed of eIF4A, eIF4E, eIF4B, and eIF4G, assembles on the 5' end of the mRNA to generate an activated messenger ribonucleoprotein (mRNP) for initiation. The 5' cap of the mRNA is bound by eIF4E which is stabilized by eIF4A slightly downstream on the mRNA. The two factors are bridged by eIF4G, which establishes its own interactions with poly(A) binding protein (PABP) coating the 3' poly-(A) tail of the mRNA. This contact between PABP and the eIF4F complex leads to circularization of the mRNA. Subsequent recruitment of the RNA helicase eIF4B is quickly followed by ATP hydrolyses and unwinding of the 5' UTR (Park et al., 2013). In the activated mRNP, the circularised mRNA positions eFI4g for interaction with components of the eIF3 complex on the 43S PIC, which allows for formation of the mature 48S initiation complex (IC).Assembly of the 48S IC is completed with the mRNP being loaded onto the 43S PIC, scanning of the mRNA in the 5'-3' direction until an AUG start codon, and dissociation of eIF4F. With the 48S IC positioned at the start codon, eIF5 stimulate the hydrolysis of GTP by eIF2, promoting dissociation of eIF3, eIF1, eIF5, and eIF2-GDP, while eIF5b-GTP binds to the remaining eIF1A in the A site. Finally, GTP hydrolysis by eIF5B promotes dissociation of eIF1A and eIF5B and joining of the ribosomal LSU. *Adapted from (Melnikov et al., 2012)*

complex: IF1 blocks the A site, IF2 promotes binding of fMet-tRNA$_i^{fMet}$ in the P site, and IF3 controls mRNA binding (Allen et al., 2005; Milon and Rodnina, 2012). With subsequent joining of the LSU, translation can proceed to the next step, elongation.

Eukaryotic initiation is vastly more complex with even further variability observed between yeast and higher metazoan systems. Where prokaryotes employ only 3 IFs, 12-13 eukaryotic IFs (eIFs) are required during initiation. Eukaryotic initiation begins with assembly of the 43S pre initiation complex (PIC) which will mature into a 48S initiation complex (IC) (Figure 3) (Aitken and Lorsch, 2012; Hinnebusch and Lorsch, 2012; Hussain et al., 2014). The 48S IC scans along the mRNA until the AUG start codon is recognised and positioned in the A site. Then, the IC dissembles, and the ribosomal LSU joins before translation proceeds to the next phase, elongation. Importantly, an anti-association factor, eIF6, is bound on the subunit interface of the LSU to inhibit premature subunit joining. As such, removal of eIF6 from the LSU precludes 80S assembly (Weis et al., 2015). Once assembled, 80S ribosomes loaded with mRNA and Met-tRNA$_i^{Met}$ are ready to proceed with the process of elongation (Jackson et al., 2010).

Elongation

During elongation, ribosomes move along mRNA in the 5' to 3' direction, decoding the open reading frame (ORF) and simultaneously joining together amino acids for generation of nascent protein (Figure 1). Aminoacyl-tRNAs (aa-tRNAs) are delivered to the A-site by eEF1A. At this point the ribosome carries out the process of decoding, wherein the mRNA codon in the A site base pairs with the anticodon stem loop of tRNAs, specifically positions 34-36 of the tRNA, forming a short A-helix. Proper decoding is sensed by two critical adenosine residues of the SSU rRNA. In prokaryotes, this is made up of A1492 and A1493 on h44 corresponding to A1754 and A1755 in *S.c.* or A1824 and A1825 of human 18S rRNA. Theses residues flip out and probe for the minor groove on the codon-anticodon helix to detect cognate, or Watson Crick base pairing. Only when tRNAs bear the correct anticodon complement to the mRNA in the A site will they be accommodated by the ribosome. The process of decoding is signalled to eEF1A, likely via the A site tRNA making contact with the ribosomal LSU, and, thereby allosterically transmitting an activation signal for GTPases located near the GAC where the hydrolysis of GTP promotes their dissociation from the ribosome (Loveland et al., 2017; Schuette et al., 2009; Taylor et al., 2007).

When elongation begins, the ribosome has an empty A-site and de-acetylated Met-tRNA$_i^{Met}$ in the P-site (Figure 4A) (Budkevich et al., 2014; Schmeing and Ramakrishnan, 2009; Voorhees and Ramakrishnan, 2013). In this state, ribosomes are in the non-rotated confirmation, referring to the movements of the SSU relative to the LSU. In this state the E site is empty and the A site is opened up in order to accommodate translation factors (Loveland et al., 2017; Spahn et al., 2004).

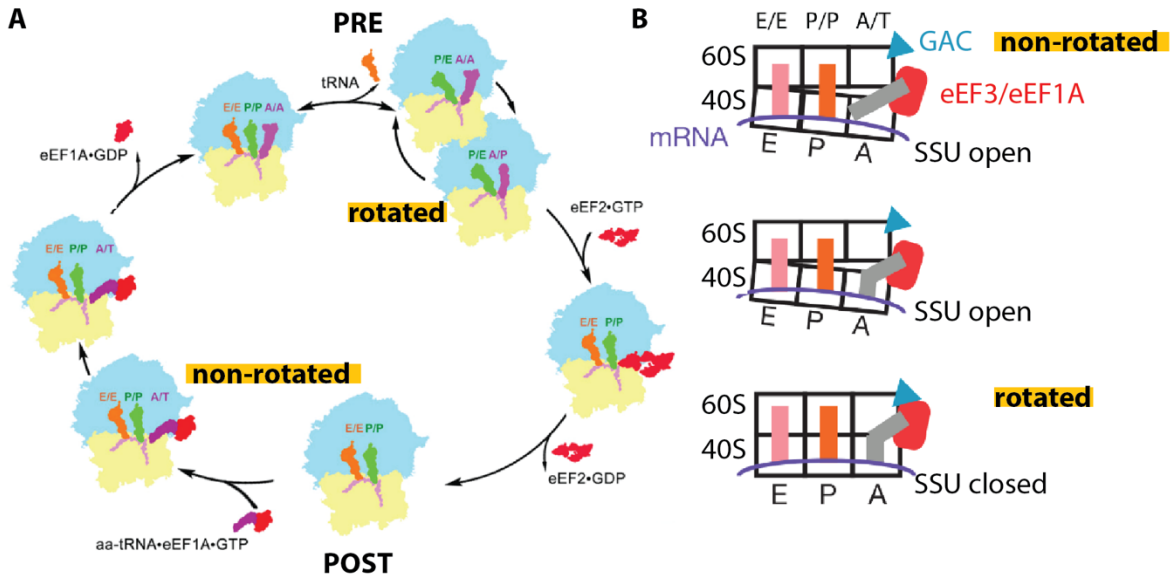

Figure 4: Ribosome movement during translation elongation
(A) Elongation proceeds in a cycle with the ribosomes alternating between the PRE and POST states (B) Movements of the SSU relative to the LSU affects changes in the A site, which can be distinguished between rotated and non-rotated confirmations. *Adapted from (Budkevich et al., 2014; Loveland et al., 2017)*

During elongation (Figure 4), non-rotated ribosomes with an empty A site are said to be in the POST state, as in POST-peptidyl transfer. During decoding, the ribosome transitions from the POST to the PRE state, marked by a conformational change in the ribosome with the SSU rolling 6° relative to the LSU. At this point, the ribosome bears A/A and P/P tRNAs and is said to be in the PRE state (Figure 4B). In the PRE state, the anticodon stem loop of tRNAs remain aligned with the mRNA, while the 3' CCA ends rearrange to promote peptide bond formation. After peptidyl transfer has occurred, tRNA structure reorients itself once again adopting 'hybrid-states' (Budkevich et al., 2014). Formation of hybrid state tRNAs depends on additional structural changes in the ribosome; rachet-like subunit rearrangement (RSR) of the SSU leads to a 13-15 Å decrease in the area of the of the A site and opening of the E

site by ~6-7 Å (Budkevich et al., 2014). Ribosomes in the PRE state therefore exist in equilibrium, where both non-rotated ribosomes bearing A/A – P/P tRNAs, and the rotated ribosomes bearing hybrid (A/P – P/E) tRNAs are represented until peptidyl transfer occurs. Peptidyl transfer occurs at various rates for each amino acid (Wohlgemuth et al., 2008), but always proceeds with the α-amino group of the A site aminoacyl tRNA launching a nucleophilic attack on the carbonyl carbon of the peptidyl tRNA in the P site (Simonovic and Steitz, 2009). After peptidyl transfer, translocation along the mRNA is aided by elongation factor eEF2 which binds to hybrid state, rotated ribosomes, and facilitates transition back to the POST state.

Termination

After successful translation of an mRNA ORF, the ribosome eventually reaches a STOP codon, which serves as the signal to dissociate from the mRNA and release the nascent protein so that ribosomal subunits can be recycled for translation to begin anew. Termination represents another point of divergence between bacterial and eukaryotic systems, and the factors responsible for carrying out this process are structurally unrelated. Prokaryotes possess two class-I release factors, RF1 and RF2, which specifically recognize particular STOP codons. At this point, RF3 releases RF1 or RF2 from the A site which, when vacant, can be subsequently accessed by ribosome recycling factors.

The eukaryotic release factor 1 (eRF1) is capable of recognizing all three stop codons, a function fulfilled by the N-terminal domain (NTD) (Bertram et al., 2000). eRF1 binds to the ribosome as a ternary complex with the translational GTPase and class-II release factor, eRF3. The STOP codon, uniquely read as a nucleotide quadruplet, forms a UNR-type U turn which is accommodated by a pocket formed between the NTD of eRF1 and the 18S rRNA within the DCC (Brown et al., 2015; Matheisl et al., 2015). Subsequently, eRF3 hydrolyses GTP and dissociates from the ribosome allowing eRF1 to be fully accommodated into the A site, positioning the conserved GGQ motif on the central domain of eRF1 within range of the PTC for hydrolysis and release of the nascent protein (Preis et al., 2014).

Recycling

In the case of eukaryotes, termination is coupled with ribosome recycling, wherein the ribosome is split into populations of SSU and LSU which will later feed back into the

cycle again at the point of initiation. The eukaryotic termination complex is composed of an 80S ribosome bound by mRNA, P/P tRNA in the P site (still associated with the nascent protein), and release factor eRF1 positioned in the A site. Release factor binding in the A site is essential for allowing the splitting factor ABCE1 to be accommodated. ABCE1 is an ABC-E type protein with two nucleotide binding domains (NBDs), and conserved iron sulphur cluster (FeS) (Karcher et al., 2008). Upon binding to the eRF1 containing termination complex, ABCE1 hydrolyses ATP, pushes the FeS domain into the inter-subunit cleft, and closes its NBDs (Heuer et al., 2017; Preis et al., 2014). The force generated by ABCE1 helps pry apart the ribosomal subunits. After splitting, ABCE1 may remain associated with the SSU throughout assembly of the 43S PIC (Schuller and Green, 2018).

1.3. mRNA decay

Translational activity is largely influenced by cytoplasmic mRNA. Cells are constantly carrying out the process of mRNA synthesis and degradation, which allows translation to be tuned to accommodate the dynamic needs of any variety of growth states or conditions (Bernstein et al., 2002; Wang et al., 2002; Yang et al., 2003). Canonical mRNA decay describes the normal regulatory process for discriminating and degrading mRNAs which should no longer be targeted to the ribosome for translation and, begins with removing critical features of mature mRNA; first the 3'-poly(A) tail, and then the 5'-cap, thereby disrupting the process of translation initiation. Subsequently, mRNAs will be targeted for degradation by cytoplasmic endonucleases. Importantly, the rate of translation is inversely related to mRNA decay. While this relationship was initially postulated over 30 years ago, ongoing works continue to provide evidence supporting the notion of interplay between mRNA decay and translation (Parker, 2012).

Deadenylation and decapping: signals for normal eukaryotic mRNA turnover

In eukaryotes, regular cytoplasmic mRNA turnover begins with deadenylation, the process by which the 3' poly-(A) tail of mature mRNA is shortened, and the rate limiting step in mRNA decay (De Leon et al., 1983). Deadenylation is carried out

temporally by two deadenlyation complexes, first by the RNase D-type catalytic poly(A)-nuclease deadenylation complex subunit 2 (Pan2) in complex with Pan3, whose activity is promoted by poly(A) binding protein 1 (PABP) which coats the poly(A) tail of mRNAs (Boeck et al., 1996), mRNAs will be subsequently targeted by the primary eukaryotic deadenlyase, the CCR4/Not complex (Parker, 2012).The CCR4-Not complex is a large, multimeric protein complex with diverse activities for regulation of gene expression in both the nucleus and cytoplasm (Buschauer et al., 2020; Collart, 2016; Denis and Chen, 2003; Kuzuoglu-Ozturk et al., 2016; Webster et al., 2018). The CCR4-Not deadenylase complex is composed of 9 subunits, Not1-5, Caf proteins 1, 40, and 130, and the ExoIII nuclease CCR4.

After deadenylation and dissociation of PABP from the 3' mRNA end, a ring-like structure formed by Lsm1-7 (Ling et al., 2011) assembles on the deadenylated 3' mRNA end. Along with the scaffold protein Pat1 and the DEAD box helicase Dhh1 (Nissan et al., 2010), Lsm1-7 forms a larger complex which serves to repress translation initiation, as well as stabilizing circularised mRNA for decapping, given that degradation of mRNA in the 5'-3' direction first requires removal of the 5'-cap. Decapping is carried out by a complex of two decappling factors, Dcp1 and the catalytic Dcp2, whose activity is stimulated by components of the Lsm complex at the mRNAs 3'-end (Figure 5A).

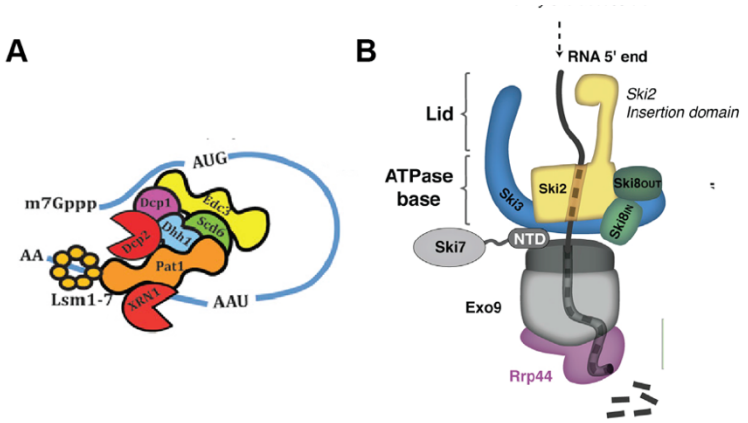

Figure 5: Complexes which stabilize mRNA during normal mRNA turnover
(A) The decapping complex associating with circularised mRNA *(Adapted from (Parker, 2012)* (B) the Ski Exosome complex responsible for 3'-5' mRNA decay *(Adapted from (Halbach et al., 2013)*

After decapping, mRNAs can be degraded by one of two cytoplasmic nucleases: mRNA may be degraded in the 5' to 3' direction by the exonuclease Xrn1 (Tesina et al., 2019), Anderson and parker 1998), or, directly targeted to the exosome by the Ski complex for 3'-5' degradation (Figure 5B) (Halbach et al., 2013; Liu et al., 2006; Schmidt et al., 2016; Zinoviev et al., 2020).

mRNA surveillance

Beyond the realm of normal mRNA turnover and decay, faulty mRNA messages may be targeted for specialised decay pathways. Unlike canonical mRNA decay, these mRNAs are problematic and must be targeted for degradation while still associated with the ribosome. During specialised mRNA decay, numerous factors act at and bind to the ribosome, in regulatory processes which recognise and recover translational stalling, wherein, the ribosome becomes stuck on the mRNA such that translation cannot proceed. When a translating ribosome encounters a problematic region of mRNA and becomes stalled, it becomes a roadblock for the following 3' ribosome translating on the same mRNA. Collision of the downstream ribosome with the stalled ribosome is accepted to be the trigger for both no-go decay (NGD) and ribosome-associated quality control (RQC) (below).

Importantly, stalling is observed under a number of circumstances: translation of rare codons (Doma and Parker, 2006; Richter and Coller, 2015), problematic di-codons (Gamble et al., 2016), oxidised mRNAs (Simms et al., 2014), or the mRNA poly(A) tail(Dimitrova et al., 2009), all induce translational stalling with differential kinetics that contrast with the stalls induced by translation of poly-proline regions, stalling peptides in the ribosomal tunnel, mRNAs with secondary structures, or mRNAs bearing premature stop codons or truncations within the ORF (Ikeuchi et al., 2018). Metabolic conditions such as tRNA deficiency (Ishimura et al., 2014) and amino acid starvation (Guydosh and Green, 2014) may additionally stall translation by specialised regulatory cascades, or, endogenous stalling may occur as a means of co-translational gene regulation.

Nonsense Mediated Decay (NMD)

Frameshifting during the process of translation may cause a STOP codon to be positioned in the ribosomal A site prematurely. In such cases, cells must be able to discriminate between an in frame or premature stop codon to prevent the production of *nonsense* proteins accumulating in the cell. Likewise, the mRNAs coding for such faulty products must be similarly identified and degraded in order that subsequent rounds of translation on the same faulty message can be prevented. This process,

appropriately named nonsense-mediated decay (NMD), is one of three non-canonical decay pathways which fall into the category of 'mRNA surveillance' (Shoemaker and Green, 2012). Though the sequence and series of events which take place during NMD have yet to be fully elucidated, the factors which participate in NMD have been broadly characterised (Chang et al., 2007; Ivanov et al., 2008; Kervestin and Jacobson, 2012). The key regulator of NMD is upstream frameshifting protein (Upf1), which interacts with Upf2 and Upf3, as well as PABP and the termination factors RF1 and RF3 during NMD. During NMD, the presence of a STOP codon in the A site leads to recruitment of eRF1 and eRF3 to the ribosomal A site, as occurs normally during translation termination. Localisation of Upf1 to the termination complex is accepted as the signal that NMD should be initiated (Kervestin et al., 2012; Serdar et al., 2016). As degradation of NMD complex occurs so rapidly within the cell, structural studies seeking to localise Upf1 in the NMD complex have to date been unsuccessful. As such, there are currently two models for how NMD may occur (Figure 6).

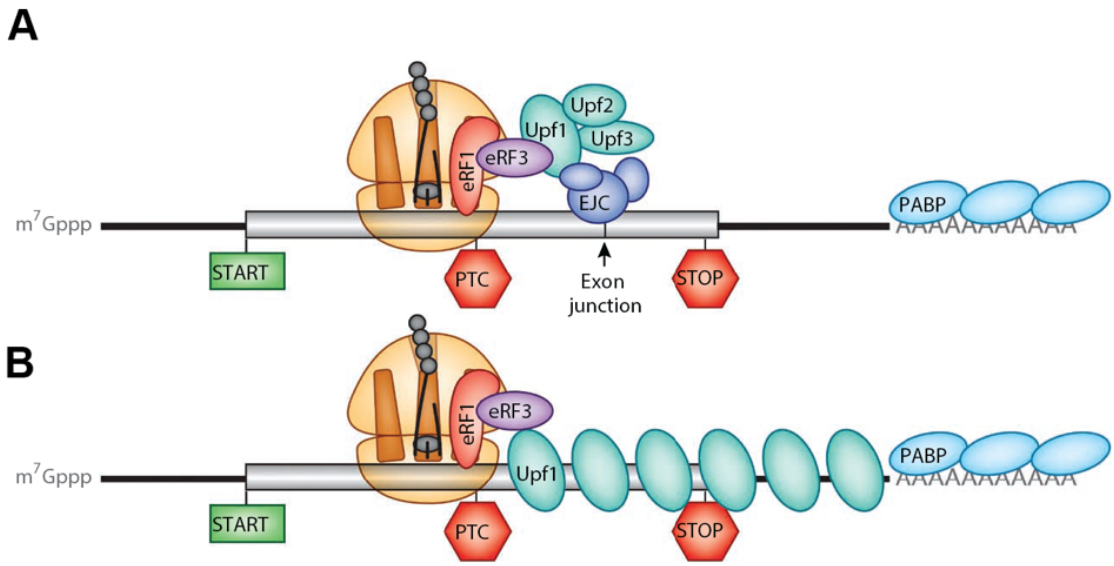

Figure 6: Models for recovery by Upf1 during NMD
A) In one model, NMD is regulated in higher eukaryotes via interplay between eRF1 and eRF3 bound in the ribosomal A site, and Upf proteins which sense downstream EJC complexes, or perhaps PABP proteins allowing premature termination to be distinguished during NMD. B) the second model for NMD suggests Upf1 coats the 3' UTR of NMD mRNAs, thereby modulating NMD on the basis of a direct ribosome association. though Upf1 associates with PABP in the model, it is inconsequential for the NMD reaction. *Adapted from (Shoemaker and Green, 2012)*

Non-stop decay (NSD)

Non-stop decay (NSD) is another of the three classical mRNA surveillance pathways and refers to the decay of mRNAs lacking an in-frame STOP codon (van Hoof et al., 2002). Endogenous NSD targets manifest as a result of truncations within the ORF, or, translation through the poly(A) tail. Translation of the poly(A), which codes for poly-Lys, induces translational stalling as a result of inhibitory interactions between large charged K regions and the rRNA within the LSU nascent protein tunnel (Arthur and Djuranovic, 2018). In recent years, it has come to light that there is a significant degree of overlap between both the targets and processes of NSD with the third mRNA surveillance pathway, no-go decay (NGD). For clarity, NSD can be generally considered to refer to process employed for 3'-5' mRNA degradation by the exosome. Importantly, mRNAs with 3' non-ribosome protected overhangs of ~10-20nt are preferred targets of NSD, as these regions are bound by the Ski complex (Schmidt et al., 2016). Recent work has found that Ski in complex with the exosome is capable of fully extracting and degrading NSD mRNAs, leaving the 80S ribosome-nascent chain complex (RNC) bearing Peptidyl tRNA and nascent protein to be resolved by the factors involved in NGD and RQC (Zinoviev et al., 2020).

No-Go Decay (NGD)

Initially, NGD was characterised with mRNAs bearing stable stem loop secondary structures, which serve as roadblocks barring the completion of translation for any given ORF (Doma and Parker, 2006). Later, endogenous biological targets for NGD were identified when it was found that inhibitory dicodon pairs, often utilising the CGA Arg codon, perturb the process of decoding by engaging wobble or non-Watson Crick base pairing interactions between position 34 of the tRNA anticodon stem loop and the third base of the mRNA codon (Gamble et al., 2016). The primary signal for initiating NGD is endonucleitic cleavage of the mRNA. Subsequently, NGD substrates are recognised and mono-ubiquitinated on eS7 by the RING-type E3 ligase Not4 of the CCR4-Not complex (Matsuo et al., 2017), before K63 linked polyubiquitination of eS7 is extended by the E3 ligase Hel2 (Ikeuchi et al., 2019). When decay is initiated, mRNA cleavage upstream of the stalled ribosome by the endonuclease Cue2 generates a 5' NGD intermediate of an 80S in the PRE, rotated-state bearing hybrid tRNAs, and a 3' 80S NGD intermediate in the POST state (D'Orazio et al., 2019). The mRNA from the 3' NGD intermediates are degraded by the exonuclease Xrn1, while the ribosome on

this fragment may either be dissociated, or, continue with translation in cases where additional regulatory factors can recover stalling (Ikeuchi et al., 2018). Finally, stalled ribosomes can be recycled by either the Dom34 system (below), or, by components of the RQC trigger complex (RQT).

Recycling of the ribosomal LSU in ribosome-associated quality control (RQC)

In RQC, collided ribosomes are first recognised and polyubiquitinated at uS10 by Hel2 (Ikeuchi et al., 2019). The dissociation of RQC disomes has been attributed to the so called RQC-Trigger complex (RQT) composed of Slh1, Cue3, and YKR023W. Though the components of the RQT complex have been characterised in both yeast and human (Hashimoto et al., 2020; Matsuo et al., 2017; Shen et al., 2015) how these events are coordinated is still a matter of some debate.

Still, RQC describes the process for recycling of the ribosomal LSU and tRNAs after the stalled disome has been dissociated. First, the remaining 60S, P tRNA, nascent protein complex is bound by the E3 ligase Ltn1, which adopts an elongated structure. Therefore, Ltn1 makes contact with the ribosome near the PTC, as well as near the ribosomal tunnel exit where the catalytic domain is found (Brandman and Hegde, 2016). In this position, Ltn1 conjugates K63-linked poly-ubiquitin to any available, non-ribosome protected Lys residues of the faulty nascent protein outside the tunnel. Meanwhile, Rqc2 bound near the PTC carries out a process known as CAT tailing, adding additional residues to the nascent protein which serves to push the remaining ribosomal protected protein terminus out of the tunnel. CAT tailing proteins helps target them for degradation and may additionally reveal more Lys residues of the nascent protein for Ltn1 ubiquitination. The ubiquitination of nascent protein serves as a signal for the cell to recruit the CDC48/p97 system which will extract and degrade the truncated peptide. With faulty proteins targeted for degradation, the final step of RQC is the release of the NC and tRNA bound to the LSU. Unexpectedly, rather than hydrolysing the peptide bond from the tRNA as occurs normally during translation termination, the endonuclease domain of Vms1 (human ANKZNF1) binds local to the PTC, and, with the help of Arb1, cleaves off the NC and the 3'CCA end, leaving the tRNA truncated (Su et al., 2019; Verma et al., 2018; Yip et al., 2019; Yip et al., 2020).

The Dom34 splitting system

In most cases, non-canonical mRNA decay employs an alternative mechanism for ribosome recycling known as the Dom34 splitting system (Doma and Parker, 2006). Recycling with Dom34 is very similar to canonical recycling (Heuer et al., 2017; Preis et al., 2014), although instead of eRF1 being delivered to the A site by eRF3, Dom34 is delivered to the A site by Hbs1. These factors, Dom34 and Hbs1, exhibit a high degree of structural similarity with the two termination factors respectively (Graille et al., 2008; Lee et al., 2007). Importantly, ribosome splitting by the Dom34 system occurs without a 'stop' codon in the A site. Due to structural differences between Dom34 and eRF1, Dom34 recycling is not accompanied by hydrolysis and release of the nascent protein as in a normal recycling reaction (Pisareva et al., 2011). As such, the LSU remains associated with a P tRNA covalently linked to the nascent protein, which if necessary, can be recovered by the downstream process of RQC.

Codon optimality as a trigger for canonical mRNA decay

Ribosome collision has also been discovered in a new context. One branch of mRNA decay of emerging interest has called into question the role of codon optimality in mRNA stability. The degeneracy of the genetic code allows numerous codons to code for a single amino acid, long observed to manifest in species-specific codons preference (Lagerkvist, 1978; Ohno et al., 2001; Sharp et al., 1986). However, in 2015, genome-wide RNA decay analysis in *S.c.* revealed a link between codon-optimality and mRNA stability, in that substitution of non-optimal codons reduced mRNA half-lives. The work went on to demonstrate the effects of codon-optimality on ribosomal translocation, linking declined rates of translation elongation with mRNA decay, and concluded by providing a novel rubric deemed 'the codon occurrence to mRNA stability correlation coefficient' for ranking codon optimality based on global mRNA stabilities (Presnyak et al., 2015). The study followed previous work which demonstrated that substitution of rare codons slowed ribosomal movement and promoted mRNA decay, implicating the DEAD-box helicase Dhh1 in repression of translation initiation and promotion of decapping and mRNA decay, as well as demonstrating the proteins association with slow moving polyribosomes (Sweet et al., 2012). As Dhh1 is known to repress translation of mRNAs by activating 5'-3' degradation by Xrn1 (Carroll et al., 2011), and is conserved across bacterial and eukaryotic species with above 70% protein sequence identity in orthologues from

yeast, *Drosophila*, and vertebrae (Weston and Sommerville, 2006), researchers began to speculate that Dhh1 may be filling a more significant role for recognising non-optimally coded mRNAs and targeting them for degradation (Hanson and Coller, 2018; Harigaya and Parker, 2016; Radhakrishnan et al., 2016). However to date, the significance of, and regulatory mechanisms for, recognising, targeting, and degrading non-optimally coded mRNAs remains enigmatic.

1.4. Ribosome Arrest Peptides (RAPs)

In some cases, endogenous translational stalling occurs as form of gene regulation, where elongation and termination is tuned by an upstream open reading frame (uORF). In such cases, stalling is mediated by the translation product of the this uORF, a so-called stalling peptide or ribosome arrest peptide (RAPs). Peptide mediated stalling usually results as a repercussion of the peptide NC tightly interacting with rRNA and proteins in the ribosomal tunnel, causing relays which disrupt orientation of PTC bases (Wilson et al., 2016). Unlike mRNA surveillance and quality control processes, which regulate translation in *trans*, stalling peptides act in *cis* via induction of conformational changes to ribosomal active sites for modulation of translation (Ito and Chiba, 2013)**.** There are three categories which describe the consequences of RAP stalling; transcription antitermination, translation induction, or translation termination (table 1) (Wilson et al., 2016; Wilson and Beckmann, 2011).

Table 1: Ribosome Arrest Peptides
Common RAPs along with the point durin translation where stalling occurs (When), the downstream effect of the RAP stalling, the name of the AP (uORF/AP), and downstream gene being regulated (dORF) and where relevant, the small which controls stalling (Regulator).

When	Effect	uROF/RAP	dORF	Regulator	Kingdon
termination	*transcription antitermination*	tnaC	tnaA/B	Trp	prokaryotic
elongation	*translation induction*	secM	secA	N/A	prokaryotic
		mifM	yidc2	N/A	prokaryotic
		VemP	secDC2	N/A	prokaryotic
		ermCL	ermC	Ery	prokaryotic
		catA86L	catA86	Cam	prokaryotic
termination	*translation termination*	AAP	arg2/CPA7	Arg	eukaryotic
		CMV	gp48/UL4	N/A	eukaryotic
		uORF SAM-DC	SAM-DC	N/A	eukaryotic

There are general mechanisms by which RAPs can induce translational stalling (Figure 7). In most cases, conformational rearrangements of PTC bases disrupts peptidyl transfer or perturb access to incoming A-site tRNA. Secondary structure formations or interactions between the nascent peptide and ribosomal constriction site proteins may congest the ribosomal tunnel. In some bacterial species, this type of stalling is utilised for gene regulation where additional binding factors generate a pulling force for release of the NC e.g. bacterial RAPs SecM, MifM, and VemP (Chiba and Ito, 2012; Sohmen et al., 2015; Su et al., 2017; Tsai et al., 2014). Other RAPs mediate stalling where interactions in the tunnel relay back to PTC bases, as is the case in bacterial RAPs TnaC and ErmCL, and likely the fungal arginine attenuator peptide (AAP) (Arenz et al., 2014a; Arenz et al., 2014b; Seidelt et al., 2009). In such cases, the NC serves as a binding pocket for regulators, allowing small molecules to serve as negative regulators for translation of their biosynthetic enzymes. With these regulators bound, PTC bases are forced into flipped out positions causing translational to arrest. RAPs may need only employ short poly-Pro stretches to force the geometry of PTC bases into the uninduced positions. Proline is generally difficult to translate and is both a poor A site acceptor and P site donor. As few as three prolines are enough to induce translational stalling in mammalian cells, though residues flanking proline residues will also influence whether the geometry of the PTC can be maintained in the induced position or will be disrupted. Though their mechanisms may vary, all RAPs take advantage of the necessity for PTC bases to be properly oriented in the 'induced' conformation in order that translation may proceed. Deformation of the PTC bases by RAPs may trap them in the 'uninduced,' or flipped out conformations such that translation can no longer proceed (Wilson et al., 2016).

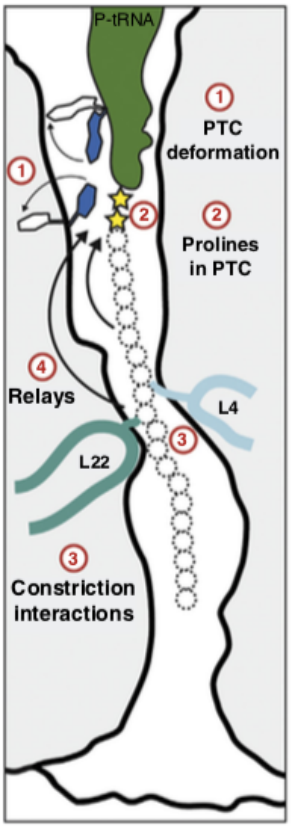

Figure 7: Mechanisms of peptide meditated stalling

(1) Deformation of PTC bases (2) Prolines in the PTC (3) NC interactions with constriction site proteins (4) NC secondary structure formation relaying back to PTC bases *Adapted from (Wilson et al., 2016)*

In prokaryotes, stalling peptides are generally responsible for upregulation of downstream cistrons, enacting either transcription antitermination or perturbations to elongation. In stalling on the bacterial TnaC uORF, the ribosomes become stalled in a position on the mRNA which blocks the binding site for the Rho transcription terminator which results in transcription antitermination for the downstream ORF (Seidelt et al., 2009). Stalling on the TnaC uORF is dependent on Trp, allowing ribosomes to regulate the downstream TnaA/B ORF, which codes for an enzyme responsible for degradation of L-Trp via pyruvate. As such, TnaC serves to control Trp metabolism in response to intracellular Trp bioavailability. Other prokaryotic stallers arrest translation at the point of elongation. Ribosomes arrest in a position on the mRNA which disrupts downstream stem-loop formation, thereby exposing the ribosome binding SD sequences required for translation of the downstream cistrons and thereby inducing translation of these genes (Table 1).

Conversely, eukaryotic RAPs are responsible for downregulating the translation of and therefore blocking protein expression for downstream cistrons. In eukaryotes, RAPs arrest translation at the point of termination, thereby initiating translation termination and ribosome recycling and preventing ribosomes from scanning and translating the downstream ORF. In the case of the human cytomegalovirus (CMV)

peptide, stalling is mediated by two C-terminal proline residues of the 22 amino acid RAP, which restrict the geometry of the PTC. In the ribosomal tunnel, the nascent CMV adopts an α-helical structure spanning from residues 11-19. In conjunction, the secondary structure from the CMV RAP forces the PTC base U2585 (U4493 in *H.s.*) to rotate by 90°C to the uninduced position, as a result of steric inhibition from residue P21 of the RAP. By promoting stalling at the end of the uORF, the hCMV RAP prevents ribosome scanning and therefore translation of the downstream gp48 cistron (Matheisl et al., 2015). Another eukaryotic staller, XBP1u was found to mediate an 'intermediate' level of translational arrest during the unfolded protein response (UPR), allowing stalled RNCs to be recognised by the signal recognition peptide (SRP) (Halic and Beckmann, 2005; Halic et al., 2006) and targeted to the ER lumen where local IRE1α transmembrane proteins splice the XBP1u mRNA. 8 residues of the XBP1u RAP is stabilized in the tunnel by a number of hydrogen bonding, salt bridge, and base stacking interactions with rRNA and constriction site proteins, though mutational analysis revealed the remaining 12 of the 20 critical stalling residues could be optimised to increase the level of translational arrest. Structural analysis was able to show that stalling on the Xbp1 RAP were a repercussion of C-terminal residues forcing the geometry of one PTC base (*E.c.* A2602), thereby blocking A site accessibility to incoming tRNAs and arresting translation (Shanmuganathan et al., 2019). In both cases, eukaryotic RAPs have been found to induce translation termination by promoting ribosome arrest via perturbations of PTC bases.

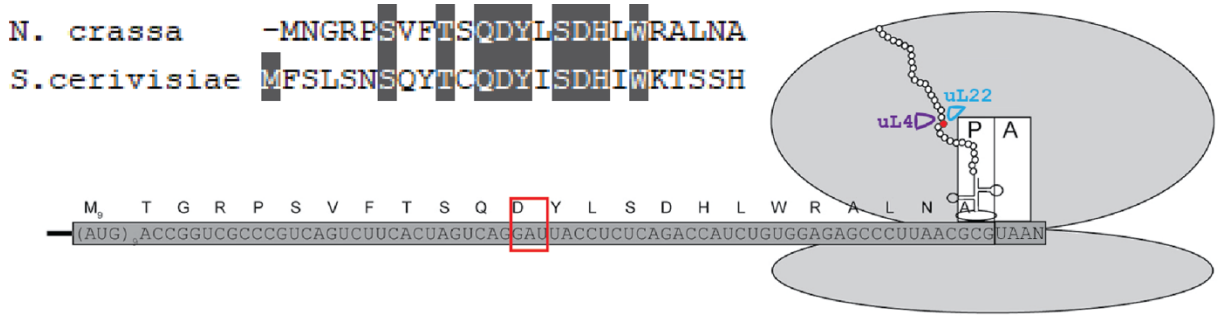

Figure 8: The fungal arginine attenuator peptide
Protein alignment for the AAP uORF in *N. c.* and *S.c.* reveals relatively low identity between species, exhibiting almost no preference for the most C-terminal residues local to the PTC. Instead, a conserved -Q-D-Y- motif midway along the peptide sequence mediates stalling. This critical aspartic acid, displayed in red, is essential for translational arrest, and is expected to localise to the tunnel constriction site as indicated by the position of uL4 (purple) and uL22 (blue). *Adapted from (Wei et al., 2012)*

One eukaryotic RAP of long-standing interest is the fungal arginine attenuator peptide (AAP). While AAP has been the subject of extensive biochemical investigations, it has to date, eluded structural resolution. Stalling on the AAP uORF, like TnaC, is dependent on intracellular availability of an amino acid, in this case arginine (Arg). When the intracellular bioavailability of Arg is adequate, > 2mM *in vivo*, stalling on the AAP RAP blocks translation of the downstream CPA1 cistron, which codes for carbamoyl synthetase, one of the first enzymes required during *de novo* Arg synthesis (Gaba et al., 2001; Werner et al., 1987). Arg dependent stalling on the AAP has been demonstrated in *in vitro* translations with wheat germ, *N.c.,* and rabbit reticulocyte cell free extracts, indicating cross-species conservation of the stalling mechanism (Fang et al., 2004). Though protein sequence does vary considerably between species, demonstrated by the 36% sequence identity between the *S.c.* and *N.c.* AAP, a critically conserved -Q-D-Y- motif midway through the peptide sequence has been implicated in the stalling mechanism (Figure 8). Stalling is dependent on the critical aspartic acid with D12N mutants, in *S,c.* D13N, exhibiting completely abolished activity (Gaba et al., 2005; Hood et al., 2007). Pulse chase analysis implicate residues 9-20 as the minimal region for the RAP to maintain regulatory stalling, agreeing with the position of the -Q-D-Y- motif, expected to localise to the tunnel constriction site (Spevak et al., 2010). Probing the mechanism for Arg dependent stalling further, one study applied chemical crosslinking to investigate the interactions between AAP and the ribosomal tunnel. The work found crosslinks to tunnel residues using probes spanning the length of the ribosome protected AAP peptide, concluding with the suggestion that flexibility of the RAP in the tunnel may be integral to its mechanism, which may present a challenge for structural investigation (Wu et al., 2012).

1.5. Metabolic Feedback

In addition to mRNA mediated decay and translational downregulation by RAPs, metabolic conditions such as tRNA deficiency (Ishimura et al., 2014) and amino acid starvation (Guydosh and Green, 2014) may additionally shut down translation by employing specialised regulatory cascades.

The Integrated Stress Response (ISR)

Ribosomal and mRNA mediated translational regulation are hardly the only means by

which cells modulate protein production. Given that translation is an energetically expensive process, eukaryotes have developed something known as the integrated stress response (ISR) which allows translation to be tuned in response to a variety of stress and metabolic conditions. Activation of the ISR results in phosphorylation of eIF2, the factor responsible for delivery of Met-tRNA$_i^{Met}$ to the 43s PIC during translation initiation (Figure 3). Phosphorylated eIF2 acts as a competitive inhibitor of eIF2β, the factor responsible for catalysing the GDP to GTP nucleotide exchange on eIF2 prior to 43S assembly (Dever et al., 1995; Rowlands et al., 1988). Thereby, activation of the ISR sequesters eIF2β, causing an overall reduction of the active pool of eIF2 and a global remodelling of the translational output (Nika et al., 2001). The activated ISR results in a global repression of translation initiation, though translation of specific mRNAs may be stimulated depending on the mode of ISR activation.

There are four mammalian protein kinases which phosphorylate the eIF2 α-subunit at Ser-51 and initiate the ISR, remodelling the translatome in response to environmental signals (Castilho et al., 2014). In erythroid cells, the bioavailability of heavy metals is monitored by heme-regulated eIF2 kinase (HRI) which allows the production of globin, the primary translational product in erythroid cells, to be tightly coupled with the availability of heme (Han et al., 2001). Another ISR activator is protein kinase R (PKR), which is regulated by its binding primarily to viral dsRNA, which serves as an innate immune response to globally downregulates translation during a viral infection. The third ISR eIF2 kinase, PKR-like endoplasmic reticulum kinase (PERK), serves to respond to endoplasmic reticulum (ER) stress (Baird and Wek, 2012; Walter and Ron, 2011). Once again, PERK activation reduces translation globally, excepting the transcriptional activator AFT4 which is upregulated.

The fourth eIF2 kinase is conserved in virtually all eukaryotes, and activated by accumulation of uncharged, de-acylated tRNAs in the cytoplasm. This allows the cell to sense and overcome amino acid deprivation via general control non-derepressible 2 (GCN2), which serves as the key regulator of translation during nutrient starvation. GCN2 interacts with ribosomes directly, and, in complex with Gcn20 and Gcn4, is monosome and polysome associated, which allows tRNA availability to be carefully monitored co-translationally as GCN2 is capable of sensing each amino acid indiscriminately (Hinnebusch, 2005). GCN2 has been studied extensively in yeast and

vertebrates (Chaveroux et al., 2010; Sood et al., 2000; Zhang et al., 2002), and like PERK, specifically upregulates one transcriptional activator GCN4. Upregulating GCN4 has far reaching consequences for the translatome (Baird and Wek, 2012). As both GCN4 and AFT4 are transcription factors, their upregulation causes numerous genes to be upregulated, which in the case of GCN4, affects genes coding for amino acid transporters and biosynthetic enzymes. Still, the GCN2 kinase is part of a must larger regulatory system with far reaching consequences for an array of crucial biological processes (Castilho et al., 2014).

While the mechanism by which GCN factors in complex with the ribosome modulate translational repression remain enigmatic, the accumulation of monosomes in growth arrested eukaryotic cells has been well documented (Ashe et al., 2001; Manners and Nielsen, 1981; Montero-Lomeli et al., 2002; Uesono and Toh, 2002). It turns out that translationally inactive, hibernating ribosomes make up these monosome populations, bound by small ribosome binding factors (RBFs).

Ribosome Hibernation

In bacterial systems, growth arrest during stationary phase is accompanied by reversible translational repression known as ribosome hibernation (Ito and Chiba, 2013; Prossliner et al., 2018). During ribosome hibernation, small binding factors which facilitate formation of inactive ribosome dimers are translationally upregulated (Beckert et al., 2018; Prossliner et al., 2018). Bacterial hibernation factors bind in the ribosomal SSU, protecting the decoding center and simultaneously inhibiting binding of both mRNA and tRNA. Subsequent dimerization of ribosomes occurs via one of two distinct species-specific mechanisms, however in both cases, the resulting ribo-dimers are maintained in a translationally inactive state and retain factor binding within the mRNA channel on the SSU (Figure 9).

Gammaproteobacteria possess three hibernation factors, ribosome-associated inhibitor A (RiaA), ribosome modulation factor (RMF), and hibernation promoting factor (HPF) (Prossliner et al., 2018). RiaA binds 70S ribosomes on its own, while RMF and HPF act together during ribosome hibernation. RiaA is a structural homologue of HPF, and both share a highly conserved, hydrophobic, (β-α-β-β-β-α fold) NTD. These factors, along with the third HPF homologue long-HPF (LHPF), bind to the ribosome

in the ribosome DCC, clashing with the location occupied in actively translating ribosomes by mRNA, as well as blocking A and P tRNA sites (Beckert et al., 2017). In gammaproteobacterial, RMF binds 70S in the SSU, local to 16S rRNA, rpS2, rpS7, rpS9, and rpS21. In this position, RMF overlaps the location normally occupied by the anti-SD/SD helix between mRNA and 16S rRNA.–Subsequently, HPF binds in the tRNA cleft on the 30S, blocking A and P sites on the SSU and interacting with de-acetylated E-site tRNA. The C-terminus of HPF is presumed to interact with RMF, upon which, RMF-90S dimers are converted to inactive (top-top) RMF-HPF-100S dimers (Beckert et al., 2017; Beckert et al., 2018)). Unlike HPF, RiaA possesses a short 18aa C-terminal extension which extends down into mRNA entry tunnel allowing both functions of RMF and HPF to be modulated, though dimer formation is not induced.

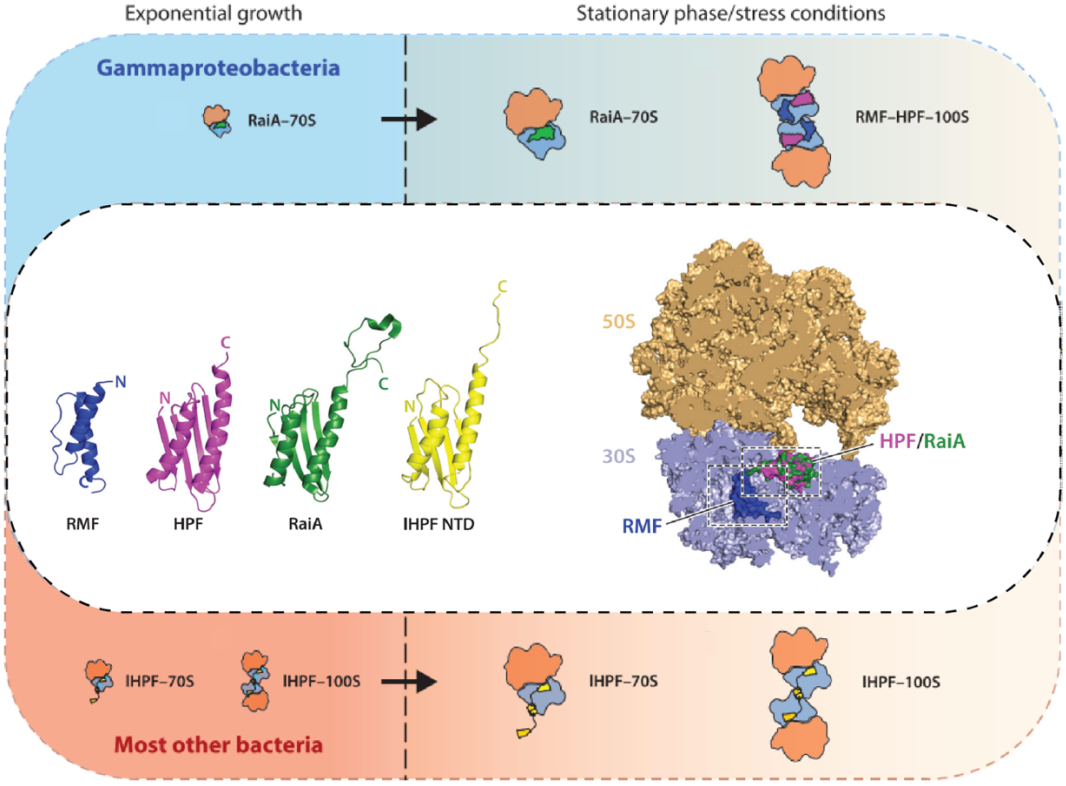

Figure 9: Bacterial hibernation factors
Bacterial ribosome hibernation has been broadly characterized by the proteins and dimerization observed. *Adapted from (Prossliner et al., 2018).*

While most gammaproteobacteria and betaproteobacteria employ some variation of RMF/HPF or RaiA for hibernation factor dependent translational repression, other bacteria and plant plastids employ LHPF in ribosome hibernation. LHPF facilitates formation of inactive 100S ribosome dimers via a distinct mechanism; in the cytosol, LHPF forms homodimers associated by their CTD. The LHPF homodimer binds

individual 70S ribosomes, sequentially engaging each NTD for ribosome inactivation and subsequent 100S dimer formation. Unlike the top-to-top orientation of the 30S interface observed in RMF-HPF-100S dimers, LHPF-100S dimers associate via side-to-side conformation (Ueta et al., 2008; Ueta et al., 2013; Ueta et al., 2005).

In eukaryotic systems, environmental stressors and nutrient deprivation have been shown to induce similar instances of temporary and reversible translational repression (Balagopal and Parker, 2011; Van Dyke et al., 2013; Wang et al., 2018). While ribosome dimerization is a hallmark of ribosome hibernation in prokaryotes, dimerization of eukaryotic ribosomes appears to be species specific, as ribo-dimers have only been observed in the polysome profiles of nutrient depleted rat and hamster cells, but not in human or mouse cells. (Krokowski et al., 2011).

The *S.c.* protein Stm1 was the first RBF described that serves a protective role during recovery of translation following quiescence in *S.c.* (Van Dyke et al., 2004). Stm1 was initially identified in genetic screens, when it was implicated as a broad regulator of mRNA degradation with links to mTOR regulation (Balagopal and Parker, 2011). Stm1 was later found to bind and sequester ribosomes with a 1:1 stoichiometry, and has also been found associated with actively translating polysomes (Correia et al., 2004; Inada et al., 2002; Van Dyke et al., 2006). Though Stm1 is non-essential protein, during starvation, stm1Δ *S.c.* cells exhibit a reduction in the monosome population where only 50% 80S are observed compared to wild type, accompanied by overall reduction of protein synthesis during quiescence as determined by monitoring ^{35}S-met incorporation (Van Dyke et al., 2013). These translational deficits are reversed in stm1Δ/dom34Δ cells, implying that activity of Dom34 antagonizes the role fulfilled by Stm1 during ribosome hibernation (van den Elzen et al., 2014).

The association of Stm1 to 80S ribosomes was first characterized structurally in a crystallographic study of the *S.c.* 80S ribosome, where a 10 minute glucose depletion was employed to promote ribosomal runoff for homogeneous crystallographic sample prep. The 30 kDa protein is composed of 96 amino acids and is largely unstructured, spare a few small helical regions. Like bacterial hibernation factors, Smt1 binds on the small subunit, weaving through the mRNA tunnel exit into the P and E sites on the SSU, where it's very N-terminus establishes contacts with the LSU on the CP (Ben-

Shem et al., 2011). This interaction was structurally characterized in the mammalian system by cryo-EM, where Stm1 homologue, SERBP1, was found associated with eukaryotic 80S ribosomes from both *H.s.* and rabbit reticulocyte systems (Anger et al., 2013; Brown et al., 2018). Once again the structure bears a striking resemblance to the binding of bacterial hibernation factors; SERBp1 binds within mRNA entrance channel, interacting with A and P sites via a DRHS motif (Brown et al., 2018). Additionally, the most abundant subset from one cryo-EM dataset was bound by tRNA in a new position, deemed the 'Z site', accompanied by an additional hibernation factor IFRD2 in intersubunit space. These ribosomes were observed in the non-rotated conformation, with the position of IFRD2 once again blocking the positions for both P and E tRNA binding, as well as mRNA binding in channel. At long last, researchers are catching up and have begun to close the gap in understanding of eukaryotic ribosome hibernation.

Recently, quantitative proteomics led to the identification of a novel eukaryotic hibernation factor responsible for aiding recovery of translation following a period of global repression: late-annotated short open reading frame 2 (Lso2) (Wang et al., 2018). Initially, ribosomal fractions from glucose-starved and -replete *S.c.* were subjected to mass spectrometry. When the protein content from the different metabolic conditions were compared, Lso2 was identified as a novel RBF. Notably, the Lso2-monosome interaction was enriched in nutrient deprived conditions, and the researchers observed that strikingly, all intracellular Lso2 was ribosome associated. Upon deletion of Lso2, recovery from quiescence took almost three times longer and was marred by translational deficits, specifically, increased pausing at AUG start codons indicative of initiation defects. At only 10.5 kDa and 92 amino acids long, Lso2 seemingly facilitates the cells ability to ultimately recover translation following long term nutrient deprivation; lso2Δ cells exhibit a 3-fold accumulation of monosomes at the expense of polysomes, relative to wild type (WT), and a 5-fold decrease in overall translation during recovery. What's more, neither WT nor lso2Δ strains increased their mature rRNA content once metabolic homeostasis was recovered, indicating that the translational defects observed during recovery from quiescence in lso2Δ cells is factor dependent, rather than manifesting as a result of an upstream failure to produce new, functional ribosomes. The study noted that all soluble Lso2 was ribosome bound, and intriguingly, unlike bacterial hibernation factors which are specifically

upregulated during nutritional deficit, the abundance of intracellular Lso2 remained constant. As such, the researchers propose that in addition to its specific function as a hibernation factor, Lso2-ribosome complexes may account for up to 15% of the total ribosomal population at any given time.

Chemical crosslinking analysis was carried out with Myc-tagged Lso2 grown in the presence of 4-thiouracil crosslinker, and irradiated at 365 nm before RNase treatment and immunoprecipitation, allowing for cDNA to be generated by PCR for rRNA contacts to be identified. The outputs from these experiments identified chemical crosslinks between the C-terminus of Lso2 and a 95 nucleotide region on the 25S rRNA, near the A site. Upon increasing RNase 10-fold during crosslinking and immunoprecipitation library preparation, additional crosslinks were identified between Lso2 and tRNAs, indicating Lso2 may be probing the ribosome for tRNAs before binding in the tRNA channel. Binding location was further assessed by comparing subunit association under physiological magnesium conditions in the presence and absence of Lso2, where Lso2 was found to increase incidence of a stable monosome population two-fold, agreeing with the proposed position of binding near the tRNA channel (Wang et al., 2018).

Excitingly, the role of *S.c.* Lso2 seems to be conserved in higher ordered species, as the study also reports on conservation of ribosomal interaction for the human Lso2 orthologue, coil-coil domain containing protein 124 (CCDC124). Like Lso2, CCDC124 is primarily enriched in the monosomal fraction of HeLa cell extracts. This interaction can be perturbed by treatment with ETDA which results in CCDC124 migrating to light, sub-ribosomal gradient fractions, consistent with the behavior of a ribosome binding protein. Chemical crosslinking experiments were repeated by replacing endogenous *LSO2* with V5 tagged CCDC124 and carrying out immunoprecipitation and PCR as before. Crosslinks were found between CCDC124 and the same region of S.c. 25S rRNA reported for Lso2, as well as for a more broad range of tRNAs. The researchers therefore conclude that the ribosome binding activity of Lso2 is conserved between yeast and human, but stipulate that higher order species likely regulate CCDC124 activity in a more complex manner. They attribute this conjecture to the observation that CCDC124 contains an additional 131 C-terminal amino acids compared to Lso2, and that although virtually all cytoplasmic Lso2 is found associated

with the ribosome, the majority of CCDC124 is detected in ribosome free soluble fractions in sucrose gradient fractionation of HeLa cell extracts (Wang et al., 2018). The conservation of Lso2 from yeast to human seemingly suggests that a more complex system exists for the regulation of eukaryotic ribosome hibernation than previously thought. If correct, a more thorough characterization of such ribosome binding proteins could uncover new mechanisms by which translation is broadly regulated, as well as clarifying the means by which eukaryotes specifically diminish the impact of nutritional deficit on translational fidelity.

Ribosome binding proteins enhance understanding of how modulations to protein synthesis contribute to the regulation of cellular homeostasis. Therefore, it is important that effective characterization of such ribosomal interactions includes structural analysis to enhance understanding via derivation of structure to function relationships within more complex regulatory cascades.

1.6. Aims

Understanding of co-translational gene regulation has been significantly enhanced by the utilisation of structural techniques for direct visualisation of RBF-ribosome complexes. In addition to providing key insights into the direct structure to function relationships within such complexes, the sequential assembly and disassembly of multi-subunit regulatory complexes, such as those which engage during mRNA surveillance and RQC, continue to benefit from application of structural techniques. Still, much of what is known today comes from pioneering studies in prokaryotic systems, calling for additional works which set out to clarify how such systems are modulated in more complex, and higher ordered eukaryotic species.

The inverse relationship between the rate of translation and mRNA decay has become a prominent focal point for investigators seeking to delineate the many mechanisms of modulating translational regulation (Balagopal and Parker, 2011). Specific mRNA features have been identified which initiate mRNA decay via distinct pathways (Shoemaker and Green, 2012). In yeast, sensing of slow or stalled translation which manifests on mRNAs enriched with non-optimal codons, has been proposed to fall upon the helicase Dhh1 (Presnyak et al., 2015). In order to understand how decay of

non-optimally coded mRNAs proceeds, whether or not Dhh1 directly binds to the ribosome must first be clarified. Initially, affinity purification of endogenous Dhh1, bearing a C-terminal affinity tag, will be used in an effort to isolate native Dhh1-ribosome complexes. Although this will represent an optimal sample for subsequent structural characterisation, recombinant overexpression and purification of the yeast protein from *E.c.* will alternatively serve this investigation. Purified protein can be incubated with yeast ribosomes in *in vitro* binding assays, allowing the optimal conditions for subsequent *in vitro* reconstitution of the putative Dhh1-ribosome complex to be identified.

Recently, a new eukaryotic RBF, Lso2, was identified in yeast, along with the conserved orthologous human protein CCDC124 (Wang et al., 2018). These factors modulate translational control during periods of nutrient deprivation, allowing ribosomes to be stored in an inactive, hibernation state and subsequently re-activated. This allows eukaryotes to regulate translation in a nutrient-dependent fashion, in response to carbon and nitrogen bioavailability (Van Dyke et al., 2006; Van Dyke et al., 2013; Van Dyke et al., 2009). To date, the Stm1-80S complex has been the only eukaryotic ribosome hibernation complex to be structurally characterised (Anger et al., 2013; Ben-Shem et al., 2011; Brown et al., 2018). Therefore, the molecular structure of the novel Lso2/CCDC124-80S complex was investigated as it may provide key insights into how this distinctive complex differs from the Stm1-80S complex, and, reveal a new structure to function relationship for how translational shutdown and re-activation is modulated during nutrient stress. Affinity purification of native hibernation complexes represent the current gold standard for molecular structural analysis and was therefore employed. As before, purified recombinant protein serves an additional utility, for *in vitro* complex assembly, to circumvent the limited yield from native complex purification. Subsequently, high concentration purified Lso2-80S can be utilised for a functional analysis, where complex disassembly as a prerequisite for translational re-activation can be assessed. Importantly, assembly of the pre-initiation complex dictates ribosome recycling must occur to regenerate the pool of ribosomal subunits for translation initiation. As such, *in vitro* splitting assays were assembled so the propensity for ribosome recycling can be derived.

In addition to *trans* regulation by RBFs, RAPs regulate translation in *cis*, allowing

eukaryotes to downregulate specific transcripts in response to specific metabolic and stress conditions (Ito and Chiba, 2013). Ribosome profiling analysis has revealed that in eukaryotes, regulatory uORFs are more widespread than previously thought. Therefore, RAP stalling events may represent a more broadly applicable form of gene regulation (Ingolia et al., 2011). To date, only three eukaryotic RAPs have been structurally resolved, while others like AAP remain elusive. Understanding the relationship between Arg metabolism and synthesis requires structural characterisation of the AAP. Following standard methodologies for *in vitro* translation and RNC purification, the study will seek to resolve the high resolution molecular structure of AAP RNCs in *N.c.*, a long standing model organism for biochemical analysis of AAP (Fang et al., 2004; Fang et al., 2000; Gaba et al., 2005; Gaba et al., 2001; Wei et al., 2012; Wu et al., 2012).

Materials and Methods

2.1. General Methodologies

This investigation employs standard methodologies for preparation of biological samples from *E.c., N.c.,* and *S.c.,* as well as the techniques required to technically assess quality and ensure the fidelity of experimental design.

2.1.0. Strains and Plasmids

Vector maps for cloning plasmids (Table 2) from this study can be found in Appendix 1.

Table 2: Cloning Plasmids
Plasmids assembled by polymerase chain reaction. (No-number, Ori- origin of replication, Origin-species of protein origin)

No.	Protein	Vector	Marker	Ori	Origin	Description
1	Dhh1	pFA6aHiFl	Nsr.	SP6	*S.c.*	His_8-$FLAG_3$ for tag integration at C-term of endogenous *DHH1*
2	Lso2	pRSF-DUET1	Kan.	RSF	*S.c.*	His_6-*SUMO* -*LSO2*
3-5	*S.c.* AAP	pEX-A2 (*S.c.*)	Amp.	pUC	*S.c.*	T7 promoter, HA-His_6-uL4A (aa2-65)-$_{S.c.}$ *AAP*- N
6-8	*N.c.* AAP	pEX-A2 (*N.c.*)	Amp.	pUC	*N.c.*	T7 promoter, HA-His_6-uL4a(aa2-65)-$_{N.c.}$ *AAP*- N

Table 3: Other plasmids for proteins used in this study
Plasmids kindly provided for use in this study, not included in PCR methodologies.

No.	Protein	Plasmid	Provided by	Origin	Description
9	Dhh1	pPROEXHtB	Prof R. Green	*S.c.*	His_6-TEV-*DHH1*
10	Upf1-1	pKB510	Dr. K. Baker	*S.c.*	nonsense mediated mRNA reporter
11	Upf1-2	pKB607	Dr. K. Baker	*S.c.*	FLAG tagged, ATP hydrolysis deficient Upf1
12	Dom34	pET24a(+)	Beckmann lab	*S.c.*	*DOM34* -His_6
13	Hbs1	pET24b(+)	Beckmann lab	*S.c.*	His_6-*HBS1*
14	Rli1 (ABCE1)	pYES2-Rli1	Beckmann lab	*S.c.*	High-copy plasmid for Rli1 overexpression in yeast under control of the *GAL1* promoter
15	Tif6 (eIF6)	p7XC3GH	Beckmann lab	*S.c.*	*TIF6* -3C-GFP-His_{10}

Table 4: Organisms used in this study
Bacterial and eukaryotic cell lines utilised in this work and corresponding description

Strain	Discription
E. coli Dh5a	Cell line for vector propagation
E. coli Rosetta (DE3)	Cell line for overexpression of recombinant yeast Dhh1
E. coli BL21 (DE3)	Cell line for overexpression of recombinant yeast Lso2
S.cerevisiae 288C	MATα; HIS3; LEU2; ura3-52; TRP1; GAL2
S.cerevisiae BY4741	MATα; ura3Δ0; leu2Δ0; his3Δ1; met15Δ0; YMR080c::kanMX4
S.cerevisiae WCGα	MATa/MATα {leu2-3,112 trp1-1 can1-100 ura3-1 ade2-1 his3-11,15}
HEK293 Flp-In T-Rex	293/tsA1609neo

2.1.1. Preparation of yeast genomic DNA

Yeast genomic DNA was used as template DNA for amplification of *S.c.* protein coding regions unless otherwise indicated. To that end, cultures of 1.5 mL YPD (2% Glucose) were inoculated with a single colony of *S.c.* BY4741 cells and incubated overnight at 30°C. Cells were pelleted with an Eppendorf table top centrifuge for 10 min at 16,000 × *g* and resuspended with 0.2 mL Lysis buffer (2% Triton-X100, 1% sodium dodecyl sulfate (SDS), 100 mM NaCl, 10 mM tris(hydroxymethyl)aminomethane (Tris)-HCl pH 8.0, 1 mM Ethylenediaminetetraacetic acid (EDTA)), before addition of 0.2 mL phenol to chelate the genomic DNA and 0.1 mL glass beads for lysis. Cells were lysed using a vortex for under the fume hood. After 5 min, 0.3 mL TE buffer (10 mM Tris-HCl pH 8.0, 1 mM EDTA) was added, and cells were vortexed for an additional 2 min. The cell lysate was clarified by centrifugation for 10 min at 21,000 × *g*. The aqueous layer (400 µL) was transferred to 1 mL 96% ethanol and mixed. Samples underwent a further centrifugation step for 20 min at 21,000 × *g* before briefly washing with 1 mL 70% ethanol. This was followed by a final centrifugation at the same speed for 1 min after which, the ethanol was decanted, and the pellet was left to stand room temperature (RT) in the fume hood until dry. Subsequently, gDNA pellet was resuspended in 0.1 mL TE buffer supplemented with 0.1 mg/mL RNAse. Finally, gDNA samples were incubated for 5 min at 60°C to inactivate DNAses. Samples were stored at -20°C and diluted 1:50 for use as template DNA in PCR reactions.

2.1.2. Polymerase Chain Reaction (PCR)

Unless otherwise indicated, PCR reactions for assembly of plasmids (Table 1) were set up in 50 µL reactions using KOD polymerase (Table 5). Reactions were carried out using BioRad 1000 Touch™ thermocycler. Settings for each reaction can be found in can be found in Appendix 2.

Table 5: Reaction setup for PCR
Reaction mix for polymerase chain reaction

50 µL KOD Polymerase reaction mix		50 µL Q5 reaction mix	
25 µL	2 × Buffer	10 µL	5 × Buffer
10 µL	2 mM dNTPs	1 µL	10 mM dNTPs
1.5 µL	FW primer	2.5 µL	FW primer
1.5 µL	RV primer	2.5 µL	RV primer
50-100 ng	template DNA	10-50 ng	template DNA
1 µL	KOD polymerase	0.5 µL	Q5 polymerase
to 50µL	nuclease free H_2O	to 50 µL	nuclease free H_2O

Plasmid 1 (pFA6a*1*-His_6-$FLAG_3$), was used for insertion of a C-terminal tag on Dhh1 at the endogenous locus in the *S.c.* genomic DNA of haploid S288C cells. The vector was designed such that insertion of the target tag would be accompanied by insertion of the gene for nourseothricin acetyltransferase under the control of an ADH1 promoter, as a resistance marker for positive clonal selection. The plasmid was kindly provided by Dr. B. Beatrix bearing a $FLAG_3$-TEV-ProteinA_2 tag and was modified for this study. Primers (Table 6) were designed with complementary 3' non-annealing regions, per manufacturer protocols for ligation using Gibson Assembly (NEB). Amplification of the His_6-$FLAG_3$ region utilised a template plasmid kindly provided by Herr V. Shanmuganathan. Therefore, the insert and backbone were first amplified using in PCR reactions 1 and 2 (Appendix 2), before linear PCR products were ligated by Gibson Assembly (NEB) according to the user manual, and used for transfection of chemically competent *E.c.* DH5α cells. The resulting plasmid was purified and subjected to sequencing (section 2.6 and 2.7, below). Upon sequence validation, a linear DNA fragment was generated in a 150µL PCR (reaction 3, Appendix 2) using primers designed with extended overhangs of 60nt complementary to yeast genomic DNA, for integration of the tag and resistance marker at the C-terminus of endogenous *DHH1* (section 2.8, below).

Table 6: Primers used for assembly of plasmid 1
Red indicates complementary overhang regions for Gibson Assembly, while blue indicates regions complementary to yeast genomic DNA. (Rxn.- reaction number, Tm- Annealing temperature, FW-forward, RV- reverse)

Rxn.	Tm	Type	Sequence	Product
1	65°C	FW	5'GATTACGATATTCCAACGACCCACCATCACCATCACC ATCACCATGG 3'	His_8-$FLAG_3$ insert for gibson assembly
1	51°C	RV	5'GGGGCCTGTggcgcgccCTACTTGTCATCGTCATCC 3'	
2	64°C	FW	5' GGATGACGATGACAAGTAGggcgcgccACAGGCCCC 3'	amplification of pFA linear vector backbone for gibson assembly
2	53°C	RV	5'ATGGTGATGGTGATGGTGATGGTGGGTCGTTGGA ATATCGTAATC 3'	
3	54°C	FW	5'GGGTATCCTCCACAGCAGGAACATTTCATGGCGATG CCACCTGGTCAGTCACAACCCCAGTATCGGATCCCCGG GTTAATTAA 3'	linear fragment for C-terminal tagging at genomic *DHH1* locus
3	55°C	RV	5'CGACGATTAGATCACAAAAAAAGCGTATCTCACCAC AGTAGTTATTTTTTCTTAGATATTCTATCGATGAATTC GAGCTCG 3'	

Plasmid 2 was assembled for recombinant overexpression of *S.c.* Lso2 in *E.c.* BL21(DE3) cells, for purification (section 2.3.0, below) and reconstitution with ribosomal subunits (section 2.3.2, below). The insert for the desired construct (pRSF-DUET1-*SUMO-LSO2*) was assembled using primers (Table 7) designed with complementary regions for two step PCR. As such, both the *SUMO* and the *LSO2* coding regions were first amplified from yeast genomic DNA. The forward primer for the *SUMO* insert was designed to include a BamHI restriction site, while the reverse primer was designed with 3' overhang regions complementary to the N-terminus of *LSO2*. Likewise, the forward primer for the *LSO2* insert bore 3' overhangs complementary to the C-terminus of *SUMO*, while the reverse primer was designed bearing a 3' overhang containing the sequence for the NdeI restriction enzyme cleavage site. Following generation of the two linear inserts in PCR reactions 4 and 5 (Appendix 2), the two products were mixed at a 1:1 molar ratio and included in a subsequent round of PCR (reaction 6, Appendix 2) using the *SUMO* forward and *LSO2* reverse primers from the previous reactions. As these primers were designed bearing restriction enzyme cleavage sites, the resulting linear BamHI-*SUMO-LSO2*-NdeI fragment could be easily inserted into a modified pRSF-DUET1 plasmid kindly provided by Dr. J. Cheng. As such, the *SUMO-LSO2* insert and target plasmid underwent restriction enzyme digestion and ligation (section 2.4, below) before transformation of *E.c.* DH5α cells (section 2.5, below). The resulting plasmid was

purified and subjected to sequencing (section 2.6 and 2.7, below), prior to transfection of *E.c.* BL21 (DE3) cells (section 2.5, below) for overexpression of recombinant *S.c. LSO2* (section 2.13, below).

Table 7: Primers used for assembly of plasmid 2
Purple indicates complementary overhang regions which lead to self-annealing in PCR reaction 6, while orange indicates insertion of restriction enzyme cleavage sequences. (Rxn.- reaction number, Tm- Annealing temperature, FW-forward, RV- reverse)

Rxn.	Tm	Type	Sequence	Product
4	60°C	FW	5'GCTCACAGAGAACAGATTGGTGGTGGTAAAAGATT TTCAGAATCCGCCG 3'	*S.c. LSO2* insert for 2 step cloning downstream *SUMO*, NdeI RV
4, 6	67°C	RV	5'accagactcgagTTATTTCATTTTTCTTTTACCCTTGCCAC CC 3'	
5, 6	69°C	FW	5'cagccaggatccgATGTCGGACTCAGAAGTCAATCAAG AAGC 3'	*S.c. SUMO* insert for two step cloning with *LSO2*, BamHI FW
5	61°C	RV	5'CGGCGGATTCTGAAAATCTTTTACCACCACCAATCTG TTCTCTGTGAGC 3'	

Plasmids 3-5 (T7-His_8-TEV-uL4A(aa2-65)-AAP-$_N$) were constructed for use as mRNA reporters in *in vitro S.c.* translation reactions (sections 2.27, 2.28, below). Primers (Table 8) were designed for amplification of a modified pEX-A2 vector kindly provided by Dr. P. Tesina, with long overhanging regions bearing the *S.c.* AAP coding sequence. In this way, the uORF was inserted as a fusion protein downstream the uL4A (aa2-65) coding sequence using the NEB Q5 PCR reaction mix (Table 5) and ligation with a kinase, ligase, Dpn1 KLD Ligation mix (NEB) per manufacturer protocols. Importantly, forward primers for vector amplification included an additional modification, engineering insertion of either the AAA, UUU, or GAG codon, immediately downstream the endogenous AAP UAA stop codon. Thermocycler settings for each PCR reaction can be found in Appendix 2.

Similarly, plasmids 6-8 (T7-His_8-TEV-uL4A(aa2-65)-AAP$_N$) were constructed for use as mRNA reporters in *in vitro* translation reactions and RNC purification in *N.c.* (sections 2.27, 2.29, below). As such, primers (Table 9) were designed for amplification of the pEX-A2 vector with long overhanging regions bearing the *N.c.* AAP coding sequence using the Q5 and KLD reaction kits (NEB) (Table 5). Likewise, forward primers were engineered for insertion of either AUG, UUC, or GAC codons downstream the endogenous AAP UAA stop codon. Thermocycler settings for each

PCR reaction can be found in Appendix 2.

Table 8: Primers used for assembly of plasmids 3-5
Italic regions indicate complementary overhang regions bearing the *S.c.* AAP coding sequence. Codon insertions are annotated in green. (Rxn.- reaction number, Tm- Annealing temperature, FW-forward, RV- reverse)

Rxn.	Tm	Type	Sequence	Product
7	65°C	FW	5'*catatctgaccacatctggaaaactagctcccactaa* aaaTAAA TAAATaaatatattcctccttaaacctgcttttgctcg 3'	Amplification of pEX-A2(T7-His_8-TEV-uL4A) and insertion of *S.c.AAPstop* AAA
7	63°C	RV	5'*tagtcttggcaggtgtattgagagttcgataagctaaa* ttccatCC AGGATTCAGCGGAGG 3'	
8	61°C	FW	5'*catatctgaccacatctggaaaactagctcccactaa* tttTAAAT AAATaaatatattcctccttaaacctgcttttgctcg 3'	Amplification of pEX-A2(T7-His_8-TEV-uL4A) and insertion of *S.c.AAPstop* UUU
8	63°C	RV	5'*tagtcttggcaggtgtattgagagttcgataagctaaa* ttccatCC AGGATTCAGCGGAGG 3'	
9	61°C	FW	5'*catatctgaccacatctggaaaactagctcccactaa* gagTAAA TAAATaaatatattcctccttaaacctgcttttgctcg 3'	Amplification of pEX-A2(T7-His_8-TEV-uL4A) and insertion of *S.c.AAPstop* GAG
9	63°C	RV	5'*tagtcttggcaggtgtattgagagttcgataagctaaa* ttccatCC AGGATTCAGCGGAGG 3'	

Table 9: Primers used for assembly of plasmids 6-8
Italic regions indicate complementary overhang regions bearing the *N.c.* AAP coding sequence. Codon insertions are annotated in green. (Rxn.- reaction number, Tm- Annealing temperature, FW-forward, RV- reverse)

Rxn.	Tm	Type	Sequence	Product
10	61°C	FW	5'*CCTCTCAGACCATCTGTGGAGAGCCCTTAACGCAtaa* atgTAAATAAATaaatatattcctccttaaacctgcttttgctcg 3'	Amplification of pEX-A2(T7-His_8-TEV-uL4A) and insertion of *N.c.AAPstop* ATG
10	61°C	RV	5'*TAATCCTGAGAGGTGAAGACTGACGGGCGCCCGTT* ttccatCCAGGATTCAGCGGAGG 3'	
11	60°C	FW	5'*CCTCTCAGACCATCTGTGGAGAGCCCTTAACGCAtaa* ttcTAAATAAATaaatatattcctccttaaacctgcttttgctcg 3'	Amplification of pEX-A2(T7-His_8-TEV-uL4A) and insertion of *N.c.AAPstop* TTC
11	61°C	RV	5'*TAATCCTGAGAGGTGAAGACTGACGGGCGCCCGTT* ttccatCCAGGATTCAGCGGAGG 3'	
12	61°C	FW	5'*CCTCTCAGACCATCTGTGGAGAGCCCTTAACGCAtaa* gagTAAATAAATaaatatattcctccttaaacctgcttttgctcg 3'	Amplification of pEX-A2(T7-His_8-TEV-uL4A) and insertion of *N.c.AAPstop* GAG
12	61°C	RV	5'*TAATCCTGAGAGGTGAAGACTGACGGGCGCCCGTT* ttccatCCAGGATTCAGCGGAGG 3'	

For *in vitro* translation of AAP (section 2.4), plasmids 3-8 were used as template DNA to generate a linear DNA fragment with primers from table 10. Linear DNA fragments were purified using QIAprep® PCR purification kit (Qiagen) and subjected to DNA

sequencing (section 2.1.6), before being used as template DNA for *in vitro* mRNA transcription (sections 2.4.1 below). Thermocycler conditions can be found in Appendix 2.

Table 10: Primers used for amplification of linear DNA for an AAP mRNA reporter
primers used to generate the final T7-His_8-TEV-uL4A-AAP_N mRNA reporter construct.

Rxn.	Tm	Type	Sequence	Product
13	60°C	FW	5'gcaagctaatacgactcactatagg 3'	Linear T7-His_8-TEV-uL4A-AAP DNA for *in vitro* mRNA transcription
13	60°C	RV	5'CAAGCGAGCAAAAGCAGG 3'	

2.1.3. Agarose gel electrophoresis

Agarose gel electrophoresis was used to separate DNA on the basis of size, which can be determined by comparison with defined, molecular weight standards (1kbp, NEB #3231; 10kbp, NEB #3232) as controls. Gels were prepared with 1.1%(w/v) agarose (Invitrogen) in TAE buffer (40 mM Tris base pH 8.8, 20 mM acetic acid, 2mM EDTA), which was boiled and cooled before addition of SYBRSafe® (Invitrogen) for DNA visualisation at 1:1000 the total gel volume. DNA samples were mixed 5:1 with 6 × Loading Dye (NEB) before loading. Gels were run in TAE buffer at 120V for 35 min before being visualised using an Inatas GelDoc.

2.1.4. Transformation of competent *E. coli* cells

For transformation of *E.c* cells, 50-100 ng plasmid DNA was incubated on ice with 50 µL competent *E. c.* cells, kindly prepared by Frau J. Musial, for 5 min. Cells were heat shocked for 30 sec at 42°C and transferred back to ice for another 10 min. 700 µL LB media was added and cells were incubated at 37°C for 1 hour. Cells were pelleted by centrifugation at 4,500 × *g* and 950 µL of the supernatant was removed. Cells were re-suspended in the remaining 50 µL and plated onto LB-agar plates supplemented with the appropriate antibiotic marker. Plates were incubated at 37°C overnight and colonies were selected the following day for subsequent plasmid preparation and DNA validations.

2.1.5. Plasmid Preparation

Single positive clones grown on LB-agar + antibiotic plates were used to inoculate 10 mL LB media which was left overnight at 37°C shaking at 150 rpm. Plasmids were extracted from the cells using the QIAprep® Spin Miniprep Kit (Qiagen) per manufacturer protocol. Plasmids were eluted in 31 µL water and DNA concentration was measured using IMPLEN NP80 NanoPhotometer.

2.1.6. DNA Sequencing

Samples of plasmids and linear DNA fragments were sequenced externally by Eurofins Genomics (Martinsreid, DE) according to company policies.

2.1.7. Integration of genomic tags in *S. cerevisiae*

A His_6-$FLAG_3$-nourseothricin acetyltransferase tag was added at the C-terminus of the endogenous *DHH1* gene in isogenic *S.c.* 288C cells kindly provided by Dr. B. Beatrix. Cells were grown to early log phase at 30°C in 100 mL YPD (2% glucose) media, to and OD_{600} of 0.8. Cells were pelleted by centrifugation at 1,160 × *g*, the media was discarded, and cells were washed with 25 mL water. Cells were pelleted as before and the water was discarded. Cell pellets were re-suspended in 1 mL of 100 mM lithium acetate (LiAc) before pelleting by centrifugation at 15,700 × *g* for 15 seconds. The LiAc was removed and cells were re-suspended to a final volume of 250 µL in 100 mM LiAc. Aside, single stranded salmon sperm DNA (ssDNA) was boiled for 5 min at 42°C, and transferred to ice for 5 min. 100 µL aliquots of cell suspension were centrifuged for 1 min at 1,500 × *g* and the LiAc was removed. Components of the transformation mix were applied to the cell pellets in the following order, 240 µL 50% (w/v) poly-ethylene glycol (PEG) 3,350, 36 µL 1 M LiAc, 50 µL ssDNA (2 mg/mL), and the linear PCR product from reaction 3 (Table 6, Appendix 2) diluted to 10 µg in 34µL. Cells were vortexed at max speed for 1 min until fully re-suspended, and incubated at 30°C for 45 min, after which, cells were heat shocked at 42°C for 25 min. Cells were pelleted by centrifugation at 2,500 × *g* for 1 min and the supernatant was removed. Finally, cells were re-suspended in 300 µL of 1 × TE Buffer and transferred to YPD agarose plates supplemented with nourseothricin for positive clonal selection. Plates were incubated

at 30°C for three days. Positive colonies were subsequently validated using PCR and western blotting methodologies to confirm tag integration was successful and correct.

2.1.8. SDS-PAGE

Proteins were separated according to their molecular weights using standard SDS-PAGE protocols (Laemmli, 1970). Sample were diluted 1:3 with SDS-sample buffer (50 mM Tris / HCl pH 6.8, 2% (w/v) SDS, 10% (v/v) glycerol, 0.1% (w/v) bromophenol blue, 100 mM 1,4-dithiothreitol (DTT)) and subjected to denaturation at either 95°C for 5 min, or 42°C for 10 min before loading onto 15% discontinuous polyacrylamide gels in 1 × SDS running buffer (25 mM Tris, 192 mM glycine, 0.1% (w/v) SDS), in the case of Dhh1 and Lso2. For AAP, 4-12% Nu-PAGE gradient gels in 1 × MOPS running buffer (50 mM MOPS, 50 mM Tris Base pH 7.7, 0.1% SDS, 1 mM EDTA) were used. In all cases, electrophoresis was performed, using 140 V for 10 min, followed by 180 V for 50 min.
Gels were loaded with two molecular weight markers, the unstained protein ladder ranging from 10-200 kDa from Thermo Scientific (PageRuler™ #26614) and the prestained protein ladder ranging from 10 to 180 kDa by Thermo Scientific (PageRuler™ #26616).

2.1.9. SimplyBlue staining

SDS-PAGE was either followed by protein visualization using SimplyBlue stain, or Western blot (below). For protein visualization without Western blotting, following SDS-PAGE gels were washed of SDS and in 3 washing steps where gels were submerged in 200 mL water and microwaved at 600 V for 1 min. Subsequently, water was removed, replaced with Simply Blue Coomassie staining solution (Novex), and microwaved once more. Gels were left to incubate with Simply Blue staining solution at RT and shaken for 5-10 min before de-staining with water.

2.1.10. Western blotting

After SDS-PAGE proteins were transferred onto a 0.2 µM pore PVDF membrane for semi-dry Western blotting. Blotting was performed using blotting buffer (20% (v/v)

methanol, 48 mM Tris-HCl, 39 mM glycine, 0.037% (w/v) at 150 mA per gel for 60 min.

Membranes were briefly washed to remove acetic acid using/with/in either 1×TBS (20 mM Tris-HCl pH 7.6, 150 mM NaCl) or 1×TBS-T (TBS with 0.1% (v/v) Tween) dependent on the subsequent blocking buffer conditions. For detection of recombinant *S.c.* His-Dhh1, membranes were blocked in 5% Milk/TBS. For detection of *H.s.* proteins (CCDC124, EBP1, eS6), membranes were blocked in 5% Milk/TBS-T. For detection of hemagglutinin (HA)-tagged *S.c.* and *N.c* AAP, blocking was carried out using 10% Milk/TBS-T. All blocking was carried out for 1.5 h at RT on a shaker. After blocking, *S.c* membranes were incubated with horseradish peroxidase (HRP) conjugated antibodies α-His-HRP (Abcam) diluted 1:5000 in 2% milk/TBS for His tagged proteins, or in the case of AAP, α-HA-HRP (Roche) diluted 1:1000 in 5% milk/TBS-T. For detection of *H.s.* proteins (CCDC124, EBP1, eS6), membranes first incubated with primary monoclonal antibodies (Santa Cruz) diluted 1:500 in blocking solution, followed by three, 5 min washing steps with TBS-T, before incubation with a mouse-α-human secondary HRP antibody diluted 1:3000 in 5%Milk/TBS-T. Membranes were incubated with antibodies for either 2 h at RT or overnight at 4°C. Membranes were washed briefly with TBS or TBS-T before protein transfer was assessed by staining with Amido Black (0.1% (w/v) naphthol blue black, 7.5% (v/v) acetic acid, 20% (v/v) ethanol) for 1 min under shaking conditions. Membranes were destained with water until clear bands were visible on white background. Protein signals were visualized with SuperSignal® West Dura Extended duration substrate (ThermoScientific) on an Amersham 600 Chemiluminscent Imager (GM).

2.1.11. TCA precipitation

Trichloroacetic acid (TCA) was used to precipitate proteins for concentration prior to SDS-PAGE for separation of proteins on the basis of size. When necessary, samples were topped up to 1 mL with nuclease free water. 100 µL 0.15% (v/v) Na-Deoxycholate and 100 µL 72% (v/v) TCA were added, and samples were incubated on ice for 20 min. Samples were pelleted by centrifugation for 20 min at 4°C, 17,000 × *g*. The supernatant was removed, and cells were washed with 1 mL ice cold acetone. Samples were centrifuged once more for 10 min at 4°C, 17,000 × *g* and the supernatant was removed. Samples were left uncovered in a fume hood for 20 min to allow for

evaporation of residual acetone. Finally, protein pellets were re-suspended in 15 µL 1 × SDS-sample buffer with 1 µL of 1.5 M Tris pH 8.8 for buffering out residual acetone.

2.2. Methods for investigating the postulated Dhh1-ribosome interaction

In order to assess whether *S.c.* Dhh1 behaves as an RBF for sensing translational stalling on non-optimally coded mRNAs, a genomic tag was inserted at the C-terminus of endogenous *DHH1*. These cell lines were then utilized to track Dhh1-ribosome association by combining sucrose density gradient separation and Western blotting. The same cell lines were also utilized for affinity purification in the attempts to purify endogenous Dhh1-ribosome complexes. Finally, recombinant *S.c.* Dhh1 was overexpressed and purified from *E.c.*, and included in binding assays with translating ribosomes, purified from *S.c.,* in order to determine the optimal conditions for recapitulating association with the ribosome.

2.2.0. Crosslinking and gradient fractionation of *S. cerevisiae* Dhh1

S.c. Dhh1 with a C-terminal His_8-$FLAG_3$ tag was purified from S288C cells Cells were grown to early log phase at 30°C, 125 rpm in 2 L YPD (2% glucose) media, to and OD_{600} of 0.8. Cycloheximide was added to a final concentration of 10 µM and cells were incubated under the same conditions for an additional 10 min. Formaldehyde was added at a final concentration of 0.25% (v/v), and cells were incubated for an additional 10 min under the same conditions. Finally, glycine was added at a final concentration of 125 mM to quench the crosslinking reaction. Cells were harvested by centrifugation and washed briefly with ice cold water, before being re-suspended in lysis buffer (20 mM HEPES-KOH pH 7.5, 100 mM KOAc, 10 mM $Mg(OAc)_2$, 1 mM DTT, 0.5 mM phenylmethylsulfonyl fluoride (PMSF), 10% glycerol, EDTA-free protease inhibitor cocktail pill (PIP), 10 µM cycloheximide). Cells were lysed using a freezer mill (SPEX 6970/EFM) and milled powder was stored at -80°C. Cells were thawed and re-suspended in lysis buffer, and "S100" lysates were prepared as followed. First, membrane fractions were removed by centrifugation at 28,714 × g for 15 min, then

cytosolic fractions were clarified by centrifugation at 92,387 × g for 20 min. "S100" were then loaded onto 10-50% sucrose gradients prepared in lysis buffer. Gradient fractionation was carried out using Gilson FC203B fraction collector and TRIAX Flow Cell software. TCA precipitation was carried out for gradient fractions and protein visualization was carried out by applied SDS-PAGE and western blotting.

2.2.1. Affinity purification of endogenous *S. cerevisiae* Dhh1

S.c. Dhh1 with a C-terminal His_8-$FLAG_3$ tag was purified from S288C cells to early log phase at 30°C, 125 rpm in 2 L YPD (2% glucose) media. Cells were harvested at an OD_{600} of 0.8 by centrifugation and washed briefly with ice cold water, before being re-suspended in lysis buffer (20 mM HEPES-KOH pH 7.5, 100 mM KOAc, 10 mM $Mg(OAc)_2$, 1 mM DTT, 0.5 mM PMSF, 10% glycerol, PIP). Cells were lysed using a freezer mill (SPEX 6970/EFM) and milled powder was stored at -80°C.

For purification, cells were re-suspended in lysis buffer and a cytosolic "S100" fraction was prepared. The "S100" was applied to 2 mL Talon metal affinity resin equilibrated with 5 column volumes (CV) of lysis buffer. Cells were washed with 10 CV lysis buffer supplemented with 10 mM imidazole, before protein was eluted with lysis buffer supplemented with 125 mM imidazole. Aliquots were taken throughout the purification for protein visualization with SDS-PAGE and Western blotting.

2.2.2. Affinity purification of recombinant Dhh1

S.c. Dhh1 was expressed with an N-terminal His tag in pPROEX HTb vector kindly provided by Prof R. Green (Baltimore), and was purified from Rosetta2(DE3) *E.c.* grown in LB media supplemented with ampicillin. Cells were inoculated at an OD_{600} of 0.05 and grown at 37°C to mid-log phase. When the cells reached an OD_{600} of 0.5, the temperature was reduced to 16°C for one hour at which point protein expression was induced by addition of IPTG at a final concentration of 0.5 mM. Cells were left to grow overnight and harvested after ~12 h of protein expression at a final OD_{600} ranging from 2-3. After centrifugation at 3,500 × *g* for 10 min, cell pellets were washed with then resuspended in lysis buffer (30 mM HEPES-NaOH pH 7.5, 500 mM NaCl, 9 mM imidazole, 5 mM β-mercaptoethanol (β-ME), 1 mM MgCl2, lysozyme, RNase, and 10%

(v/v) glycerol) and lysed using Branson Sonifier 250 in 6 × 30 second intervals with 25% output. The membrane fraction was removed by centrifugation at 34,000 × *g* for 45 min. Clarified lysates were then loaded onto TALON metal affinity resin equilibrated with 5 CV of lysis buffer. Dhh1 was eluted in elution buffer (30 mM HEPES-NaOH pH 7.5, 300 mM NaCl, 125 mM imidazole, 5 mM β-ME, 10% glycerol). The eluate was concentrated to 1 mL and applied on a Superdex 200 gelfiltration column in final buffer of (30 mM HEPES-NaOH pH 7.5, 125 mM NaCl, 1 mM DTT. 10% glycerol) yielding 0.3 mg purified Dhh1-His from 1 L culture.

2.2.3. Purification of cytoplasmic polysomes for binding assays

Isogenic *S.c.* S288C cells were grown to mid-log phase at 30°C to a final OD_{600} of 0.9, at which point cycloheximide was added at a final concentration of 10 µg/mL. Cells were harvested by centrifugation at 27,000 × *g* for 15 min and washed with lysis buffer (20 mM HEPES-KOH pH 7.5, 100 mM KOAc, 2.5 mM $Mg(OAc)_2$, 1 mM DTT, 0.5 mM PMSF, 10 µg/mL cycloheximide). Cells were lysed by vortexing with glass beads for 10 × 30 second intervals, resting on ice between vortexing steps. Lysates were clarified with two steps of centrifugation at 4°C, 21,000 × *g* for 10 min. RNA content was measured using Eppendorf BioPhotometer UV-VIS at 260 nm, and aliquoted appropriately to prevent overloading of sucrose gradients. 10-50% sucrose gradients were prepared with lysis buffer,and loaded with clarified lysates. Gradients were subjected to ultracentrifugation at 284,000 × *g* for 3 h before gradient fractionation was carried out using Gilson FC203B fraction collector and TRIAX Flow Cell software, and polysomal fractions were collected. Polysomal fractions were concentrated by pelleting through 1M sucrose cushion prepared in lysis buffer and centrifuged at 290,000 × *g* for 45 min. Final polysomal fractions were resuspended in lysis buffer and flash frozen before storing at -80°C.

2.2.4. Binding assays

Binding assays were assembled in 5 × 25 µL reactions with the final BA buffer condition (20 mM HEPES-KOH pH 7.5, 150 mM KOAc, 10 mM $Mg(OAc)_2$, 1 mM DTT, 0.5 mM PMSF, 1:1000 PIP). The five reactions were assembled as follows, (1) included

only 25 pmol Dhh1 as a control, though the sample was lost during ultracentrifugation; (2) included 25 pmol Dhh1 and 2.5 pmol purified polysomes; (3) included 25 pmol Dhh1, 2.5 pmol purified polysomes, and 10 mM ATP; (4) included 25 pmol Dhh1, 2.5 pmol purified polysomes, and 10 mM AMP-PNP; (5) included 25 pmol Dhh1, 2.5 pmol purified polysomes, and 10 mM AMP-PCP. Reactions were assembled and topped up to 25 µL with BA buffer before incubating on ice for 20 min. Subsequently, reactions were loaded onto a 750 mM Sucrose cushion prepared with BA buffer and subjected to ultracentrifugation for 3 h at 136,900 × *g*. Following ultracentrifugation, samples were plunge frozen in LiN_2 and tubes were cut to separate supernatant and pellet fractions. Supernatant and pellet fractions were subjected to TCA precipitation (section 2.1.11, above) for SDS-PAGE and Western blotting sample analysis.

2.3. Structural characterisation of the Lso2/CCDC124-80S hibernation complex

Visualisation of the novel Lso2/CCDC124-ribosome hibernation complex utilised standard methodologies for the preparation of ribosomal samples for cryo-EM. Specifically, recombinant S.c. Lso2 was purified and mixed with purified ribosomal subunits for complex reconstitution *in vitro*. Native hibernation complexes were also purified by applying membrane free cell lysates over sucrose density gradients for separation of ribosomal populations on the basis of size. 80S populations could then be specifically isolated by pelleting through a sucrose cushion, or, via affinity purification where affinity tagged RBFs were employed. Subsequently, cryo-EM analysis was carried out with the help of Dr. O. Berninghausen, Herr R. Buschauer, and Dr J. Cheng and molecular models could be built. Finally, upon structural resolution, structure to function relationships could be assessed by assembling an enzymatic *in vitro* assay, designed to contextualise the contribution of the hibernation complex structure in translational re-activation, during recovery from quiescence.

2.3.0. Purification of recombinant Lso2

For overexpression of recombinant Lso2, the *LSO2* gene was cloned from yeast genomic DNA into a modified pRSF-Duet1 vector downstream a SUMO coding

sequence. The resulting plasmid, coding for a SUMO-Lso2 fusion protein, was transfected into *E. c.* BL21 (DE3) and grown in LB media supplemented with ampicillin. Cells were inoculated at an OD_{600} of 0.05 and grown at 37°C to mid log phase, at which point protein expression was induced by the addition of IPTG. Cells were harvested after two h of protein expression at 37°C by centrifugation at 3,500 × *g* for 10 min. Cell pellets were resuspended in lysis buffer (50 mM Tris-HCl pH 8.0, 300 mM NaCl, 2 mM β-ME and lysed using Microfluidics M-110L microfluidizer. The membrane fraction was removed by centrifugation at 34,000 × *g* for 45 min. Clarified lysates were then loaded onto TALON metal affinity resin equilibrated with 5 CV of wash buffer (30 mM Tris-HCl pH 8.0, 300 mM NaCl, 20 mM imidazole, 2 mM β-ME). Lso2 was cleaved in batch mode by addition of de-ubiquitin protease Ulp1 over night at 4°C and eluted in wash buffer lacking imidazole. The eluate was concentrated to 1 mL and applied on a Superdex 75 gelfiltration column in 20 mM Tris-HCl pH 8.0, 150 mM NaCl, 2 mM β-ME, yielding 1.1 mg purified Lso2 from 0.5 L culture at a concentration of 3 mg/ml.

2.3.1. Purification of ribosomal subunits

Clarified cytoplasmic "S100" lysates obtained from isogenic *S.c.* S288C cells were spun through a sucrose cushion (1 M sucrose, 30 mM Tris-HCl pH 7.0, 500 mM KOAc, 25 mM $Mg(OAc)_2$, 5 mM β-ME, 0.1% Nikkol, 10 µg/mL cycloheximide) at 290,000 × *g* for 45 min. The ribosomal pellet was resuspended in buffer (50 mM Tris-HCl pH 7.4, 500 mM KOAc, 2 mM $MgCl_2$, 2 mM DTT) and treated with puromycin (1 mM final concentration) for 15 min on ice, and 10 min at 37°C. Samples were then loaded onto 10-40% sucrose gradients (50 mM HEPES-KOH pH 7.4, 500 mM KOAc, 5 mM $MgCl_2$, 0.1 mM EGTA, 2 mM DTT) and centrifuged for 3 h at 284,000 × *g*. Gradient fractionation was carried out using Gilson FC203B fraction collector and TRIAX Flow Cell software,, and 40/60S subunit fractions were pooled and concentrated to 0.5 mL in grid buffer (20 mM HEPES-KOH pH 7.4, 100 mM KOAc, 2.5 mM $Mg(OAc)_2$, 250 mM sucrose, 2 mM DTT).

2.3.2. Reconstitution of the Lso2-80S hibernation complex

Purified ribosomal subunits were mixed at a 1:1 molar ratio and incubated under re-association conditions in grid buffer containing 10 mM $Mg(OAc)_2$, 0.1% Nikkol for 10 min. Afterwards a ten-fold molar excess of purified Lso2 was added 10 min prior to blotting.

2.3.3. Native Lso2-80S complexes from *S. cerevisiae*

Lso2-containing ribosomes were identified by cryo-EM in several samples, where ribosomal complexes were purified from yeast cells grown in minimal media and overexpressing different target proteins on plasmids. The sample analyzed here was initially targeted at obtaining 80S-NMD complexes. As such, Upf1-containing ribosomal complexes from BY4741 yeast cells harboring the plasmids pKB510 overexpressing a nonsense-mediated mRNA decay reporter and pKB607 overexpressing a FLAG-tagged ATP-hydrolysis-deficient Upf1 mutant. Cryo-EM analysis of the elution fractions revealed a vast majority of idle 80S ribosomes lacking any density for Upf1, however, a subclass of Lso2-bound ribosomes was identified.

Cells were grown in minimal media (Yeast Nitrogen Base; -Leu-Ura dropout media and 2% glucose) at 30°C to an OD600 of about 0.75. Cells were lysed using a freezer mill (SPEX 6970/EFM) before resuspended in lysis buffer (20 mM HEPES-KOH pH 7.4, 100 mM KOAc, 10 mM MgCl2, 0.5% Triton X-100, 1:1000 protease inhibitor pill (Roche: 04-693-132-001)). For the preparation 40 g of lysed cell powder was used and a cytosolic “S100” fraction was prepared. The “S100” was added onto 300 µl of magnetic FLAG beads (Sigma-M8823) equilibrated with lysis buffer and incubated for 2 h at 4°C. After washing three times with lysis buffer lacking Triton X-100, the sample was eluted with FLAG peptide (Sigma F4799). Ribosomal eluate was spun through a 750 mM sucrose cushion prepared in elution buffer for 45 min at 290,000 × *g*. Pellets were resuspended in elution buffer and adjusted to a final concentration of ~4 A260 nm ml–1 for cryo-EM sample preparation. As mentioned above, only Lso2 could be visualized in this sample as additional ribosome binder. Similar observations were made when using the same protocol to obtain ribosomal complexes with other tagged

proteins indicating that the presence of Lso2 on vacant ribosomes is independent of the nature of the tagged bait protein.

2.3.4. Antibiotic treatment of human cells for probing 80S enrichment with CCDC124 or EBP1

HEK293-T cells (ThermoFisher Scientific, R78007) were kindly prepared by Herr Buschauer on 10 × 15 cm plates in DMEM media and harvested by washing with 1 × phosphate buffered saline (PBS) and gently scraping to remove adherent cells. Cells were harvested at moderate confluency, one day after plating to representing standard, non-stressed growth conditions. Cells were pelleted by centrifugation for 10 min at 150 × *g* and re-suspended in 1.5 mL lysis buffer (20 mM HEPES-NaOH pH 7.4, 100 mM KOAc, 10 mM $Mg(OAc)_2$, 100 mM sucrose, 1 mM DTT, 0.5 mM PMSF, 0.5 % IGEPAL/NP-40, protease inhibitor pill). Immediately, cell suspensions were divides into 5 × 300 µL aliquots. Aliquots were supplemented with either blasticidin S (20 µg/mL), cycloheximide (100 µg/mL), puromycin (2 mM), tigecycline (10 µg/mL), or no additional antibiotic, and incubated on ice for 30 min for cell lysis. Subsequently, membrane fractions were pelleted and clarified lysates were loaded onto 10-50% sucrose gradients prepared without IGEPAL. Gradients were additionally supplemented with appropriate antibiotics corresponding to the lysis conditions for each sample. Gradients were subjected to ultracentrifugation for 3 h at 284,000 × *g* before gradient fractionation was carried out using Gilson FC203B fraction collector and TRIAX Flow Cell software. Light fractions and 80S peak fractions were used for SDS-PAGE (2.1.8) and western blotting analysis (2.1.10) using specific mouse monoclonal antibodies for detection of CCDC124 and EBP1.

2.3.5. Native human hibernation complexes

Were kindly provided by Herr R. Buschauer.

2.3.6. Purification of idle 80S ribosomes bound by Stm1

80S ribosomes with Stm1 were prepared according to (Ben-Shem et al., 2011). Therefore, wild type BY4741 *S.c.* cells were grown to mid-log phase in YPD before

pelleting at 30°C and incubated in YP for a further 10 min at 30°C. Cells were pelleted and washed three times in wash buffer (30mM HEPES-KOH pH 7.4, 50 mM KCl, 2.5 mM $Mg(OAc)_2$, 0.5 mM EDTA, 2 mM DTT, PIP, 10% glycerol). After washing, cells were flash frozen in liquid nitrogen and lysed using a freezer mill (SPEX 6970/EFM), lysed cell powder was stored at -80°C. Clarified "S100" lysates resuspended in wash buffer were loaded onto 10-50% sucrose gradients in wash buffer lacking glycerol. After gradient fractionation, 80S peaks were pelleted through a 1 M sucrose cushion prepared in wash buffer, by centrifugation at 417,000 × *g* for 45 min. Finally, purified ribosomal pellets were resuspended in storage buffer (20 mM HEPES-KOH pH 7.5, 100 mM KOAc, 5 mM $Mg(OAc)_2$, 1 mM DTT). Aliquots were flash frozen and stored at -80°C.

2.3.7. Purification of puromycin treated 80S ribosomes

S.c. BY4741 cells were grown to mid log phase in YPD at 30°C, and harvested at a final OD_{600} of 2.5. Cells were pelleted and washed once with water and once with 1% KCl, before being resuspended in 100 mM Tris-HCl pH 8, 10 mM DTT and incubated at room temperature for 15 min. After a final pelleting step, cells were resuspended in lysis buffer (10 mM HEPES-KOH pH 7.5, 100 mM KOAc, 7.5 mM $Mg(OAc)_2$, 125 mM sucrose, 1 mM DTT, 0.5 mM PMSF, protease inhibitor pill), before being lysed using Microfluidics M-110L microfluidizer. Lysates were clarified and a cytosolic "S100" fraction was prepared. Ribosomal fractions were then isolated by centrifugation through a double layer 1.5 M/2 M sucrose cushion (20 mM HEPES-KOH pH 7.5, 500 mM KOAc, 5 mM $Mg(OAc)_2$, 1 mM DTT, 0.5 mM PMSF) at 246,500 × *g* for 21 h. Supernatant fractions were discarded, and ribosomal pellets were resuspended in nuclease free water. Ribosomes were mixed 1:1 with 2 × puromycin buffer (40 mM HEPES-KOH pH 7.5, 1 M KOAc, 25 mM $Mg(OAc)_2$, 2 mM puromycin, 2 mM DTT, and Amicon Anti-RNase (AM2692)) and incubated for 30 min at room temperature. Puromycin treated ribosomes were loaded onto 10-40% sucrose gradients in buffer conditions matching the previous sucrose cushion, and subjected to ultracentrifugation at 4°C, 21,000 × *g* for 20 h. 80S fractions were manually harvested from the gradients by monitoring absorption at 260 nm, and ribosomes were pelleted at 417,000 × *g* at 4°C for 45 min. Finally, puromycin treated 80S pellets were

resuspended in storage buffer (20 mM HEPES-KOH pH 7.5, 100 mM KOAc, 5 mM $Mg(OAc)_2$, 1 mM DTT). Aliquots were flash frozen and stored at -80°C.

2.3.8. Purification of splitting factors

Purified *S.c.* Dom34 was kindly provided by Frau H. Sieber. Fully prepared as described (Becker et al., 2011a; Becker et al., 2011b).

Purified *S.c.* Hbs1 was kindly provided by Frau H. Sieber as previously described (Becker et al., 2011a).

S.c. Rli1p (ABCE1) was purified from *S.c.* strain WCGα with the help of Frau H. Sieber, who provided a high copy pYES2Rli1 vector for protein overexpression. Cells were grown 30°C to mid-log phase in YP -ura, 2% galactose, 1% raffinose media and were harvested at a final OD_{600} of 1.0. Before flash freezing, cell pellets were washed with ice cold water. Cell pellets were stored at -80°C until lysis, when pellets were thawed and washed once with 1% KCl for cell wall destabilization. Cells were then resuspended in 100 mM Tris pH 8.0, 14 mM β-ME and incubating at room temperature for 15 min. Subsequently, cells were pelleted and resuspended in lysis buffer (75 mM HEPES-NaOH pH 8.0, 300 mM NaCl, 5 mM β-ME, 1% Tween, 20 mM imidazole, 2 mM $MgCl_2$, 10% glycerol) and lysed using Microfluidics M-110L microfluidizer. a cytosolic "S100" fraction was prepared and filtered through 0.45 µm filter before loading onto HisTrap-HP 5mL affinity column using the ÄKTA pure system. The column was washed with 8 CV wash buffer (50 mM HEPES-NaOH pH 8.0, 500 mM NaCl, 5 mM β-ME, 20 mM imidazole, 2 mM $MgCl_2$, 10% glycerol) before eluting with 8 CV over a 0-100% gradient from wash to elution buffer (wash buffer with 300 mM imidazole). Peak fractions were concentrated to 1 mL before loading onto Superdex 200 for size exclusion chromatography. Aliquots of pure ABCE1 in 20 mM Tris pH 7.5, 200 mM NaCl, 5 mM β-ME, and 5% glycerol were flash frozen and stored at -80°C.

Purified *S.c.* eIF6 was kindly provided by Frau J. Musial.

2.3.9. Splitting assays

Splitting assays were carried out in collaboration with Herr T. Mackens-Kiani. 50 µL reactions were assembled for splitting assays with the final SA buffer condition (20

mM Tris pH 7.5, 100 mM KOAc, 4 mM $Mg(OAc)_2$, 5 mM β-ME). The splitting assay was initially tested using 80S ribosomes reconstituted in a high magnesium buffer, as in the reconstitution of Lso2-80S complexes (section 2.3.2, above), and components were incubated for 5 min at RT. Later, splitting assay reactions were optimized and these reconstituted 80S control were replaced by puromycin treated, non-split, purified 80S ribosomes for a control. The puromycin treated 80S provided a more stable base line for the subsequent comparison between the splitting of structurally distinct Lso2-80S and Stm1-80S. Furthermore, final splitting reactions were instead incubated for 30 min on ice. Under these conditions, the extended incubation time compensated for the decrease in temperature, such that enzymatic activity was maintained in the reaction. For validation, splitting assay controls were carried out where individual splitting factors or nucleotides were excluded. This confirmed the functionality of each enzymatic component in the assay. Additionally, both puromycin treated 80S and Lso2-80S complexes responded in the same way to exclusion of individual components in the reaction. Final splitting reactions were carried out in triplicate and included 5 pmol purified ribosomes (either Stm1-80S, Lso2-80S, or puromycin treated 80S which served as a control), a 5 × molar excess (25 pmol) of each splitting factor in the reaction (Dom34, Hbs1, Rli1, Tif6), 1 mM ATP and 1 mM GTP. Negative controls for each reaction were assembled also assembled in triplicate with ribosomes and eIF6 only.

After 30 min incubation on ice, splitting reactions were loaded onto 10-50% sucrose SA buffer gradients and subjected to ultracentrifugation for 3 h at 284,000 × *g*. Sucrose density gradients were subjected Gradient fractionation using Gilson FC203B fraction collector and TRIAX Flow Cell software. Quantification of peaks was performed with the help of Herr T. Mackens-Kiani, by estimating the integral using the trapezoid rule (Kalambet et al., 2018). Where ($x_n \mid A_n$) is the data points recorded with x , the distance along gradient, and A is the absorption at 260 nm, the area S_{ab} under one peak from x_a to x_b was approximated as

$$S_{ab} = \sum_{n=a}^{b-1} 0.5\ (A_n + A_{n+1})\ (x_{n+1} - x_n)$$

Relative splitting efficiencies were calculated as ratios of peak areas and averaged across experiments. Errors shown in normalized results were estimated assuming linear propagation of statistical uncertainties.

2.4. The stalling mechanism of AAP

To investigate translational regulation in *cis* by the eukaryotic AAP RAP required the preparation of components for *in vitro* translation reactions. *In vitro* translation is a principle method for the synthesis and purification of RNCs. These reactions utilise mRNAs specifically designed to program translational stalling. Subsequently, RNCs can be purified for structural analysis by standard methodologies for affinity purification. This is made possible by mRNA design, wherein, N-terminal affinity tags are first translated by the ribosome, followed by a short linker region, in this case uL4A(aa2-65) to ensure the affinity tags are not protected by the ribosomal tunnel. Finally, the most C-terminal coding sequence on the mRNA contains the sequence for the RAP, such that, ribosomes will become stalled in the *in vitro* translation reaction. Ribosomal stalling can be observed by Western blotting, as the synthesis of the mRNA reporter and covalent association with P-tRNA can be detected on the basis of size at ~35 kDa. This signal is distinct from free, non-ribosomally associated peptides synethesised in the reaction, which run at a much lower molecular weight as these peptides are not covalently linked to tRNAs as is the case when stalling occurs.

2.4.0. Preparation of mRNA

For preparation of mRNA, linear DNA was first prepared via PCR reaction 13 (Table 7, Appendix 2), subjected to purification using Qiagon PCR purification kit (#28106) per user manual. Aliquots were sent for DNA sequencing and the remaining DNA was included in *in vitro* transcription reactions carried out with the T7 mMessageMachine™ kit (Invitrogen) according to the manual. Reactions were incubated for 7 h at 37°C and the RNA was precipitated in an overnight incubation at -20°C following addition of a 1:1 H20 and LiCl solution (Ambion). Precipitated RNA was first pelleted by centrifugation (20 min, 4°C, 14000 rpm), washed with 1 ml EtOH, and pelleted again (10 min, 4°C, 14000 rpm). Finally, the pellet was dried at room temperature for 20 min before being resuspended in 15 µl nuclease-free H2O + RNase-

IN. Concentrations were measured with IMPLEN NP80 NanoPhotometer , mRNA was flash frozen and stored at -80°C.

2.4.1. *In vitro* transcription of AAP mRNA

In vitro transcription reactions were carried out with the Ambion T7 mMESSAGE mMACHINE Kit according to the manual. Reactions were incubated for 7 h at 37°C and the RNA was precipitated in an overnight incubation at -20°C following addition of a 1:1 H20 and LiCl solution (Ambion). Precipitated RNA was first pelleted by centrifugation (20 min, 4°C, 14000 rpm), washed with 1 ml EtOH, and pelleted again (10 min, 4°C, 14000 rpm). Finally, the pellet was dried at room temperature for 20 min before being resuspended in 15 µl nuclease-free H2O + RNase-IN. Concentrations were measured with an IMPLEN NP80 NanoPhotometer, mRNA was flash frozen and stored at -80°C.

2.4.2. *In vitro* translation of *S. cerevisiae* AAP

Translation of *S.c.* AAP reporter mRNAs was carried out in 50 µl *in vitro* translation reactions as described (Ikeuchi et al., 2019; Waters and Blobel, 1986) using 0.5-2 µg mRNA per reaction and cell-free extracts prepared from *S.c.* Δski2 S288C cells, kindly provided by Frau H. Sieber. Reactions were incubated for 5 min at 25°C before 5 µL aliquots were removed for SDS-PAGE and Western blot analysis.

2.4.3. *In vitro* translation and purification of *N. crassa* AAP RNCs

Ribosome nascent chain complexes (RNCs) were purified by programming ribosomes in a *N.c.* cell-free translation system with uL4A-AAP-UUC-4xSTOP mRNA similarly to experiments carried out using *S.c.* and RRL systems before (Beckmann et al., 2001; Halic et al., 2004; Ikeuchi et al., 2019; Tesina et al., 2019). 300 µl *in vitro* translation reactions were assembled exactly as described (Fang et al., 2000) using 13 µg mRNA per reaction and cell-free extracts prepared from WT *N.c.* OR74A cells, kindly provided by Prof. M. Sachs and incubated for 5 min at 25°C. Reactions were immediately diluted to 2 ml with ice cold AAP wash buffer (50 mM HEPES-KOH pH 7.5, 100 mM KOAc, 25 mM Mg(OAc)2, 5 mM Arg, 0.1% nikkol, 2 mM b-ME) and

transferred to 400 µl of Dynabeads-His coupled magnetic bead affinity resin slurry, pre equilibrated with 250/tRNA buffer (250 buffer with 10 µg/ml tRNA). Translation reactions were incubated with magnetic beads for incubated on a rotating wheel for 15 min at 4°C. Subsequently, the flow through was collected and beads were washed with 6 mL wash buffer. RNCs were eluted following incubation for 5 min with 400 µl wash buffer supplemented with imidazole at a final concentration of 300 mM.

The eluate was next loaded onto 10-40% sucrose gradient prepared in AAP wash buffer and subjected to ultracentrifugation at 284,000 × *g* for 3 h. Gradient fractionation was carried out using Gilson FC203B fraction collector and TRIAX Flow Cell software, and fractions were collected for the 80S, disome, and trisome RNCs. Ribosomal populations were concentrated by pelleting through a sucrose cushion (1 M sucrose prepared in AAP wash buffer) at 290,000 × *g* for 45 min. Finally, the RNCs were resuspended in grid buffer (20 mM HEPES-KOH pH 7.2, 50 mM KOAc, 5 mM $MgCl_2$, 1 mM DTT, 0.05% Nikkol, PIP, 0.01 U/µl RNAsin). concentrations were measured with UV-Vis photometer (1:70 dilution; 1 A_{260} = 20 pmol 80S ribosomes). RNCs were immediately frozen on Quantifoil R3/3 grids for cryo-EM. Aliquots taken throughout the purification were subjected to western blot analysis for detection of HA conjugated peptidyl-tRNA signal at ~35 kDa.

2.5. Cryo-EM and molecular models

2.5.0. Cryo-EM Data Collection

For samples from *S.c.* and *N. c.,* ~ 2.5 - 6 $A_{260\ nm}$ ml^{-1} of ribosomes were applied to 2 nm precoated Quantifoil R3/3 holey carbon support grids. Data was kindly collected by Dr O. Berninghausen who employed either a Titan Krios TEM (Thermo Fisher) equipped with a Falcon II direct detector or with Falcon III detector, at 300 keV under low-dose conditions using approximately 28 electrons per $Å^2$ for ten frames in total. The defocus range was between −1.1 to −2.3 µm for samples collected with Falcon II detector, or -0.8 to -3.2 um using Falcon III detector. Data was collected under semi-automated data acquisition mode using the software EM-TOOLS (TVIPS). Magnification settings resulted in a pixel size of 1.084 Å $pixel^{-1}$ using Falcon II detector, and 1.059 Å $pixel^{-1}$ with Falcon III detector. Original image stacks were

summed and corrected for drift and beam-induced motion at the micrograph level using MotionCorr2 (Zheng et al., 2017). CTF estimation and the resolution range of each micrograph was performed with Gctf (Zhang, 2016).

2.5.1. Structure of the *in vitro* reconstituted Lso2-80S complex

After manual screening for ice quality, 10,313 micrographs were used for automated particle picking in Gautomatch (http://www.mrc-lmb.cam.ac.uk/kzhang/) yielding 1,413,783 initial particles. Upon 2D classification in RELION 3.0, 781,257 particles were selected for a consensus 3D refinement. After 3D classification, a Lso2-containing class (88,523 particles) was obtained and refined including CTF refinement to an average resolution of 3.4 Å with local resolution ranging from 3-7 Å (3.2-4.5 for Lso2). All other classes contained only 80S ribosomes with no additional factors, tRNA, or mRNA.

2.5.2. Structure of the native Lso2-80S complex

After manual screening for ice quality, 8,600 micrographs were used for automated particle picking in Gautomatch (http://www.mrc-lmb.cam.ac.uk/kzhang/) yielding 585,801 initial particles. Upon 2D classification in RELION 3.0, 486,383 particles were selected for a consensus 3D refinement. Two rounds of 3D classification and 3D refinement and resulted in reconstructions of a low resolution Lso2-80S complex from 29,735 particles. This dataset was later merged with a subsequent data set, wherein, 8,400 micrographs underwent automated particle picking in Gautomatch (http://www.mrc-lmb.cam.ac.uk/kzhang/) yielding 381,233 initial particles. After 2D classification in RELION 3.0, 163,303 particles were selected for a consensus 3D refinement. 3D classification and 3D refinement and resulted in reconstructions of a low resolution Lso2-80S complex from 24,085 particles. The resulting merged data set of 53,820 particles underwent a consensus 3D refinement before focused sorting on the intersubunit space (A and P site tRNA positions) resulting in one tRNA containing class of 18,869 particles and one Lso2 containing class of 34,951 particles. The Lso2 containing class underwent one final round of 3D refinement and CTF

refinement resulting in an Lso2-80S complex reconstruction at 3.5 Å. Discarded classes contained 80S ribosomes with no additional factors, tRNA, or mRNA.

2.5.3. Molecular models of hibernating ribosomes

Molecular models were kindly built by Dr. J. Cheng or Herr R. Buschauer.

Results

3.1 Investigating the role of Dhh1 as a sensor for translational stalling on non-optimally coded mRNAs

In 2016, the ~60 kDa helicase Dhh1 was thought to be responsible for specifically sensing translational stalling on non-optimal codon stretches, which has been associated with decreased mRNA half-life (Hanson and Coller, 2018; Miller et al., 2018; Presnyak et al., 2015; Radhakrishnan et al., 2016). Therefore, to visualize the proposed interaction between Dhh1 and eukaryotic 80S ribosomes, endogenous Dhh1 was tagged at the C-terminus generating an *S.c.* 288C *DHH1*-His_6-$FLAG_3$ cell line. Cells were grown to early log phase in YPD (2% glucose), lysed with standard methodologies and membrane fractions were removed, before cytoplasmic fractions were loaded on TALON metal affinity resin for affinity purification of Dhh1 via the His tag. In these native pullouts however, Dhh1 did not appear to co-precipitate with ribosomal proteins (Fig 10A). Therefore, lysates were treated briefly with chemical crosslinker before loading over 10-50% sucrose gradients. Dhh1 was detected by western blotting for the α-His across the length of the gradient, seemingly enriched in the high molecular weight fractions in agreement with its documented role in P-body formation (Figure 10B) (Mugler et al., 2016). This indicated the proposed interaction between Dhh1 and the ribosome may be transient, low affinity, or low incidence under standard growth conditions. Therefore, to assess whether the putative interaction could be recapitulated *in vitro* under optimized conditions, binding assays were assembled where Dhh1 was supplemented at a 10-fold molar excess to ribosomes. Assays were additionally supplemented with ATP or non-hydrolysable analog to test whether the ATPase activity of Dhh1 would be required for ribosome binding. To that end, recombinant *S.c.* Dhh1 with a C-terminal His_6 tag was overexpressed and purified from *E.c.* Rosetta (DE3) cells (Figure 10C), yielding 0.3 mg from 1 L cell culture, and subjected to binding assays with a high concentration of purified *S.c.* polysomes (Figure 10D). Unfortunately, binding was not observed in any of the tested conditions.

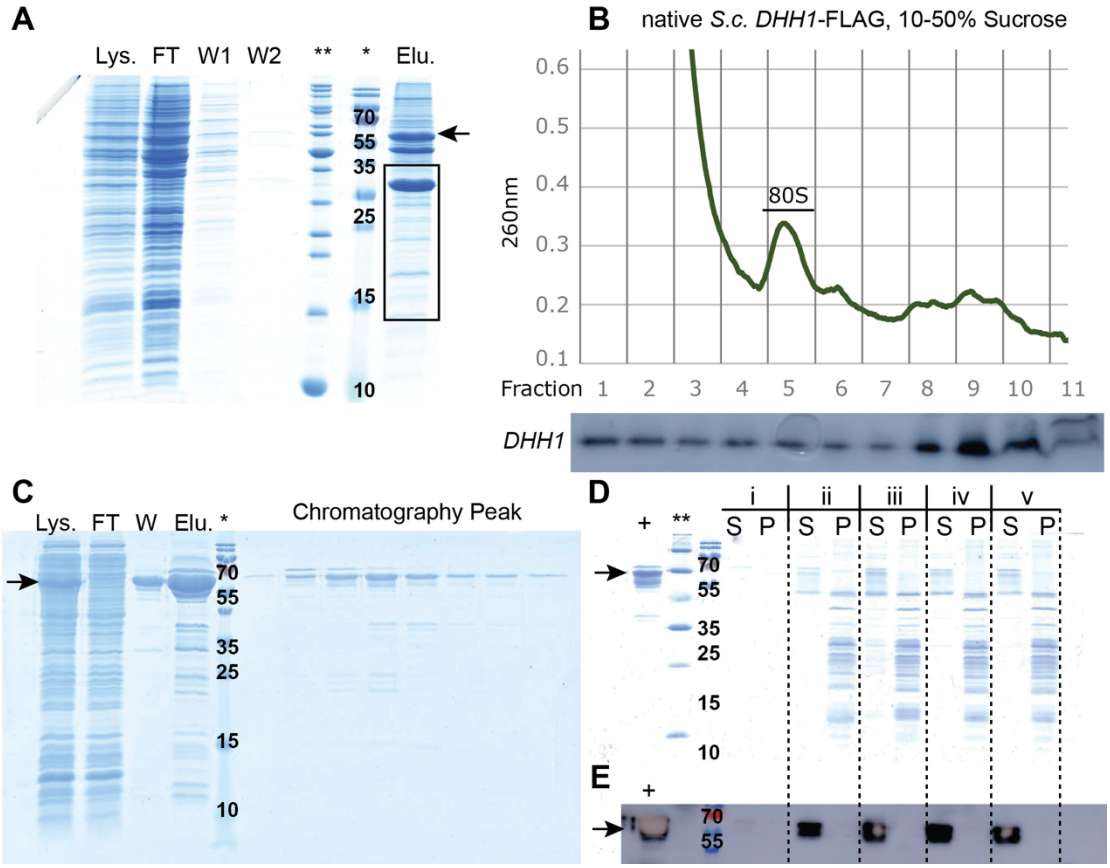

Figure 10: Biochemical analysis of the proposed Dhh1-ribosome interaction

Dhh1 migrates on SDS-PAGE to approx. 60 kDa and is annotated throughout with a black arrow. (A) SDS-PAGE for the purification of endogenous *DHH1* tagged at the C-terminus with His_6-$FLAG_3$ in *S.c.* 288C haploid cells. Membrane free cell lysates (Lys) were loaded onto Talon Metal affinity resin and the flow through (FT) was collected. Beads were washed twice (W1, W2), before eluting (Elu.) with 100 mM imidazole. Dhh1 did not appear to co-purify with ribosomes as indicated by a black box, highlighting the molecular weight range where ribosomal proteins should be detected. (B) 10-50% Sucrose gradient profile from cell lysates of *S.c.*288C *DHH1*-His_6-$FLAG_3$ cells, which were treated briefly with formaldehyde crosslinker. Below, the corresponding western blot for gradient fractions, where Dhh1-His_6-$FLAG_3$ was visualized using an anti-FLAG antibody. (C) SDS-PAGE for the purification of recombinant Dhh1-$His_6$from *E.c.* Rosetta (DE3) cells. Membrane free cell lysates (Lys) were loaded onto Talon Metal affinity resin and the flow through (FT) was collected. Beads were washed (W), and eluted (Elu.) with 125 mM imidazole, before loading onto a Superdex 200 column for size exclusion chromatography. 0.3 mg of rDhh1 was ultimately purified from 1 L cell culture and used for subsequent binding assays. (D) SDS-PAGE for binding assays between purified Dhh1 with C-terminal His tag, and purified polysomes in the presence and absence of nucleotide analogues. Binding was not observed in any of the tested conditions, (i- broken UC tube on Dhh1 only control; ii- Dhh1 and polysomes; iii- Dhh1, polysomes, and ATP; iv- Dhh1, polysomes, and AMP-PNP; v- Dhh1, polysomes, and AMP-PCP) confirmed by western blotting (E) where chemiluminescent signal for visualization of Dhh1-His using α-His-HRP antibody is found in soluble supernatant (S) but not pellet (P) fractions, where ribosomes migrate. (**-unstained molecular weight marker, *- pre-stained molecular weight marker, +- positive loading control)

At the same time, new evidence emerged implicating components of the CCR4-Not complex in the sensing of translational stalling on non-optimally coded mRNAs (Buschauer et al., 2020; Hanson and Coller, 2018; Miller et al., 2018). Importantly, the CCR4-Not complex serves as primary eukaryotic deadenlylase, which precedes decapping, during canonical mRNA decay. Dhh1 is also known to participate in canonical mRNA decay, where it acts as a scaffold, bridging the decapping complex with CCR4-Not, via interaction with the MIF4G domain of Not4, on circularized mRNA. Discovery of the Not5 domain in the E-site implies the hypothesized role of Dhh1 as a sensor for recognition of non-opt codons is actually being carried out by CCR4-Not. What's more, developments in the field of mRNA decay reveal additional roles for CCR4-Not in translational quality control, where the E3 ligase activity of Not4 provides a means by which ubiquitination could serve to broadly signal a translational defect, and call for recruitment of the quality control, mRNA degredation, and ribosome recycling machinery (Brandman and Hegde, 2016; Ikeuchi et al., 2018; Ikeuchi et al., 2019; Juszkiewicz et al., 2018; Matsuo et al., 2017; Shao and Hegde, 2016), In light of these findings, it became clear that that the hypothesized role for Dhh1 in the recognition of codon-dependent polysomal stalling was incorrect. While Dhh1 serves to stabilize circularized mRNAs during mRNA decay, its role in the broader context of translation is limited to that of a metabolic scaffold, rather than serving a specific regulatory function for non-optimally coded mRNAs. In this sense, the investigation was able to reveal that Dhh1 is not an RBF, as previously thought.

3.2 Identification of a novel eukaryotic ribosome hibernation complex

Canonical translation proceeds cyclically, beginning and ending with the ribosomes split into subunits. As such, accumulation of a translationally inactive monosome population during nutrient deprivation raises a number of questions about what this means for translational reactivation. Therefore, the identification of *S.c.* Lso2 and the orthologous *H.s.* protein CCDC124 as RBFs presented an exciting opportunity to structurally characterise this novel, eukaryotic hibernation complex (Wang et al., 2018).

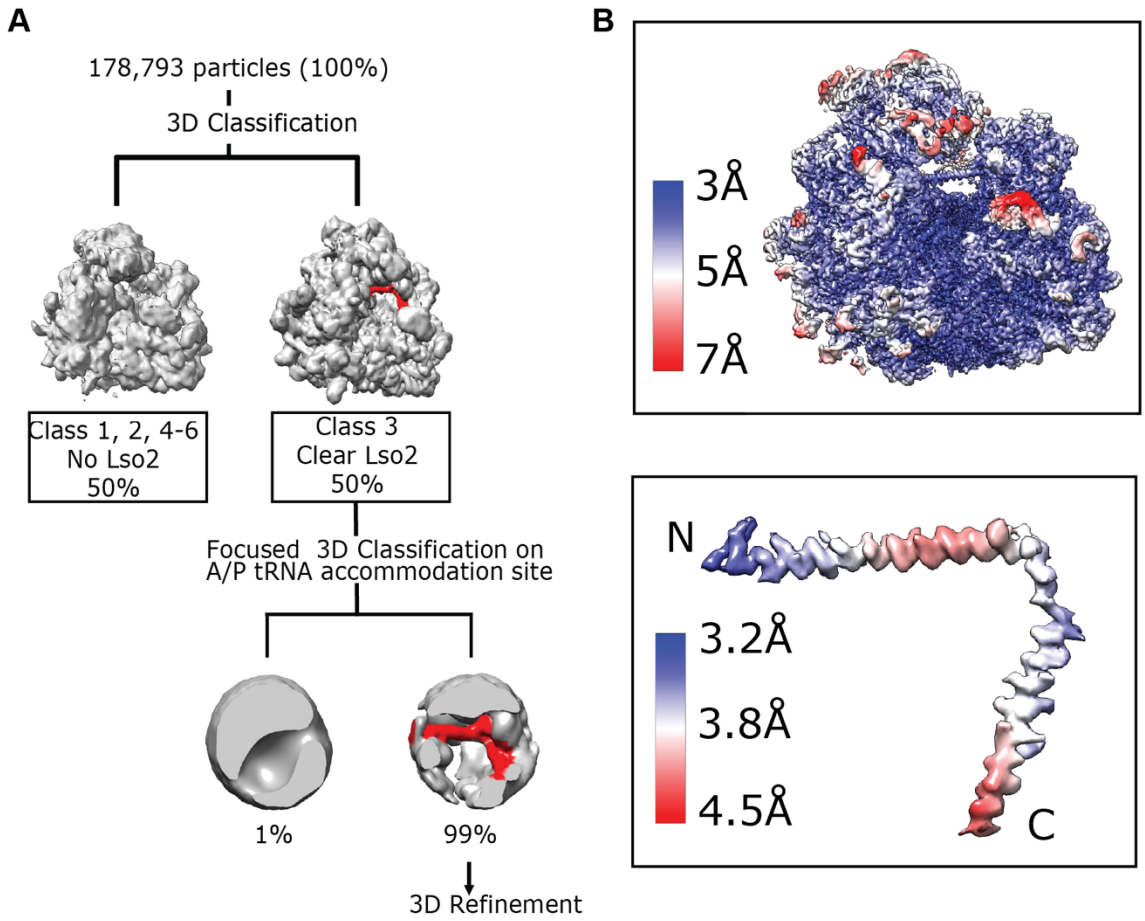

Figure 11: CryoEM analysis of the reconstituted Lso2-80S hibernation complex

A) The sorting scheme used for classification, resulting in the final 3.4 Å Lso2-80S map: after 2D classification of particles picked using Gautomatch, 178,793 particles were included in an initial 3D refinement. The initial model was sorted without masking into 6 classes. Lso2 was identified in the intersubunit space of ribosomes in one class, which contained 50% of the total particles. Subsequently, focused sorting with a mask on the Lso2 helices was used to remove any additional non-Lso2 bound particles from the subset which accounted for 1%. B) The final Lso2-containing subset was refined to a final average resolution of 3.4 Å. The average local resolution for Lso2 (3.8 Å) was sufficient for building a molecular model.

Lso2 bound 80S complexes were reconstituted *in vitro* and visualized using single particle cryo-electron microscopy (cryo-EM). First, small and large ribosomal subunits were purified from *S.c.* under high salt, low magnesium conditions. Then, Lso2 was recombinantly expressed and purified from *E.c.* BL21 (DE3) cells yielding 1.1 mg from 0.5 L cell culture. Purified subunits were then mixed at a 1:1 molar ratio under defined magnesium conditions and incubated with a 10 × molar excess of *S.c.* wtLso2 for 10 min, before freezing grids for single particle analysis (Materials and Methods). Data was collected on a Titan Krios and processed using Relion 3.0. Lso2 bound 80S ribosomes were identified in the output of 3D classification at 50% occupancy, by two

clear helices bridging the intersubunit space, without mRNA, tRNAs, or nascent protein being bound (Figure 11A). The reconstituted Lso2-80S hibernation complex was ultimately refined to an average resolution of 3.4 Å with a local resolution of 3.2-4.5 Å for Lso2 itself (Figure 11B, right).

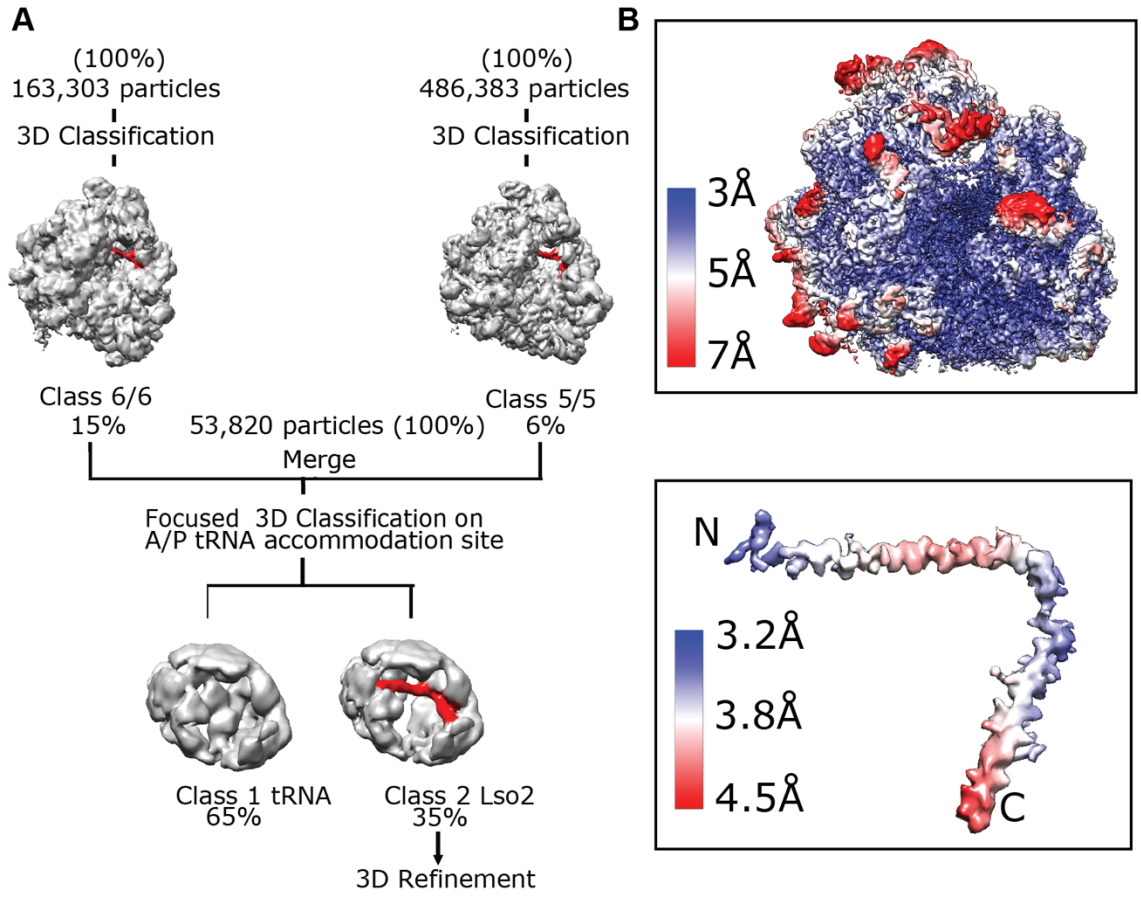

<u>Figure 12:</u> Cryo-EM analysis of the native Lso2-80S hibernation complex
A) The sorting scheme used for classification, resulting in the final 3.5 Å native Lso2-80S map. Lso2 was identified in the intersubunit space of ribosomes from two datasets, one at 15% occupancy, one at 6% occupancy. Lso2 containing classes were merged, and the 52,820 particles were subjected to focused sorting using a mask on the intersubunit space for removal of non-Lso2 bound particles (65%). The final Lso2-containing particles were selected for 3D refinement yielding a final 3.5 Å map of the native Lso2-80S complex. B) The final Lso2-containing subset was refined to a final average resolution of 3.5 Å. The average local resolution for Lso2 was in good agreement with the structures obtained from *in vitro* reconstitution of the hibernation complex.

In addition to the reconstituted Lso2-80S complex, native Lso2 bound to ribosomes could also be observed. These complexes were found in native pullouts of tagged mRNA decay factors overexpressed in yeast growing in minimal medium (see Materials and Methods for details). Translationally inactive Lso2-80S complexes were

first identified at low occupancy (6%) in the output of a 3D classification from a cryo-EM dataset prepared from 80S ribosomes, purified via a tagged mutant of the NMD factor Upf1 (Figure 12A). The ATP-hydrolysis deficient Upf1 mutant was overexpressed in an upf1Δ background in an attempt to stabilize short lived NMD intermediates for structural resolution. Though Upf1-bound NMD RNCs could not be resolved, the native Lso2-80S hibernation complex was readily identified within this dataset. Subsequently, the same hibernation complex was found in a similar cryo-EM dataset, this time at 15% occupancy (Figure 12A). Once again, the sample was purified from the 80S fractions of *S.c* exhibiting defective growth, this time harboring mutant pYKR023W, which was used to purify cytoplasmic ribosomes in an investigation seeking to stabilize and visualize the RQT complex (Hashimoto et al., 2020). Particles containing the intersubunit density were extracted and merged into a single dataset which was ultimately refined to yield a high resolution (3.5 Å) map (Figure 12B). Agreement between the native *S.c.* Lso2-80S structure and the reconstituted Lso2-80S structure was taken as validation that the reconstituted structures adequately represent those appearing *in vivo*. Though the absence tRNA and mRNA is a rather atypical observation for 80S ribosomes obtained from native pullouts, this is consistent with the role of Lso2 as a hibernation factor. The near atomic local resolution for the reconstituted structure was adequate for building a molecular model, carried out by Dr. J. Cheng (Figure 13A). Standard model to map validation was carried out for both the 3.4 Å reconstituted Lso2-80S map (Figure 13B) and the final 3.5 Å native Lso2-80s map (Figure 13C).

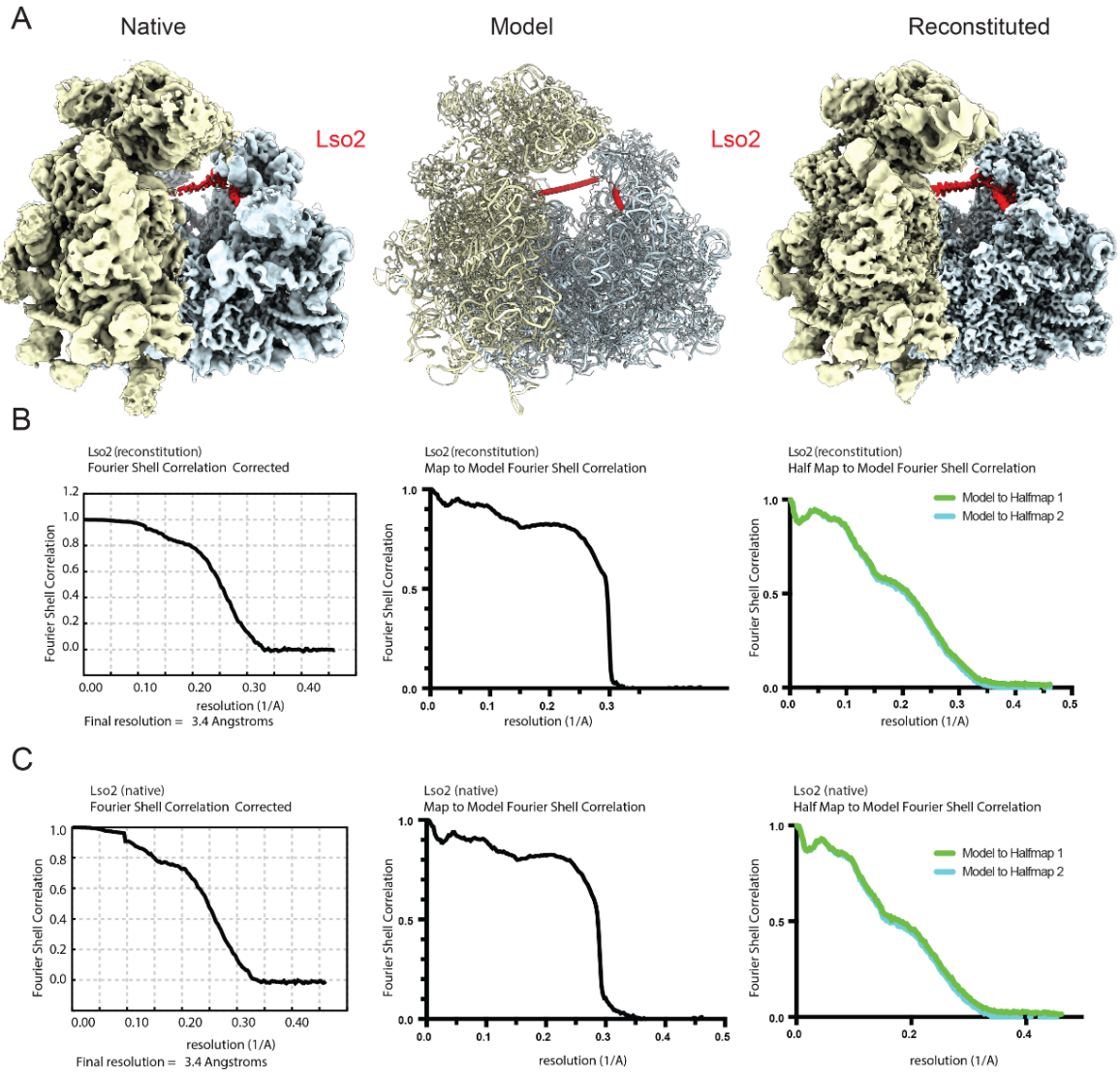

<u>Figure 13</u>: Final Lso2-80S maps, molecular model, and map to model statistics
(A) Final Lso2-80S maps and model (left) reconstituted Lso2-80S map displayed at contour level 0.03 σ (centre) Final molecular model built by Dr J. Cheng, (right) native Lso2-80S map displayed at contour level 0.03 σ (B-C) FSC curves, map to model FSC curves, and half map to model FSC curves for validation of the Lso2-80S model fitting the reconstituted (B) and native (C) Lso2-80S reconstructions, to ensure models were not overfitted (Brown et al., 2015)

3.3 Molecular interactions between Lso2 and the ribosome

Lso2 can be observed interacting with the SSU (Fig 14A, top), with its positively charged N-terminus making numerous contacts with the 18S rRNA of the 40S, which normally participates in decoding and translocation (Figure 14A, bottom).

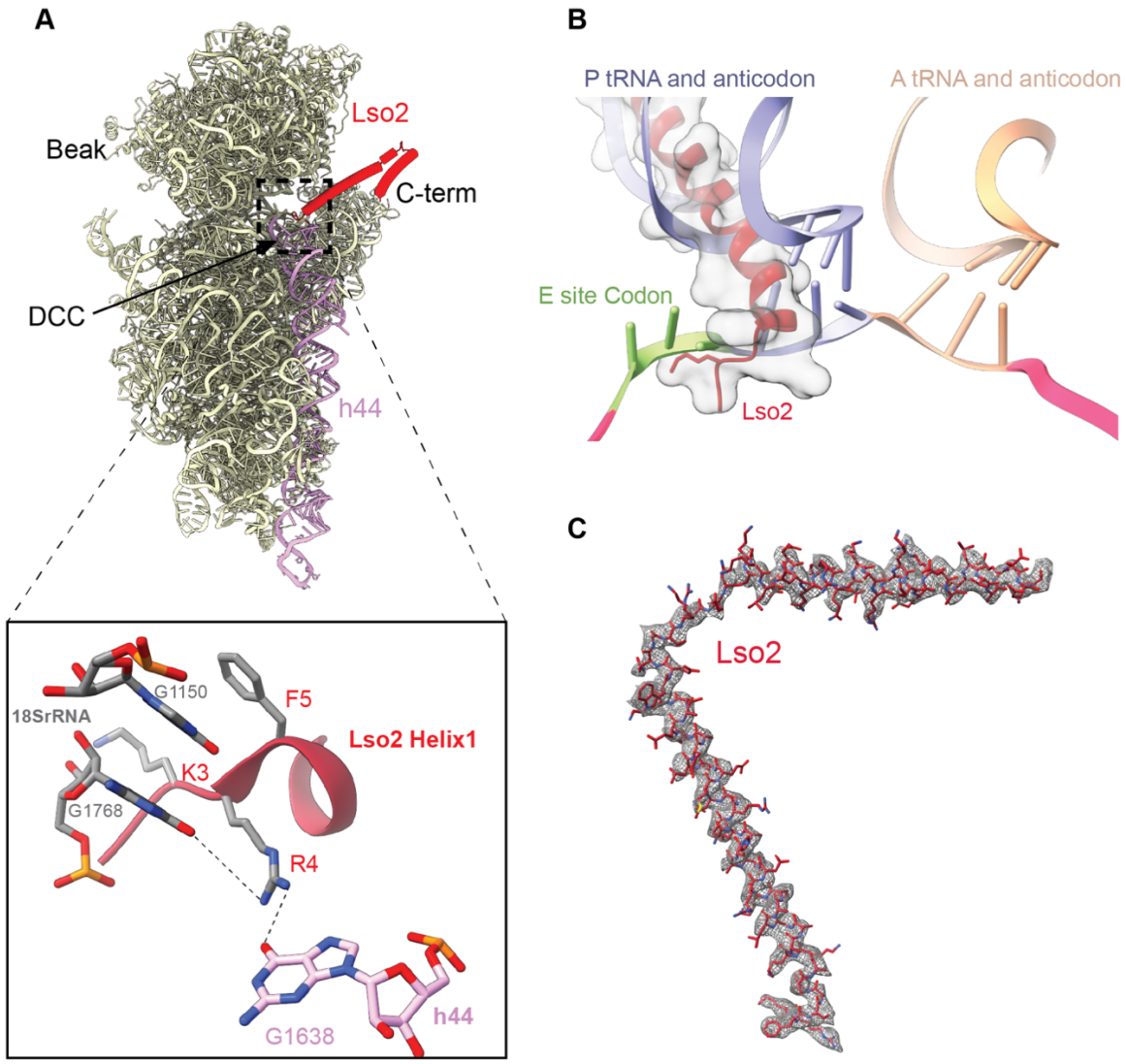

Figure 14: Lso2 interacts with the small ribosomal subunit
(A) The N-terminus of Lso2 reaches down into the ribosome decoding centre on the small subunit, coordinated by interactions with bases of the 18S rRNA and h44. (B) In this location, the very terminus of Lso2 clashes with the position normally occupied by mRNA in the P and E-site. Additionally, Helix 1 of Lso2 occupies the position in the intersubnuit space normally occupied by P-site tRNAs, which cannot be accommodated while Lso2 is bound. (C) Electron density maps, shown as a grey mesh, provide adequate high-resolution molecular detail to allow confident assignment of Lso2 side chain orientation, specifically in regions stabilized by interaction with the ribosome.

More specifically, the unstructured terminal residues G2 to S6 are wedged between a cleft normally occupied by P and E-site mRNA (Figure 14B). On the 18S, helices h24, h28, and h44 (Figure 14A) directly participate in coordinating N-terminal residues of Lso2, with K3 extending towards the E-site, only 2 Å distal to the location occupied by the phosphate between the first two residues of an E-site codon. The peptide bond between residues R4 and F5 of Lso2 is positioned 2.6 Å from the carbonyl oxygen of

G1150 of h28, which stacks with the benzene ring of F5 and G1768 of h44 while the positively charged guanidinium group of R4 is coordinated between the carbonyl oxygens from G1768 of h45 (4.8 Å) and G1638 of h44 (2.9 Å) (Figure 14A). The described interactions are likely supported by a number of salt bridges and hydrogen bonds, due to the local negative charge from the rRNA and the high incidence of positively charged residues in this region of Lso2 (K3, R4, K11, K12) At the very terminus of helix 1, which extends away from the DCC into the intersubunit space, residues S6-A15 pass directly through the position of codon-anticodon base pairing between P/P tRNA and bases 2 and 3 of P codon (Figure 14B). The final local resolution for Lso2 was within the range for side-chain resolution (Figure 14C), providing confidence in the molecular models, and thus analysis of the molecular interaction with the ribosome. In conclusion, the location occupied by the N-terminus of Lso2 in the SSU directly occupies the area from base 2 of the P-site codon to base 2 of the E-site codon.

The first Lso2 helix extends away from the decoding centre, spanning the intersubunit space until it reaches the large subunit below the central protuberance (Figure 14B 15A). The helix ends with a hinge region, positioned below the central protuberance, where it contacts the ribosome at an interface formed between uL5 and eL42 (Figure 15A). Residue W42 of Lso2 is accommodated in a pocket formed between R55 and R60 of uL5, and F106 of eL42 (Figure 15A, inset). Further interactions between Lso2 residues E38, G45 and R47 with uL5 Y52 (Figure 15B) and R55 as well as between Lso2 N50, K52 and K53 and the phosphate backbone of 25S rRNA helices H84 and H85 are well resolved. The hinge connecting the two Lso2 helices includes an 85.5° kink, such that the second helix of Lso2 continues almost perpendicular to helix 1, crossing from the P to the A-site on the large subunit along the so called “A-site finger” (Komoda et al., 2006), which follows the major groove of H38A (Figure 15C). Helix 2 ends local to uL16, ~22 Å from the stalk base of the ribosomal P stalk and ~40 Å away from the GAC (Figure 15A). As mentioned above, the position occupied by the Lso2 C-terminal helix 2 clashes with the location of the T loop for AAs in the A- and P-site, and it’s blocking the contact sites with rRNA helix 89 and uL16. Importantly, both the A-site finger and uL16 are contact sites for the elbow region of A-site tRNA during accommodation and translocation (Frank et al., 2007; Petrov et al., 2008; Whitford et al., 2010). Lso2 binding therefore blocks translation factors from accessing these critical contact sites.

RNA crosslinking (ePAR-CLIP) data suggested direct interaction of Lso2 with H43/H44 of the GAC (Wang et al., 2018). This interaction is most likely established by the ultimate C-terminus of Lso2, which is not resolved most likely as a repercussion of flexibility in this region (Figure 14C).

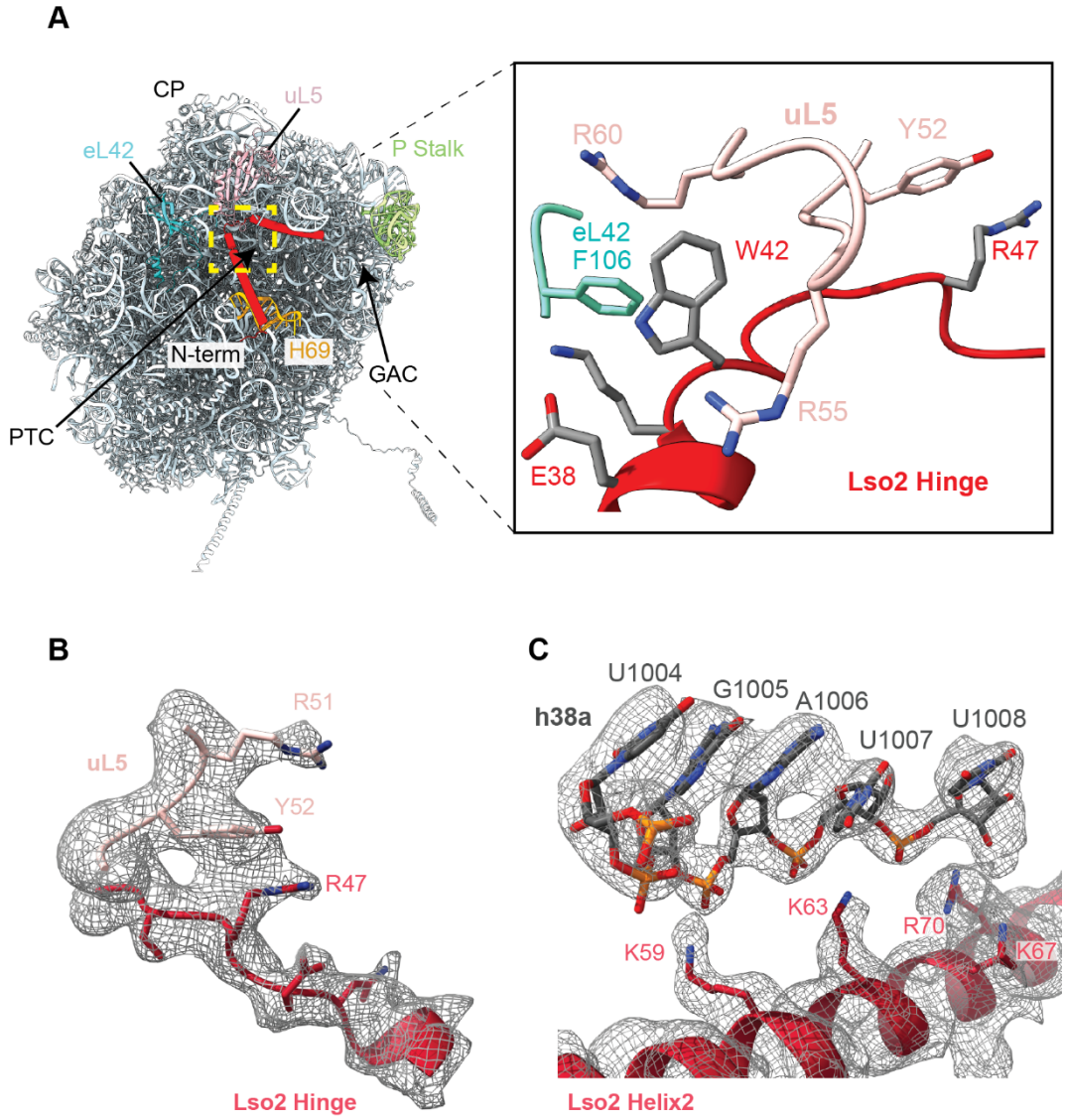

Figure 15: Lso2 interacts with the large ribosomal subunit
(A) Helix 1 of Lso2 extends away from the small subunit, passing through the intersubunit space towards the large subunit. Helix 1 ends with a hinge region positioned below the central protuberance (CP), and is coordinated by ribosomal proteins eL42 and uL5, which form a binding pocket and coordinate stable Lso2 binding via residue W42 of Lso2 (inset). Electron density maps shown as a grey mesh, provide adequate high resolution molecular detail to allow confident assignment of Lso2 residues interacting with the ribosome, such as (B), the stacking between R47 of Lso2 with R51 of uL5 and (C) coordination of helix2 by H38a of the 25S rRNA.

3.4 Visualisation of the orthologous human hibernation complex reveals 80S are bound by CCDC124 and an additional factor, EBP1

Having resolved the structure of the yeast Lso2-80S hibernation complex, the next step was to assess how these structures compare with the human Lso2 homologue, CCDC124 (Wang et al., 2018). Adherent HEK293T-Rex cells were grown to high density, mimicking starvation conditions, before purification and preparation of 80S fractions for cryo-EM. Samples were subjected to mass spectrometry, which confirmed the presence of CCDC124 as well as SERBP1, the human homologue of the other known yeast hibernation factor Stm1. Cryo-EM analysis from the hibernating human 80S sample was carried out by Herr R. Buschauer. Initial 3D reconstitutions underwent several rounds of classification which were refined by factor occupancy. The majority class was refined, yielding a final 3.1 Å map which accounted for 54% of the dataset, and contained CCDC124, an E-site tRNA, and EBP1 a homolog of ribosome biogenesis and nuclear export factor Arx1 at the peptide exit tunnel (Figure 16) (Barrio-Garcia et al., 2016; Bradatsch et al., 2012; Greber et al., 2016).

The sample also contained a class containing the other known eukaryotic hibernation complex at 48% occupancy; rotated 80S containing eEF2, and the homologue of yeast hibernation factor Stm1, SERBP1. This structure is consistent with other metazoan hibernation complexes from *H.s.* and *D.m.* (Anger et al., 2013; Brown et al., 2018).

The occupancy of the E-site tRNA in the *H.s.* CCDC124-80S complex but not the homologues *S.c.* Lso2-80S complex structure is likely attributable to the higher stability of E-site tRNA in metazoan species compared to yeast, owing to the expanded structure and expansion segments found in the ribosomes of higher metazoan species. The incidence of stably associated E-site tRNA in the *H.s.* structure could therefore explain crosslinking data from W. Gilbert which identified low incidence of Lso2-tRNA crosslinks.

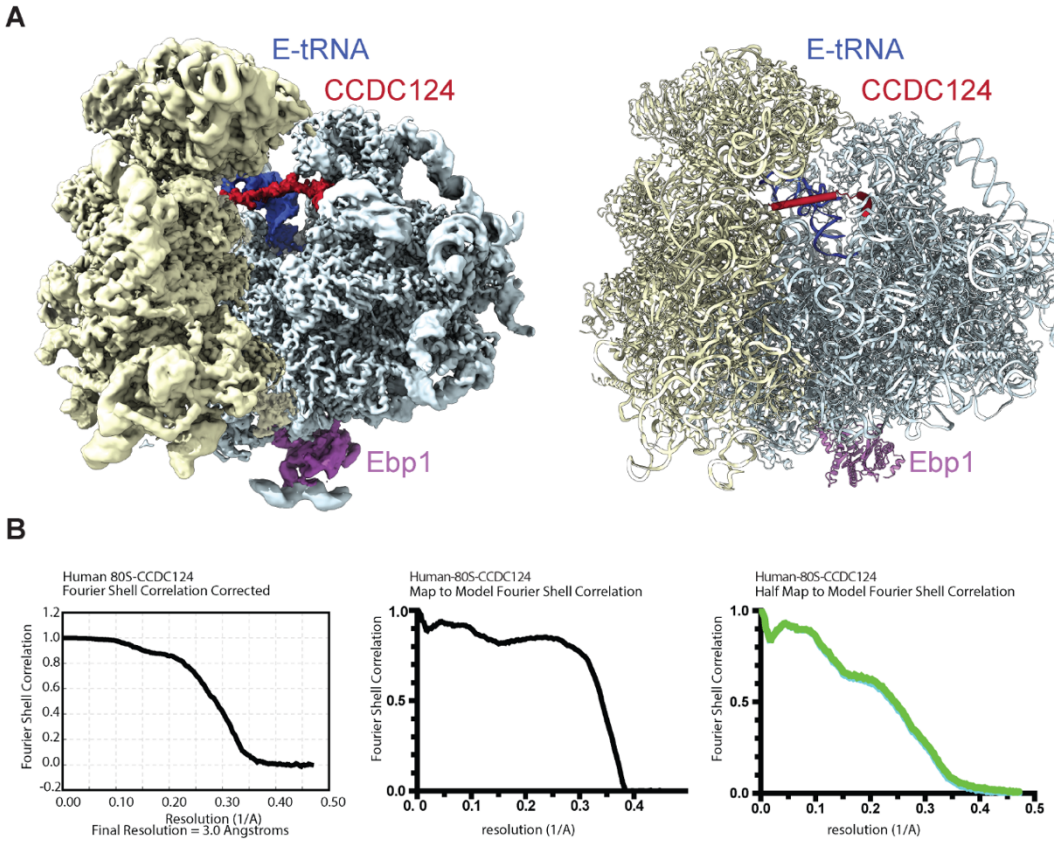

<u>Figure 16:</u> Final map, molecular model, and map to model statistics for the human hibernation complex
(A) (Left) The final molecular map for the human hibernation complex containing CCDC124 (red), E-site tRNA (blue), and EBP1 (purple) is displayed at a contour level of 0.03 σ (Right) The final molecular model, corresponding to the human hibernation complex. (B) FSC curves, map to model FSC curves, and half map to model FSC curves for validation of the CCDC124-EBO1-80S model fitting the final 3.1 Å map to ensure models were not overfitted (Brown et al., 2015).

3.5 The ribosome binding mechanism for Lso2 and CCDC124 is highly conserved

As indicated by the sequence alignment (Figure 17A), most of the key residues mediating the association with 80S ribosome are highly conserved, specifically, F5 and W39, or in *S.c.* W42. Upon superimposition of the *S.c.* and *H.s.* molecular models, based on the 28S rRNA of the CCDC124-ribosome and the 25S rRNA of the Lso2-ribosome, it is clear the factors adopt the same conformation and both protein helices align very well with each other (Figure 17B). Due to the high flexibility of the 40S head domain, the very N-terminus of CCDC124 could not be confidently modelled.

However, it is clear that in both cases, the factors extend towards the decoding centre and prevent the mRNA binding. In both cases, the second helix spans the 60S underneath the central protuberance to the P stalk, excluding both A- and P-tRNA binding.

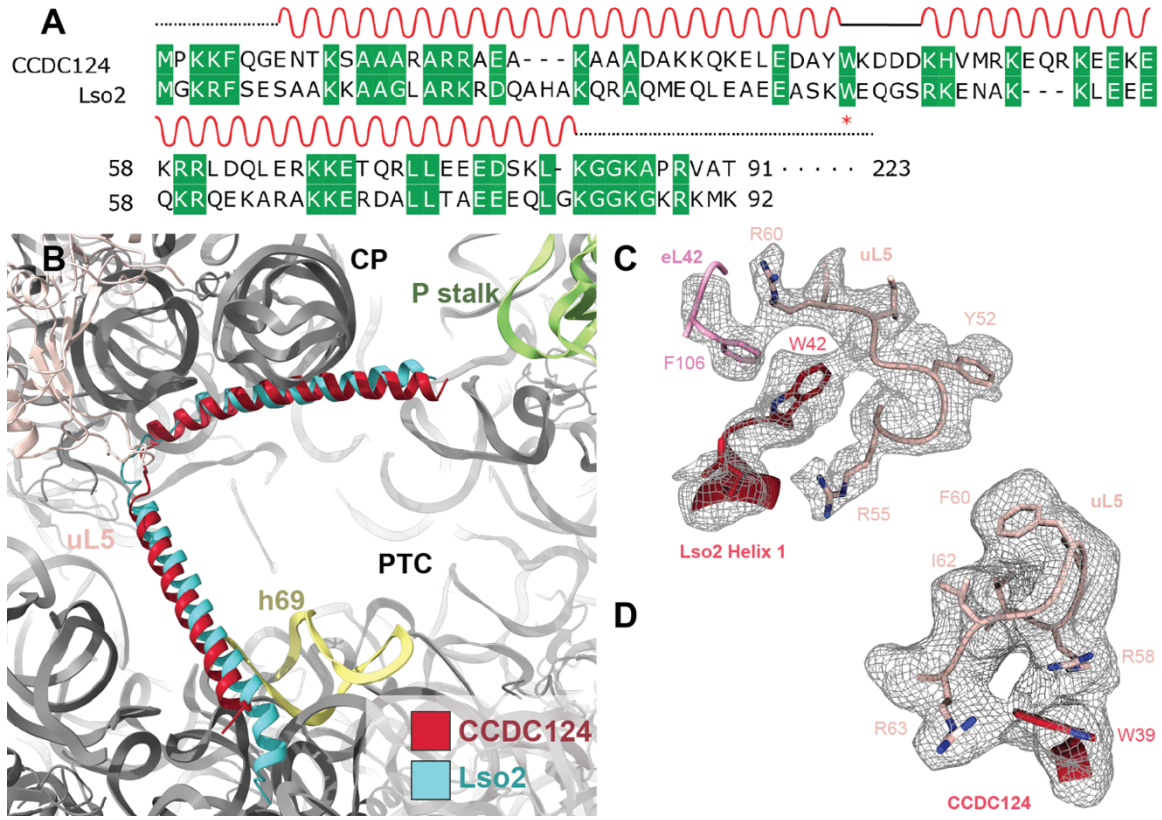

<u>Figure 17:</u> Lso2 and CCDC124 exhibit highly conserved ribosome binding interactions
(A) Domain organisation and protein alignment for Lso2 and CCDC124 shows a high degree of conservation between the two proteins. Specifically, key residues which facilitate ribosome interaction such as F5 and W39 are highly conserved (B) By overlaying the molecular structures of Lso2 and CCDC124, is it clear they occupy nearly the same position on the ribosome, with only slight differences in the path of the first helix crossing the intersubunit space. In both cases, the protein's N-terminus localises near h69 and the peptidyl-transferase centre (PTC). (C) The binding pocket for residue W42 on the hinge of Lso2 is coordinated on the large subunit by two ribosomal proteins, eL42 and uL5. (D) Similarly, the binding pocket for W39 of CCDC124 is coordinated by uL5 only, without the help of eL42.

There is a slight change in the path followed by the spacing loop between Lso2 and CCDC124, approaching helix 2. As such, there is a slight change in the binding pocket which accommodates the critically conserved W39/42 residue. While W42 of Lso2 is stabilized by both uL5 and F106 of eL42 (Figure 17C), W39 of CCDC124 is coordinated only by residues R58 and R63 of uL5 (Figure 17D). Nevertheless, Lso2/CCDC124

inactivate the ribosome in the same way, in agreement with the suggestion that this represents a highly conserved factor both in yeast and humans (Wang et al., 2018).

3.6 The Lso2/CCDC124 hibernation complex is exclusively observed on non-rotated ribosomes

In addition to the most notable feature of the Lso2 bound 80S structures, the absence mRNA and tRNA, all Lso2 bound 80S were observed in the non-rotated conformation. Non-rotated ribosomes are represented in the translocational POST state, where the A-site is not occupied and subunit rolling occurs (Budkevich et al., 2014; Loveland et al., 2017; Tesina et al., 2019). Importantly, POST state ribosomes are targeted for recycling by the Dom34, Hbs1, Rli1 recycling machinery, all of which can still be accommodated alongside Lso2 binding (Figure 18). That Lso2 binding to non-rotated ribosomes is observed in structures assembled *in vitro* and *in vivo* suggests that these structures accurately represent the endogenous *S.c.* Lso2-80S hibernation complex, where ribosomes exclusively adopt the non-rotated conformation when factor bound.

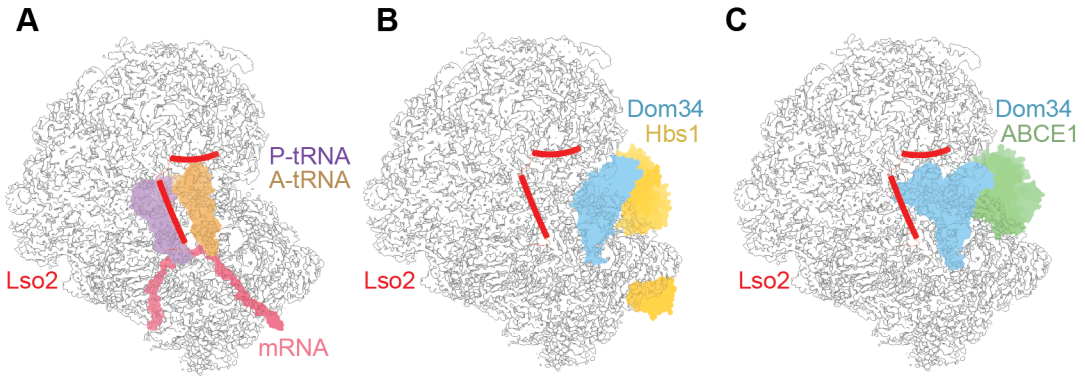

Figure 18: Lso2 binding to non-rotated ribosomes excludes translational machinery while still allowing recycling factors to be accommodated
(A) Upon overlaying the position of accommodated A- and P- site tRNAs and mRNA (PDB: 5MC6, (Schmidt et al., 2016)) with the Lso2-80S structure in the non-rotated state (displayed as cartoon), it is clear that binding of Lso2 or translational machinery to 80S ribosomes is mutually exclusive (B) The non-rotated Lso2-80S structure (displayed as cartoon) was overlaid with ribosome rescue factors Dom34 and Hbs1, PDB: 3IZQ (Becker et al., 2011) (B) or Dom34 and ABCE1, PDB: 3J16 (Becker et al., 2012) (C). In both conformations, Dom34 could accommodate within the A-site of the 40S and would not clash with Lso2, leading to the hypothesis that the Dom34 splitting system preferably splits Lso2-80S.

3.7 CCDC124 binding to the ribosome cannot be chemically enriched, and is always accompanied by binding of EBP1

Given that Human CCDC124-EBP1-80S hibernation complexes could be purified from HEK293T cells at high confluency, it was important to investigate the conditions under which these complexes could be detected. To that end, density gradient separation and western blotting confirmed the binding of CCDC124 and EBP1 to 80S fractions in cells grown under standard, non-depleted growth conditions (Figure 19A). To assess whether CCDC124 and EBP1 - 80S interactions could be promoted by specific perturbations to translationally active ribosomal regions, HEK293T cells were grown and harvested at 65% confluency before treating with a series of antibiotics, each targeting different catalytic centres on the ribosome. Lysates were left untreated or incubated with blasticidin S (20 μg/mL), cycloheximide (100 μg/mL), puromycin (2 mM), or tigecycline (10 μg/mL) and were subjected to sucrose gradient density separation. Contents of the 80S peaks were then compared with light fractions containing soluble protein, by western blotting for CCDC124 and EBP1 (Figure 19B). Interestingly, free CCDC124 unbound to ribosomes is detected at a much higher molecular weight than when associated with ribosomes. I postulate that this represents homodimerization of CCDC124 within cytoplasmic fractions. This hypothesis is currently being tested in ongoing work by the Gilbert lab.

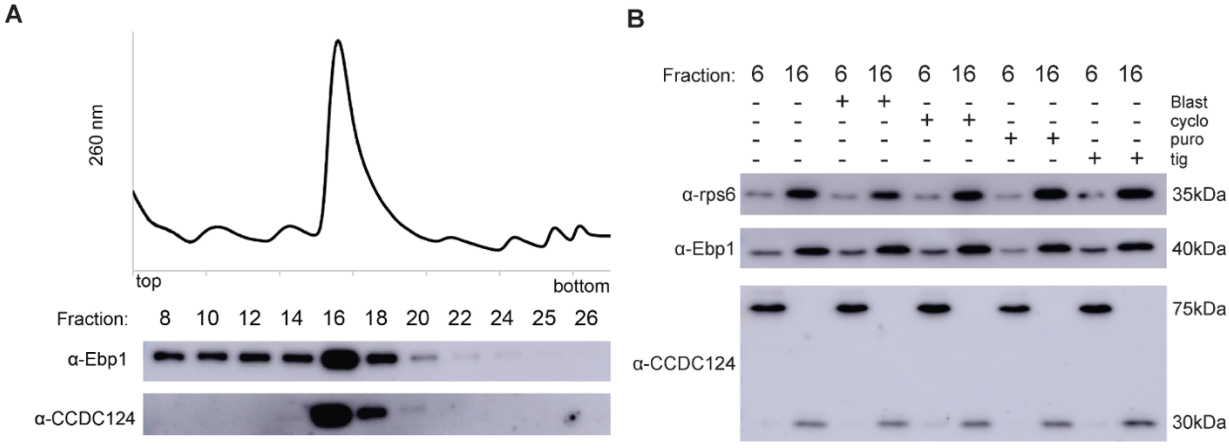

Figure 19: CCDC124 and Ebp1 interaction with human 80S ribosomes (A) Sucrose gradient profiles and western blotting detects both CCDC124 and EBP1 binding to 80S fractions in HEK 293T cells under standard growth conditions. (B) In Hek293T REx cells treated with a series of antibiotics (blasticidin S, cycloheximide, puromycin, tigecycline), ribosome binding was neither enriched or abolished for CCDC124 or EBP1, indicating these interactions were not affected by perturbations to critical catalytic centers on the ribosome.

.

For both CCDC124 and EBP1, a shift from the lighter, soluble fractions to the heavy, ribosomal fractions was not observed under any of the tested conditions. This indicates that poisoning with a single antibiotic is not enough to induce recruitment of either CCDC124 or EBP1. Taken together, these results suggest there is a stable background of 80S associated with CCDC124 and EBP1 at any given time within the cell, as postulated (Wang et al., 2018).

3.8 Implications for recycling: Lso2-bound but not Stm1-bound 80S are split by canonical recycling factors

Cryo-EM analysis of human hibernating 80S suggests that in eukaryotes, at least two clearly distinguishable populations of idle, translationally repressed 80S exist: 80S bound to Stm1 and SERBP1/eEF2, and 80S bound to Lso2(CCDC124). While both 80S cannot be bound by mRNA or tRNAs while factor bound, factor binding location and overall ribosomal conformation suggest each is recycled by a distinct mechanism. Importantly, Stm1/SERBP1-containing 80S have been almost exclusively observed in rotated states (Abeyrathne et al., 2016; Anger et al., 2013; Ben-Shem et al., 2011; Brown et al., 2018) whereas the Lso2/CCDC124-bound 80S has only been found in the non-rotated state. Therefore, Stm1 80S are most similar to PRE- state ribosomes whereas Lso2/CCDC124 80S hibernation complexes are similar to the POST-translocational state, where tRNAs occupy the P- and E-sites while the A-site remains vacant (Budkevich et al., 2014). Thereby, Lso2(CCDC124) 80S seemingly enrich the non-translating ribosome pool with non-rotated ribosomes, the conformation favourable for binding of Dom34-Hbs1 and Dom34-ABCE1 complexes (Figure 18, 20A). For deeper analysis, the molecular model for Dom34 from the Dom34-ABCE1 complex (PDB: 3IZQ) was docked into the molecular models of rotated and non-rotated ribosomes (Figure 20B). Due to the structural rearrangements of the SSU during ribosome rotation, in its normal catalytic position Dom34 would clash with h34 and h18 of 80S ribosomes in the rotated conformation (Figure 20C). This led to the hypothesis that Lso2-80S are the preferential clients for splitting by the Dom34-splitting system during translational recovery following quiescence in yeast.

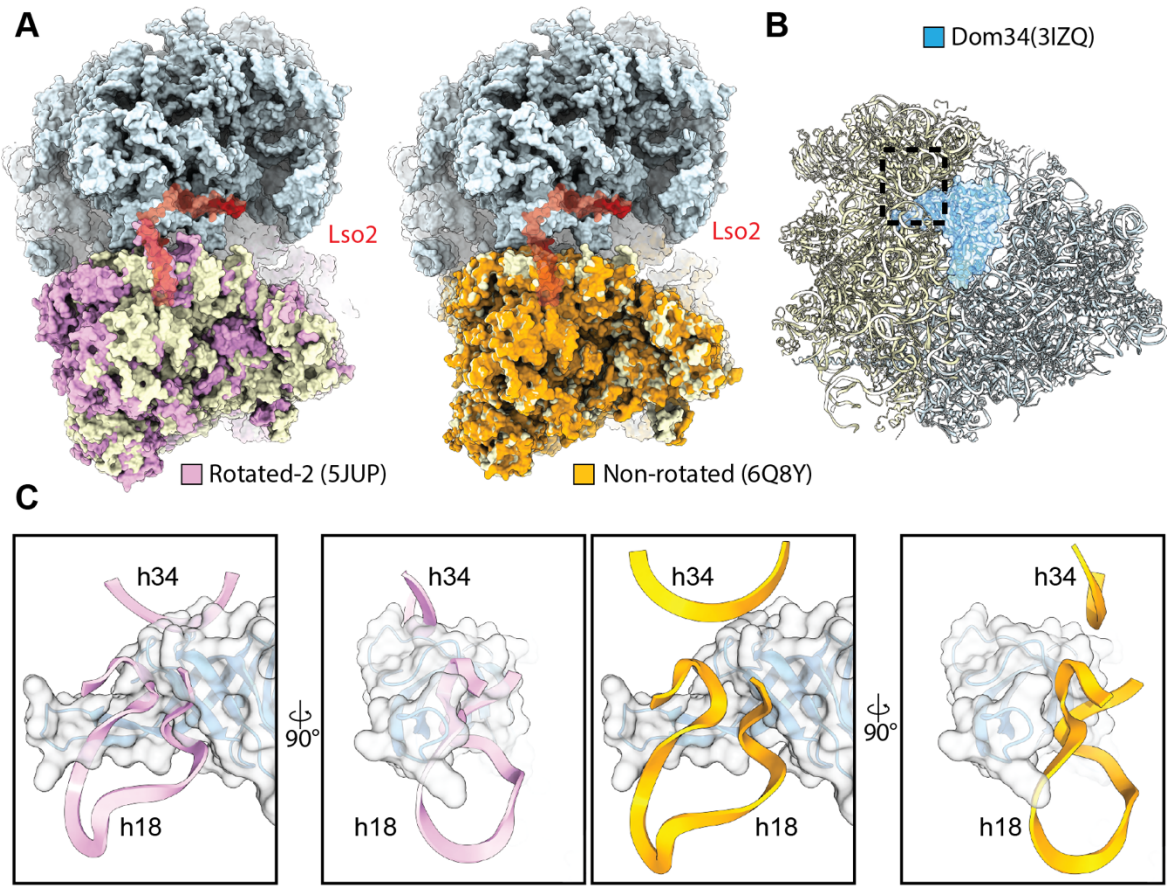

Figure 20: Docking Dom34 into rotated and non-rotated structures reveals a clash between the rRNA of the SSU and Dom34 in ribosomes in the rotated conformation
(A) Overlay of the Lso2-80S structures with yeast 80S in the rotated-2 state (pink) (PDB: 5JUP, (Abeyrathne et al., 2016)) and non-rotated 80S (PDB: 6Q8Y, (Tesina et al., 2019)), showing differences between SSU rRNA in the two rotational states. (B) Docking Dom34 (taken from PDB: 3IZQ, (Becker et al., 2011)) (C) into rotated and non-rotated ribosomes, reveals Dom34 would clash with 18S rRNA helix h18 and h34 in the rotated-2 state, indicating that the non-rotated 80S ribosome can be split by the Dom34 splitting system, while rotated (Stm1-containing) 80S ribosomes should not be split.

To test the hypothesis that Lso2-bound but not Stm1-bound 80S are targeted by the Dom34/Hbs1-ABCE1 recycling system, *in vitro* ribosome splitting assays were carried out. 80S were incubated with a 5-fold molar excess of purified Dom34, Hbs1-GTP, Rli1-ATP (yeast ABCE1) and Tif6 (yeast eIF6), to prevent subunit reassociation. Splitting reactions were subjected to density gradient centrifugation in sucrose gradients and UV profiles were collected at 260 nm.

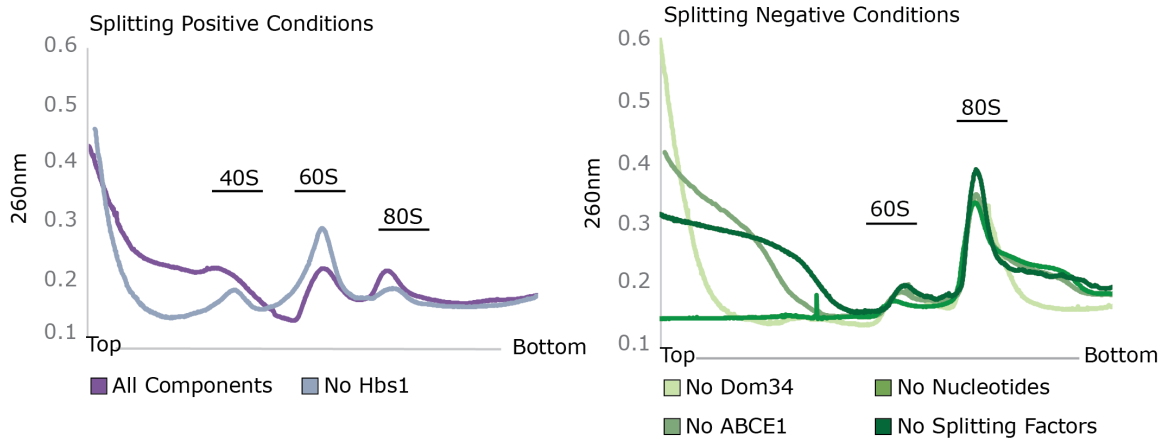

Figure 21: Control of splitting assay
In vitro splitting assays were assembled with 80S ribosomes reconstituted with Lso2, omitting individual factors or nucleotides as annotated. UV profiles for splitting assays were collected following separation over a 10-50% sucrose gradient and absorption profiles were collected at 260 nm. Splitting was observed in reactions when all components (eIF6, ABCE1, Hbs1, Dom34, 1mM ATP, 1mM GTP) were present, or in the absence of Hbs1. Conversely, splitting was not observed when Dom34, Hbs1, or nucleotides were omitted from the reaction, or in reactions containing eIF6 and nucleotides without other factors.

To assess whether the system was functional, and to validate fidelity of the enzymatic components in the reactions, a splitting assay control was carried out (Figure 21). Using Lso2-80S as the target, splitting could be observed when all components of the system were present, but not upon exclusion of Dom34, ABCE1, or nucleotides in the splitting reaction. Consistent with the established role of Hbs1 being limited to the delivery of Dom34 to the ribosome, exclusion of Hbs1 from the reaction did not result in a splitting negative condition (Pisareva et al., 2011; Shoemaker and Green, 2012). The same results were obtained when control 80S were substituted for Lso2-80S. These results were taken as validation for control in this *in vitro* splitting system; thus, execution of experimental splitting assays could proceed.

For comparative splitting analysis, Stm1-enriched 80S were prepared following established methodologies (Materials and Methods), employed for crystallographic studies (Ben-Shem et al., 2011). Cells were grown to mid-log phase at 30°C in YPD (2% glucose) media, at which point they were pelleted at 25°C before resuspending in YP media without glucose and incubating for an additional 10 min at 30°C. Ribosomes were then purified following standard protocols and included in the comparative splitting assays. 80S ribosomes which remained after splitting were subjected to cryo-EM analysis, which confirmed that a vast majority, 90% of the remaining 80S, indeed

adopted the rotated state. Furthermore, in 50% of the ribosomes Stm1 could be observed in its previously reported binding position (Figure 22).

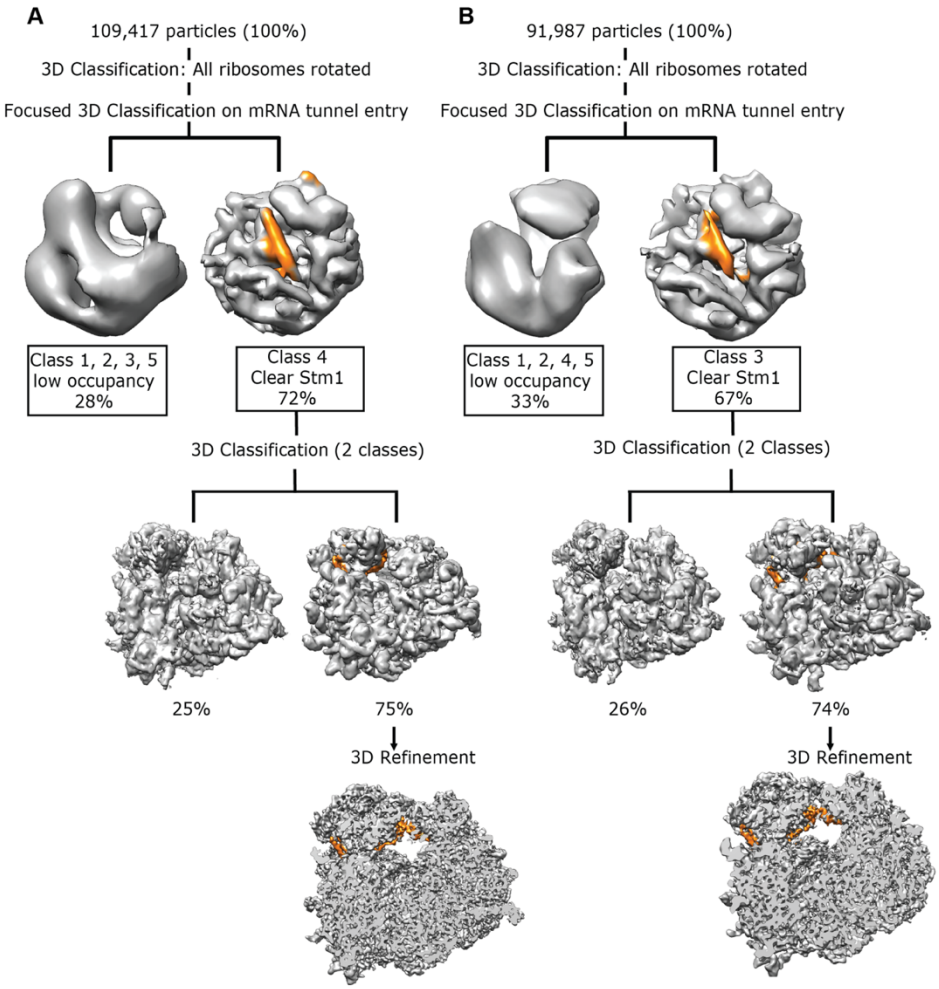

<u>Figure 22:</u> Cryo-EM sorting scheme for identification of Stm1 enrichment in splitting negative 80S fractions
Stm1-80S were prepared exactly as described for Stm1 binding to be enriched, and used in *in vitro* splitting reactions (Ben-Shem et al., 2011). Stm1-80S were collected from the sucrose gradient following *in vitro* splitting reactions with (A) and without (B) splitting factors. These 80S fractions were analysed by cryo-EM where particles were assessed for ribosome rotational states and presence of Stm1. In both cases, an initial 3D classification revealed that a vast majority (90%) of 80S are in the rotated state. These particles were further subjected to local classification using an ellipsoid mask covering the region of the mRNA channel of the 40S to classify for Stm1-containing particles (~50%) which were further refined. Stm1 density is displayed in orange.

Finally, splitting assays were performed in triplicate for reconstituted Lso2-80S, and Stm1-80S (Figure 23A). As a control, 80S ribosomes treated with puromycin and purified under high salt conditions were used, representing non-factor bound ribosomes free to adopt either rotated or non-rotated conformations. Splitting data

was normalised to the puromycin 80S control, such that under conditions where control 80S were only partially split (4 mM Mg(OAc)2 and 100 mM KOAc), splitting of the Lso2-80S was observed with almost 4 fold, quantitative splitting (Figure 23B). Conversely, almost no splitting occurred with the Stm1 bound 80S (Figure 23B). Consistent with the hypothesis, Lso2 bound but not Stm1 bound 80S ribosomes are the preferred clients for splitting by the Dom34 splitting system *in vivo* in *S.c.*, revealing the functional significance of ribosome rotational state within the Lso2-80S complex.

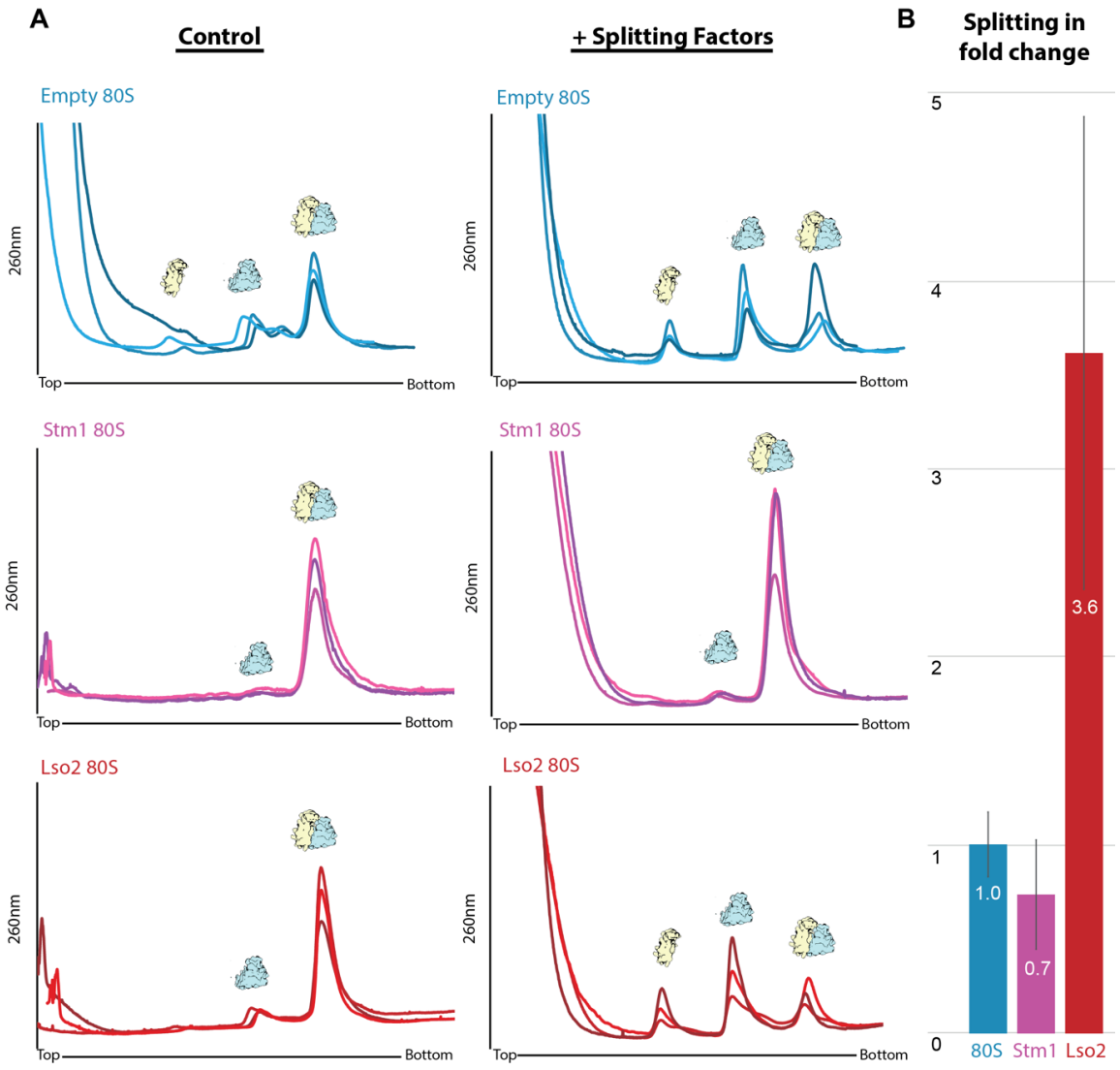

Figure 23: Profiles for 10-40% sucrose gradients following incubation with splitting factors, and quantification of observed splitting
(A) Splitting assays were carried out in triplicate for empty, puromycin treated 80S (blue), Lso2-80S complexes (red), and Stm1 enriched 80S (pink), with or without splitting factors, and sucrose gradient profiles were collected at 260 nm. (B) Quantification of relative splitting is displayed as fold change over control, normalized to experiment using propensity of splitting observed in the control (puromycin-treated) empty 80S.

3.9 Stalling on AAP has a preference for U in the +4 position of the A-site codon *in vitro*

In eukaryotes, RAP mediated translational regulation provides a means for specifically downregulating translation of certain genes, as cellular conditions are signaled to the ribosome. This type of regulation is distinct from translational regulation in *trans* by RBFs, as here the ribosome itself serves as the key regulator in *cis*. As such, resolving the mechanism of Arg dependent stalling on the AAP considers translational regulation from an alternative perspective when compared to the work done on the Lso2/CCDC124 hibernation complex. Though metabolic feedback remains at the center of AAP mediated translational repression, in this case, meaningful structure to function relationships may only be derived upon resolution of extremely high-resolution molecular models.

As all previous attempts to resolve the stalling mechanism of AAP have failed, this investigation called for a modified experimental approach. Specifically, new mRNA reporter constructs were designed to assess whether mRNA-rRNA interactions in the A-site on the SSU may play a role AAP stalling. Though Arg dependent stalling on AAP has observed in in *vitro* translations using yeast, RRL, and *N.c.* cell free extracts mRNA and protein sequences exhibit a low degree of cross species conservation (Figure 24A) (Fang et al., 2000). In order to minimize the potential that nuanced species specific differences (e.g. the absence of splicing in *S.c.*) mRNA constructs were designed for species specific analysis using either *S.c.* or *N.c.* mRNA reporters and respective cell free extracts (Figure 24A).

In vitro translation reactions utilized mRNA truncated after the UAA stop codon as a positive control, as truncated mRNAs are known to induce translational stalling targeted for NGD. Importantly, AAP induces translational repression at the point of translation termination, where progress in the field has revealed the unique sensing of the eukaryotic stop codon as a quadruplet (Matheisl et al., 2015). Similarly, unique mRNA-rRNA base stacking interactions observed with stalling on poly(A) sequence and endogenous NMD target SDD1 suggests that in eukaryotes, mRNA in the A-site may additionally serve in translation regulation (Chandrasekaran et al., 2019; Tesina et al., 2020).

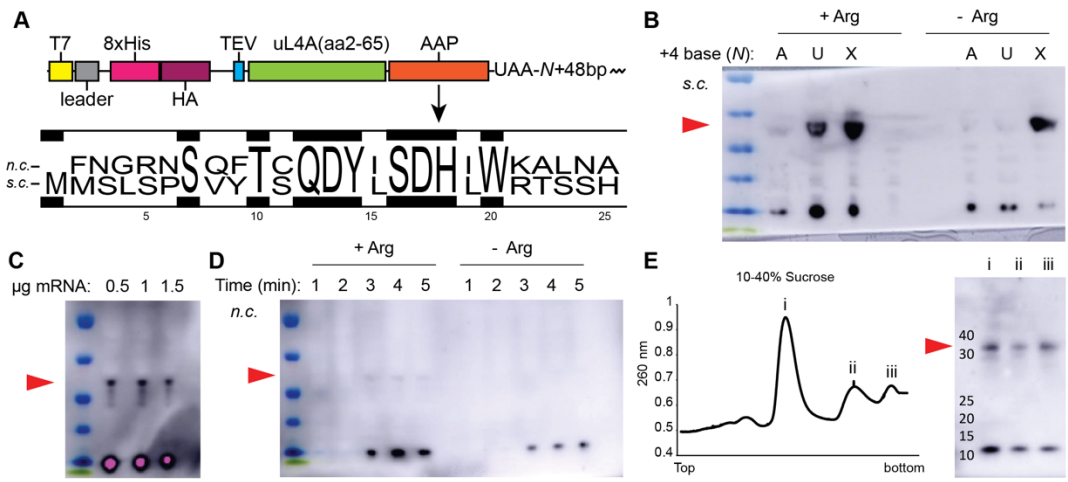

Figure 24: *In vitro* translation of the arginine attenuator peptide in *S.c.* and *N.c.* cell free extracts
(A) Reporter mRNA was designed for IVT. The coding sequence for AAP from N.c. and S.c. were inserted downstream uL4A(aa2-65), which served as a linker to ensure the N-terminal His_8-HA tag would extend outside the ribosomal tunnel and be detectible by western blotting with the reaction complete. Importantly, the protein coding sequence for AAP shows a low degree of cross-species conservation. (B) Western blotting to detect translational stalling in S.c. cell free translations, wherein Arg dependent stalling is detected using mRNA reporters bearing U in the +4 position of the canonical UAA stop codon. Stalling is also observed using mRNA truncated before the STOP codon (X), representing the experimental positive control. (C) Western blotting to determine optimal the mRNA content for IVT reactions in N.c. for generation of RNCs stalled on the AAP. (D) Western blotting to determine optimal incubation times for IVT reactions in *N.c.* (E) UV profiles from 10-40% sucrose gradients loaded with 300µL *N.c.* IVT reactions displaying monosomes (i) disome (ii) and trisome (iii) populations of RNCs stalled on the AAP, and corresponding Western blot to verify RNC programming. (Red arrows indicate signal from His8-tagged AAP, covalently associated with peptidyl-tRNA. Free peptide can be found at ~10 kDa)

Therefore, a series of mRNA reporter constructs were first engineered by polymerase chain reaction (PCR) for the *N.c.* and *S.c.* AAP bearing different nucleobases in +4 position following the UAA STOP codon (Figure 24A). After validating the sequences with DNA sequencing, mRNA was synthesized with a 5' cap using the mMessageMachine t7 kit and included cell free *in vitro* translation reactions. Arg dependent translational stalling was observed in both species with U in the +4 position, which could be identified by western blotting by the incidence of an ~35 kDa signal attributable to nascent protein conjugated to peptidyl tRNA. In both species, Arg dependent stalling was observed when the +4 position was occupied by U (Figure 24B).

Subsequently, *in vitro* translation reactions were optimized for mRNA input (Figure 24C), incubation temperature, and incubation time (Figure 24D) before reactions were scaled up for purification of ribosome nascent-chain complexes (RNCs). AAP

stalled RNCs were first prepared by *in vitro* translation using *N.c.* cell-free extracts, kindly provided by Prof. M. Sachs, following established methodologies (Fang et al., 2000). Programmed RNCs were affinity purified (materials and methods), and grids ultimately frozen for isolated 80S RNC fractions (Figure 24E).

3.10 Cryo-EM analysis of *N. crassa* AAP

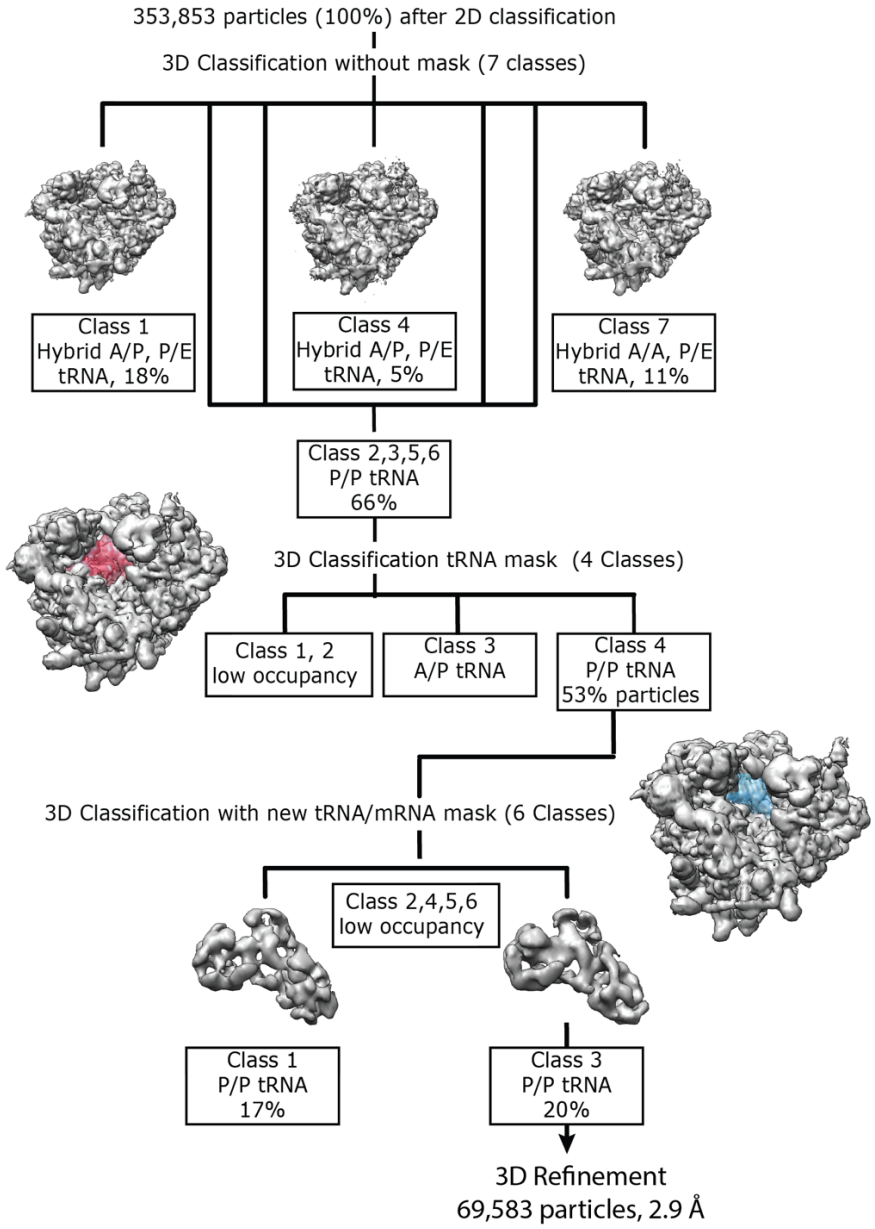

Figure 25: Cryo-EM analysis of purified *N.c.* 80S RNCs stalled with the AAP
The sorting scheme used for classification of single particle 80S

Single particle cryo-EM data was collected for purified 80S AAP RNCs on a Titan Krios by Dr O. Berninghausen. The data was subjected to heavy sorting (Figure 25), in the

hopes of resolving atomic level detail for the areas of interest; the ribosomal PTC, the reporter mRNA, and AAP NC.

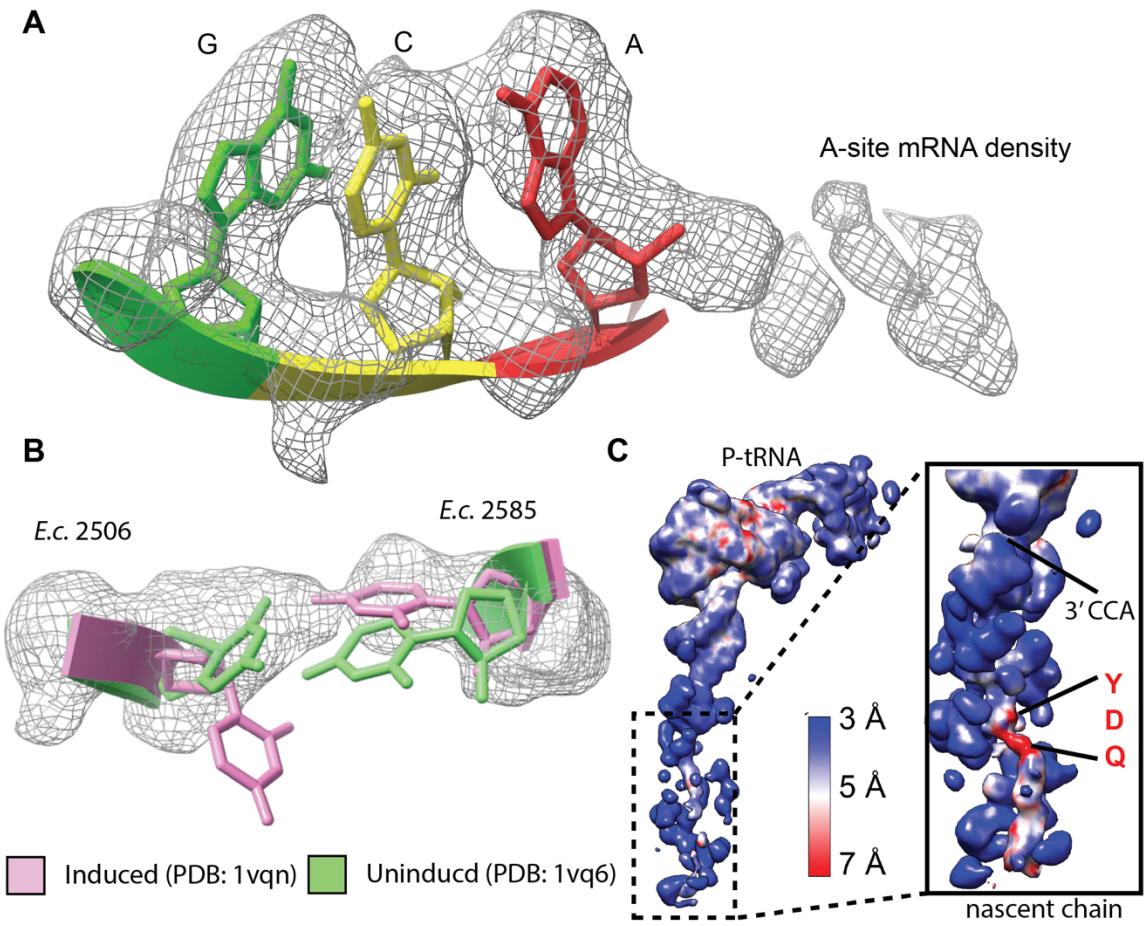

Figure 26: Preliminary results from the structural investigation of the AAP
(A) Electron density (grey mesh) for the mRNA codon occupying the P-site corresponds with the expected GCA Ala which precedes the endogenous stop codon in *N.c.* AAP. Poor local resolution in the A-site prohibits model building for this region of mRNA. (B) By docking molecular models from the *H. marismortui* 50S into the AAP electron density map (grey mesh) reveals PTC base corresponding to *E.c.* U2585 is flipped down in a position not conducive with peptidyl transferase activity (Schmeing et al., 2005). (C) Electron density showing the local resolution for the P-tRNA and NC displayed at a contour level of 0.005 σ after applying a low pass gaussian filter. NC resolution quickly devolves extending away from the 3' CCA end of the tRNA (inset), with the lowest resolution localizing to the expected position of the critical -Q-D-Y- motif. This speculation is based on attempts to build a molecular model for the AAP NC, beginning with A24 after the 3' CCA of the tRNA.

Density for the P-tRNA codon was in agreement with the expected GCA, 'Ala,' in this position, based on the design of the reporter mRNA sequence (Figure 26A). Unfortunately, density for the mRNA in the ribosomal A-site was poorly resolved, preventing observation of interactions between the mRNA stop codon and the rRNA

of the SSU. Similarly, PTC bases were observed in mixed conformations an in most cases, neither the induced or uninduced orientation could be confidently assigned. Indeed only the density for the base corresponding to U2506 in *E.c.* appears to adopt the uninduced conformation, when compared to molecular structures from *Haloarcula marismortui* 50S ribosomes with induced, and non-induced PTC bases (Figure 26B) (Schmeing et al., 2005). For localisation of the critical Arg moiety, unmodeled blobs were identified as low confidence candidates, but lacked high resolution detail for confident assignment and would therefore require further validation, in the form of additional datasets for confident assignment. Finally, although the density for the most C-terminal residues the NC reached near-atomic resolution (~4.5 Å), attempts to build a molecular model were unsuccessful as the density became fragmented extending away from the 3'CCA of the P-site tRNA. Indeed the resolution for the NC only worsens along the tunnel, and by the tunnel constriction site, the NC density becomes indistinguishable from noise. Only by applying a gaussian low-pass filter to the electron density in this region does it become clear that the local resolution of ~7 in this region (Figure 26C) suggests a high degree of conformational freedom and movement for residues in this position. Assuming the AAP NC forms a simple helix between the 3' CCA of the tRNA and the tunnel constriction site, would position the critical -Q-D-Y- stalling motif in exactly the position where this low resolution, flexible density is observed. If correct, this would consistent with earlier observations made in crosslinking analysis (Wu, 2012). Sadly, that the flexible region of the NC could not be resolved with a structural approach may represent current limitations for this methodology.

Discussion

In this thesis, ribosomal regulation of gene expression was addressed in three contexts. The first topic addressed the question of how translation is coupled with mRNA degradation. Here, the goal was to investigate the role the DEAD box helicase and ATPase Dhh1 in complex with ribosomes translating on non-optimal mRNA. Therefore, using standard methodologies for affinity purification and *in vitro* reconstitution, this work attempted to generate a Dhh1-ribosome sample for cryo-EM analysis. As the investigation progressed, it became clear that Dhh1 did not interact directly with the ribosome. Instead, new data emerged implicating the CCR4-Not in sensing translational stalling on non-optimal mRNAs (Buschauer et al., 2020). Taken together, these works provide a model wherein the fates of non-optimally coded mRNAs are determined by the sensor CCR4-Not, and when appropriate, targeted for mRNA decay via recruitment of decapping factors like Dhh1.

The second aspect of this work dealt with the question of how eukaryotic cells maintain the ribosomal population and simultaneously reduce protein production in response to fluctuating nutrient bioavailability. While the translational status of non-proliferating bacterial cells has been the subject of extensive research, far less is known about how eukaryotic cells modulate physiology and fitness under similar environmental conditions of metabolic deficit (Beckert et al., 2017; Beckert et al., 2018; Flygaard et al., 2018; Ueta et al., 2008; Ueta et al., 2013; Ueta et al., 2005). First, cryo-EM samples were prepared for native eukaryotic 80S ribosomes in complex with the recently identified hibernation factor Lso2, to find out what ribosomes look like during the global shut-down of translation that occurs when eukaryotic cells are starved of carbon and nitrogen. Conservation of this system in *H.s.* was also confirmed with similar cryo-EM analysis. Intriguingly, Lso2/CCDC124-bound ribosomes could be observed in a different rotational state then has been observed when ribosomes are bound by the only other characterised eukaryotic hibernation factor Stm1 (SERBP1 in H.s.) (Anger et al., 2013; Ben-Shem et al., 2011; Brown et al., 2018a). In order to assess the functional significance of this conformational distinction, high concentrations of purified hibernation complexes were prepared for biochemical analysis. As Lso2 is present at only ~8-12k mol/cell, *S.c.* Lso2 was overexpressed in *E.c.* and purified for reconstitution with ribosomal subunits, to circumvent the issue with the yield limited

preparation of the native Lso2-80S complex (Ho et al., 2018). Cryo-EM analysis confirmed agreement between the structures for the reconstituted and native Lso2-80S hibernation complex, allowing work to proceed to the next question; are hibernating ribosomes bound by Stm1 or Lso2 recycled differently? By recapitulating Dom34 splitting *in vitro*, this work was able to demonstrate that Lso2-80S hibernation complexes are readily split by Dom34 and ABCE1, unlike the Stm1-80S which is resistant to splitting. Importantly, this work has uncovered how eukaryotic cells maintain ribosomes for quick translational reactivation following nutrient stress.

The final chapter of this investigation addressed the mechanism by which the AAP modulates translation termination stalling in its role as a regulatory uORF. As with other eukaryotic RAPs, the AAP downregulates expression of the CPA1 cistron, providing a means for negative feedback during Arg biosynthesis (Gaba et al., 2001; Hood et al., 2007; Werner et al., 1987). The instance of regulatory uORFs in eukaryotes may serve more generally in translational regulation, so understanding eukaryotic RAP mechanisms serves as an important challenge for structural investigators (Ingolia et al., 2011). To that end, reporter mRNA constructs were assembled for *in vitro S.c.* and *N.c.* cell free translation of the AAP. Reporter mRNAs were designed in consideration of emerging evidence which implicates the +4 base of the A-site codon in serving additional regulatory functions not observed in prokaryotic systems (Chandrasekaran et al., 2019; Matheisl et al., 2015; Tesina et al., 2020). Translational stalling was thus observed in both *S.c.* and *N.c.* when the endogenous stop codon was followed by a U base in an Arg dependent fashion. Therefore, *N.c.* RNCs were prepared following standard methodologies and subjected to cryo-EM analysis, resulting in a final 2.9 Å EM density map. Although this resolution has previously been found to be adequate for resolution of the of RAP stalling mechanism with Xbl1, the poor local resolution for areas of interest prevented conclusive analysis for the mechanism of stalling employed by the AAP at this time (Shanmuganathan et al., 2019).

4.1 The role of helicase Dhh1 in decay of non-optimally coded mRNA

The major challenge this study faced was that Dhh1 could not be observed binding to the ribosome, and ultimately, it became clear that this aspect of the hypothesis was incorrect. Instead, parallel work revealed that sensing of ribosomal stalling on non-optimally coded mRNAs is carried out by the CCR4-Not complex, a master regulator of translation (Buschauer et al., 2020; Collart, 2016; Denis and Chen, 2003). Excitingly, this discovery does ultimately delineate the role of Dhh1 in decay of non-optimal mRNAs, clarifying biochemical data wherein tagged-Dhh1 can be readily detected amid ribosomal fractions on sucrose density gradients. In canonical mRNA decay, deadenlyation by CCR4-Not precedes the decapping of mRNA which is carried out by Dcp1 and Dcp2 in complex with Edc3, Pat1, and Dhh1 (Nissan et al., 2010; Sharif et al., 2013; Sweet et al., 2012). As Dhh1 is known to interact with the MIF4G domain of Not4 in the CCR4-Not complex, it is unsurprising that preliminary works detected Dhh1 in their analysis of ribosomes stuck on non-optimal mRNA and, sought a functional explanation (Basquin et al., 2012; Chen et al., 2014; Presnyak et al., 2015; Radhakrishnan et al., 2016). The helicase activity of Dhh1 does suggest that this 60 kDa protein could be a prime candidate for ribosomal binding, however, a major question for this investigation sought to understand the specific mechanism by which Dhh1 would be capable of specifically sensing mRNA codon-optimality. In this regard, that the 1 MDa master regulator CCR4-Not is instead responsible for recognising translational stalling on non-optimal mRNAs, subsequently recruiting decapping factors for mRNA decay, provides a much more palpable explanation for how such problematic transcripts are regulated. Furthermore, codon optimality has since been found to be utilised by the cell for slowing translation during synthesis of certain protein domains, allowing for recruitment of protein folding chaperones (Hanson and Coller, 2018). As such, ribosomal stalling on non-optimally coded mRNAs may not always require translation termination and mRNA decay. Thus, sensing of translational stalling on non-optimally coded mRNAs should require a more sophisticated regulator than the helicase Dhh1, ultimately discovered with CCR4-Not (Buschauer et al., 2020).

4.2 Structural characterisation of a novel eukaryotic hibernation complex

In the seminal 1949 paper, Jacques Monod aptly avoids addressing bacterial cell death, or rather negative growth, except in commenting on the technological and conceptual shortcomings which would prohibit analysis of this phase at the time of writing (Monod, 1949). Luckily, understanding such negative regulation has enjoyed plenty of progress since then. In nutrient depleted environments, ribosome hibernation, or the storage of factor-bound inactive ribosome populations as 100S dimers, has been extensively characterised in prokaryotic systems (Basu and Yap, 2017; Beckert et al., 2017; Beckert et al., 2018; Flygaard et al., 2018; Ortiz et al., 2010; Prossliner et al., 2018; Ueta et al., 2008; Ueta et al., 2013; Ueta et al., 2005). Still, key differences between the prokaryotic and eukaryotic cell cycle, as well as the additional complexity of eukaryotic systems calls for further research to address how negative growth phases are regulated in eukaryotic systems. In both cases, nutrient stress is known to globally downregulate the process of translation, modulated by RBFs. In prokaryotes, hibernation factor binding is accompanied by ribosomes dimerization, though limited evidence has emerged to support conservation of this mechanism in eukaryotic systems (Krokowski et al., 2011; Prossliner et al., 2018). Instead, inactive 80S populations are often observed after exposure to osmotic stress, lithium induced stress, fusel alcohols, and in mammalian systems, following serum depletion (Ashe et al., 2001; Manners and Nielsen, 1981; Montero-Lomeli et al., 2002; Uesono and Toh, 2002). Given that the cycle of translation both begins and ends with dissociation of the ribosomes into SSU and LSU components, it is curious that upon translational shutdown, fully assembled 80S maintain the majority of the ribosomal population. Until recently, published literature has offered little in the way of a satisfactory explanation for this phenomenon.

Still, the influence of cellular metabolism on translation has been broadly characterised. Phosphorylation of eIF2 and activation of the ISR are both well-established means for negative translational regulation, as these systems allowing for global remodelling of the translatome in response to specific metabolic signals. In the case of GCN2, a direct association with the ribosome allows translation to be regulated in *trans,* by indiscriminately sensing accumulation of deacyl-amino acids and

modulating protein production accordingly (Castilho et al., 2014). The regulatory sensing carried out by Gcn2 occurs during elongation, when accumulation of deacyl-tRNAs is detected. By comparison, eukaryotic hibernation factors aid cells in recovery from quiescence, such that instead of deacyl-tRNA accumulation, the bioavailability of carbon and/or nitrogen serve as regulatory signals (Van Dyke et al., 2006; Van Dyke et al., 2013). This represents a much broader and less direct signal than occurs during ISR activation, posing a challenge for deduction of the direct mechanism by which eukaryotic hibernation factors promote initiation during recovery from quiescence.

Herein, the structure of the novel Lso2-80S hibernation complex has been solved by cryo-EM for both the native and reconstituted *S.c.* complex. Additionally, through collaboration with Herr R. Buschauer, the orthologus *H.s.* structure has been solved, and another *H.s.* hibernation complex identified. Furthermore, the functional significance of ribosome rotation in these structures, all observed in the post translocational non-rotated state, was pursued in biochemical analysis. To that end, *in vitro* splitting assays were assembled, and component analysis was carried out to verify enzymatic activity. Upon system validation, the propensity of splitting for Lso2-80S hibernation complexes was compared to the splitting observed for control empty 80S, and Stm1-80S. These data are clear, the Lso2-80S hibernation complex is readily split by the activity of Dom34 and ABCE1 while the Stm1-80S hibernation complex is not.

The most significant finding in this study was the observation that Lso2/CCDC124 bound 80S could be exclusively observed in the non-rotated conformation. Importantly, previous structural investigations have observed idle yeast 80S primarily in the rotated state (Beckmann et al., 1997; Ben-Shem et al., 2011; Jenner et al., 2012). The ribosomal states of hibernating Stm1/SERPB1 80S were compared with published molecular structures from a structural investigation which characterized cap independent translation and ribosome translocation with the Taura syndrome viral internal ribosome entry sites (IRES). This work presented five distinct molecular structures, attributed different phases of ribosome rotation. Rigid body fitting of these molecular models into previously reported Stm1/SERBP1-80S complexes (Ben Shem, 2011; Brown 2018), as well as the experimentally derived Stm1-80S complexes confirmed that in all cases, Stm1/SERBP1-80S adopt the rotated-2 confirmation

(Abeyrathne et al., 2016). Conversely, when applying the same restraints in Chimera, all Lso2/CCDC124 80S structures were observed in the non-rotated, post-translocational conformation. This is the state often observed when ribosomes are stalled with an empty A-site, as for example is the case in the structures of the stalled 80S bound to the mRNA decay factor Xrn1, and NGD structures such as 80S stalled on stem loop bearing or truncated mRNAs (Becker et al., 2011; Tesina et al., 2019).

This observation led to the hypothesis that storing two populations of dormant ribosomes in distinct rotational states could serve to inform the fates of such complexes during their nutrient recovery and translational reactivation. Specifically, that ribosomes in the non-rotated state may be preferred targets for reactivation by the Dom34 splitting system was postulated. Indeed, docking of the Dom34 molecular model in complex with ABCE1, in its active splitting conformation, into rotated and non-rotated 80S models reveals that Dom34 would clash with the rRNA of h18 and h34 on the SSU for rotated, but not non-rotated ribosomes (Figure 20). As such, *in vitro* splitting assays were assembled to recapitulate Dom34-mediated splitting *in vitro* and were able to show that Lso2-bound 80S are highly susceptible to recycling (Figure 23). An experimental control confirmed that in the assay, splitting is dependent on the enzymatic function of Dom34, ABCE1, and inclusion of nucleotides in the reaction, but not in the inclusion of Hbs1 (Figure 21). This is unsurprising given that Hbs1 is responsible for delivery of Dom34 to the ribosome, but does not participate in the splitting reaction. Considering the role of Hbs1 *in vivo* serves only to deliver Dom34 to the ribosomal A-site, under controlled conditions *in vitro*, where each factor is supplemented in excess, it is not unexpected that this system can still perform optimally when this role is not being fulfilled. Furthermore, this finding is in agreement with previous studies which have reported the activity of Hbs1 is non-essential ribosome splitting *in vitro* (Pisareva et al., 2011; Shoemaker and Green, 2012).

In *in vitro* splitting assays, the splitting of Lso2-80S was compared to the splitting observed with 80S ribosomes treated with puromycin, therefore representing an artificially 'empty' pool of 80S ribosomes. Preparing these ribosomes under high salt conditions ensures that additional factors or mRNA, tRNAs and nascent chains are not associated, and treating with puromycin ensures these ribosomes are free to alternate between the rotated and non-rotated state. Splitting quantifications were

therefore normalised to this puromycin 80S population as control, and 3.7 fold increased splitting was observed for the Lso2-80S complexes than for the control. Stm1 bound 80S ribosomes were prepared following using pre-existing protocols (Ben-Shem et al., 2011) and also subjected to splitting with the *in vitro* system. In agreement with the hypothesis, rotated-80S enriched in Stm1, whose factor occupancy and rotational state were confirmed by cryo-EM analysis (Figure 22), exhibited only 0.7 fold the splitting potential of the puromycin treated 80S controls (Figure 23).

The question remains: what determines differential binding of Stm1 and Lso2 to ribosomes? Here, interesting conclusions can be drawn by comparing experimental conditions that enrich either Stm1 or Lso2 on ribosomes. While most investigations focusing on the Stm1-80S complex carry out glucose depletion for 10 min while maintaining cell culture at 30°C, Lso2 investigations have utilised long term nutrient depletion spanning the course of days (Wang et al., 2018). This indicates that the Lso2-80S system responds preferentially during long-term nutritional deficit. By comparison, the 10 minute starvation condition used for preparation of Stm1 containing ribosomes indicates these complexes preferentially form in the extreme short-term relative to nutritional deficit (Ben-Shem et al., 2011; Wang et al., 2018) (Materials and Methods).

Previous works have shown that translational recovery during quiescence could be perturbed upon deletion of either Stm1 or Dom34 (van den Elzen et al., 2014). With respect to the recent characterization of Lso2 as a hibernation factor, one interpretation of these findings would suggest that Stm1 antagonizes the role of Dom34 during translational recovery from quiescence, in that deletion of Stm1 negates the requirement, advantage, or role fulfilled by Dom34 recycling of the Lso2- 80S hibernation complex. This suggests an alternative fate, and likely overall role, for Stm1-80S than for Lso2-80S.

Both Lso2 and Stm1 are non-essential proteins, whose deletion exhibits no phenotype under standard growth conditions (Van Dyke et al., 2013; Wang et al., 2018). However, stm1Δ do exhibit a slow growth phenotype when galactose is the primary source of carbon, exhibiting inositol auxotrophy and an increased sensitivity to mTOR signaling and rapamycin (Butcher et al., 2006; Utsugi et al., 1995; Van Dyke et al., 2009; Villa-Garcia et al., 2011; Yoshikawa et al., 2011). Stm1 has additionally been implicated in

genetic studies as an effector of mRNA decapping, seemingly promoting mRNA decay (Inada et al., 2002; Van Dyke et al., 2004; Van Dyke et al., 2006; Van Dyke et al., 2009). Given that control of translation is inversely related to mRNA degradation (Balagopal and Parker, 2011), it's no surprise that Stm1 both promotes mRNA degradation and inhibits translation, the primary functional offset of its ribosome binding activity (Van Dyke et al., 2009). Indeed, the role of Stm1 as an activator of mTOR signaling and apoptosis suggests its role may function more as an emergency response, serving mechanistically as a primary means for quickly shutting down translation. Support for this theory comes from the conditions under which Stm1-80S ribosomes become enriched, requiring only 10 minutes ~~of~~ glucose deprivation. Following an immediate and abrupt nutrient drop out, Stm1-80s are observed at 50-90% occupancy in cryo-EM 3D classifications (Figure 22) and can be prepared with a high enough degree of homogeneity to allow for preparation of a high-resolution crystallographic sample (Ben-Shem, 2011).

By comparison, within this structural investigation, native Lso2-80S complexes were represented at only 6% and 15% of the total ribosomal population. Indeed while Stm1 is present at ~35-47k mol/cell, Lso2 is quite lowly expressed at ~8-12k mol/cell (Ho et al., 2018; Van Dyke et al., 2006). Still, unlike prokaryotic hibernation factors which are translationally upregulated upon entry to stationary phase (Prossliner et al., 2018), both Lso2 and Stm1 are constitutively expressed by the cell. Given that two structurally distinct populations of factor bound inactive eukaryotic monosomes have been observed, how do cells discriminate between their assembly?

At least in the case of Lso2, there is evidence to suggest that rather than associating with the ribosome as a direct response to metabolic changes, the Lso2-80S complex may account for up to 15% of the cytoplasmic ribosome population even under standard, glucose replete conditions (Wang et al., 2018). In agreement with this hypothesis, attempts to enrich or abolish binding of CCDC124 to 80S ribosomes by treating HEK293T cell lysates with various antibiotics, each targeting distinct catalytically active sites on the ribosome such as the DCC or PTC, were unsuccessful (Figure 19). This finding led to the same conclusion; that within eukaryotic cells, a stable background of Lso2/CCDC124-associatied monosomes are represented within the ribosomal population at all times. Therefore, if the primary function of the Stm1-80S population serves to immediately and globally reduce translation, perhaps the

primary function of the Lso2-80S population serves to preserve ribosomes for fast translational reactivation. If correct, this theory could explain the advantage in establishing two seemingly redundant, albeit structurally distinct, inactive 80S populations with divergent fates.

Support for this proposed distinction, wherein Stm1-80S represents a switch to turn translation OFF and Lso2-80S is the switch to turn translation ON, could be one interpretation of the binding location of Lso2 on the ribosomal SSU. Given the position of Lso2's N-terminus within the mRNA channel, occupation by Lso2 could perhaps protect rRNA bases from chemical modification, as toxic reactive oxidative species are known to accumulate during nutrient stress. In this context that Lso2 binding stabilizes the LSU-SSU interaction and 80S association, compared to the lower stability observed for non-factor bound ribosomes (Wang et al., 2018), would extend the proposed 'protective' function for Lso2 to the subunit interface which is predominantly populated by rRNA (Spahn et al., 2004). Additional support for the theory that Lso2 binding protects the ribosome from chemical modification can be found in the observation that lso2Δ cells recovering from quiescence exhibit defective initiation, as demonstrated by the 3-fold accumulation of monosomes population compared to wild type. Furthermore, ribosome footprinting from these populations reveals that even elongating monosomes exhibit a 4-fold increase in stalling at the AUG start codon as opposed to along the ORF. Elongating ribosomes are distinguished from initiating ribosomes during ribosome footprinting based on mRNA length, producing final read fragments of 28-30 nucleotides. The study went on to confirm these effects could not be attributed to synthesis of new ribosomes, and therefore can be taken to reflect translational defects specific to Lso2 functionality (Wang et al., 2018). Taken together, these results suggest that during recovery from quiescence, Lso2 serves to protect ribosome functionality at the point of initiation either directly, by preserving the SSU rRNA responsible for mRNA binding and decoding, or indirectly, by facilitating Dom34 recycling and allowing ribosomes to be directly targeted to formation of a 43S PIC.

In higher eukaryotes, the presence of SERBP1 is accompanied by stable binding of the translation factor eEF2 in the ribosomal A-site, which has been observed in mammals (Anger et al., 2013; Brown et al., 2018b) and *in vitro* in yeast (Hayashi et al., 2018). Indeed, while eEF2 is apparently not present in the Stm1-80S complex (Figure 22),

analysis of protein content by SDS-PAGE and silver stain indicate that eEF2 is indeed present in these samples, albeit with declining occupancy in the steps preceding sample vitrification. This is not uncommon in cryo-EM, where factor occupancy may be perturbed by the harsh conditions of ultracentrifugation and grid freezing. As such, complexes existing *in vivo* are not always adequately stabilized, and therefore represented, in the samples subjected to structural analysis. Importantly, eEF2 binding in the A-site would further block access to Dom34 and render these ribosomes resistant to splitting by this system. Therefore, establishing whether or not Stm1/SERBP1 binding is exclusively accompanied by eEF2 binding *in vivo* should be addressed by future investigations seeking to delineate the fate of these hibernating Stm1-80S complexes.

Still, within this splitting analysis, the significance of ribosome rotational state is clear. While non-rotated Lso2-80S ribosomes are readily split by Dom34 and ABCE1, Stm1-bound 80S in the rotated state cannot be recycled in the same way. Therefore, the fates of Stm1-80S complexes remains to be elucidated. It seems unlikely these Stm1-80S would be simply targeted for degradation. Given that ribosome biogenesis is an energetically expensive process, employing such a destructive mechanism in response to nutrient stress would have far reaching consequences for the cell upon nutrient recovery, which are not likely to be conserved from an evolutionary perspective. As such, there is a strong suggestion that an additional mechanism for ribosome recycling has yet to be uncovered.

Indeed, there is some exciting new data in agreement with this rather provocative theory. In emerging cryo-EM data analysis, the flexible C-terminus of CCDC124 has been found associating with the ribosomal SSU (Thoms et al., 2020). In the structures presented herein, this region could not be visualised, likely, a result of being non-structured. As such, the most C-terminal region of CCDC124 which could be visualised ends with helix 2, above the GAC, on the ribosomal LSU.

Interestingly, a very recent study by the Beckmann lab focusing on the 40S interaction of the SARS-CoV-2 protein Nsp1 shows, that CCDC124 was bound to Nsp1-containing 80S in native pullouts. While a direct role of CCDC124 in translational shutdown by Nsp1 seems unlikely, the structure shows that the previously invisible C-terminal part of CCDC124 is in the ribosomal A-site. Interestingly, one subclass showed in addition,

ABCE1 and the eukaryotic termination eRF1 bound. Moreover, eRF1 is observed in an entirely new conformation, where the stop-codon decoding N-terminal domain is moved away from the A-site towards the CCDC124-bound 60S. With these new data, it is clear that when associated with the ribosome, CCDC124 adopts an overall slingshot-like tertiary structure, with its two helices acting as a wedge and the C terminus acting as a sling for eRF1.

These findings are in good agreement with this investigation, and imply CCDC124-80S recruits the eRF1-ABCE1 splitting system and Lso2-80S the Dom34-ABCE1 splitting system. As both can recruit ABCE1, this finding provides further confirmation for the theory that Lso2/CCDC124-80S indeed represent an easy-to-split 80S population.

4.3 Investigating the stalling mechanism of the fungal AAP

To date, far more progress has been made in structurally resolving the stalling mechanisms of prokaryotic RAPs than for those from eukaryotes (table 1). Indeed though countless prokaryotic RAP structures are currently available, only three structures of eukaryotic RAP arrested ribosomes have been solved; the human 80S stalled by the "CMV" stalling sequence (Matheisl et al., 2015), the rabbit 80S stalled by the Xbp1 RAP (Shanmuganathan et al., 2019); and the human ribosome stalled by a drug like molecule PF846 (Li et al., 2019). Importantly, ribosome profiling experiments have identified numerous regulatory uORFs in eukaryotic systems, hinting that RAP mediated stalling may in fact represent a more broadly applicable mechanism for translational repression in eukaryotes (Ingolia et al., 2011). Therefore, structural characterization of eukaryotic RAPs may illuminate presently unknown mechanisms for translational regulation. As such, one of the aims of this thesis was to generate purified RNCs for cryo-EM analysis of a well-characterized RAP, the fungal AAP(Fang et al., 2004; Fang et al., 2000; Spevak et al., 2010; Wei et al., 2012; Wu et al., 2012).

Therefore, reporter mRNAs bearing the coding sequence for *N.c.* and *S.c.* AAP were prepared to allow production and purification of AAP stalled RNCs for cryo-EM analysis. First the uORF sequence was inserted downstream the uL4A(aa2-65) gene in

a pEX-A2 vector kindly provided by Dr. P. Tesina, by PCR cloning. The resulting plasmid was then used for amplification of a linear DNA fragment for preparation of reporter mRNA (Materials and Methods), coding for HA-His_6-uL4A(aa2-65)-AAP under control of the T7 promoter for mRNA transcription. This uL4A(2-65) truncation has demonstrated utility for preparation of RNCs, as it provides an appropriate linker region such that the HA-His6 region of the nascent protein extends beyond the ribosomal tunnel, allowing for signal detection in subsequent experimental Western blot analysis. Additionally, mRNA reporters were designed with different nucleotides occupying the +4 position of the endogenous UAA stop codon. This approach follows recent work which has found the eukaryotic codon to be read as a quadruplet, at times forming distinctive secondary structures with rRNA as has been observed in the structures of RNCs stalled with SDD1 and poly(A) stalling (Chandrasekaran et al., 2019; Matheisl et al., 2015; Tesina et al., 2020). Therefore, we set out to assess whether the mRNA stop codon may play a role in the translation termination stalling of AAP.

Preliminary *in vitro* translation experiments were carried out using either cell free extracts from *S.c.* 288C Δski2 cells, kindly provided by Frau. H. Sieber for S.c. AAP, or cell free extracts from N.c. OR74A, kindly provided by Prof M. Sachs (College Station, Texas). In both cases stalling was observed in the presence of 4 mM Arg using mRNA reporters bearing U in the +4 position of the STOP codon. Exclusion of Arg from these reactions abolished the Western blotting signal at ~35 kDa, indicative of a covalent association between the successfully translated reporter mRNA peptides and the P-site Peptidyl-tRNA (Figure 24). This finding was somewhat unexpected, given that UAAU is considered a 'weak' stop codon compared to stop quadruplets bearing purines in the +4 position (Friedman and Honig, 1995; Tate and Mannering, 1996).

Upon identification of the optimal incubation temperature, incubation time, and mRNA input for *in vitro* translation, purified AAP RNCs from N.c. were prepared for cryo-EM analysis using the most up-to date hardware available. The data was subjected to extensive 3D classification using Relion 3.1, and a final 2.9 Å electron density map was resolved. Notably, this same resolution was demonstrated to be adequately sufficient to decipher the RAP stalling mechanism for Xbp1 (Shanmuganathan et al., 2019).

Importantly, in order for translation to proceed, the 5 critical PTC bases must be oriented in the induced positions. With one or more PTC bases disrupted, the ribosome cannot catalyse peptidyl transfer, or delivery of new aminoacyl-tRNAs in the A-site may be disrupted. As such, one of the primary goals of this investigation was to observe the orientation of PTC bases in the experimentally derived *N.c.* AAP RNCs. In this analysis, only one of the rRNA bases of the PTC, corresponding to *E.c.* residue U2585, appears to be in the flipped out from the induced conformation (Figure 26A). During peptidyl transfer, this base helps coordinate the incoming amino acid in the A-site, and disruption of this base position has been observed in the prokaryotic RAPs MifM and ErmCL, as well as in the eukaryotic termination CMV staller (Arenz et al., 2014a; Arenz et al., 2014b; Matheisl et al., 2015; Sohmen et al., 2015). Still, the ambiguity for PTC base orientation may indicate that during stalling on the AAP, bases of the PTC exhibit a degree of plasticity, rather than adopting specific orientations or states.

Support for this hypothesis comes from an investigation of the interactions between the AAP NC and the ribosomal tunnel. Site specific photo cross-linking found Arg dependent changes to the proximity of residue V7 of the AAP with the constriction site proteins uL22 and uL4. Furthermore, PEGylation assays revealed the AAP NC adopts a generally extended conformation in the presence and absence of Arg, an observation unchanged with substitution of the non-functional D12N AAP construct (Wu et al., 2012). Importantly, this excludes AAP from acting as a RAP force sensor, as is observed with prokaryotic RAPs VemP, MifM, and SecA (Chiba and Ito, 2012; Su et al., 2017; Tsai et al., 2014). These and other data, specifically that crosslinking to uL22 and uL4 could be observed for probes along the length of the AAP NC, led the authors to propose that the AAP NC rotates, or moves back and forth within the tunnel. It is tempting to suggest that the AAP NC is always in motion, and that Arg binding creates a steric hindrance which perturbs the PTC, whose bases are perpetually shifting between induced and uninduced positions. Further agreement with this hypothesis can be found in the data, where experimental densities show a clear helix extending from the 3' CCA end of the tRNA, representing the very C-term of the AAP NC (Fig 26C), which quickly devolves around the critical -Q-D-Y- motif positioned just above the constriction site. Local resolution for the NC density in the position the -Q-D-Y- motif is expected abruptly declines from ~4 to ~7 Å, indicative of flexibility (Figure

26C). Furthermore, within the SSU, the high resolution for the P-site mRNA verifies that in the final 3D reconstitution, the RNCs are indeed stalled by AAP. Clear resolution of the terminal Ala GCA codon (Figure 26A) discounts the notion that particles were not properly sorted. As such, the poor local resolution for the peptide NC should not be taken to represent heterogeneity in the data, and rather provides validation for this interpretation for flexibility within this region. The second aim of this investigation sought to identify the position occupied upon Arg binding during stalling on the fungal AAP. Unfortunately, due to the poor local resolution in this region, the work was unsuccessful in this regard. Still, this structural analysis resolves programmed AAP RNCs with near-atomic, average overall resolution. That poor local resolution in observed specifically for the A-site mRNA, the PTC, and for the peptide NC, is strongly indicative that flexibility and movement may be a factor in the stalling mechanism. Equipped with an optimized system for generating high concentrations of purified AAP RNCs in both *S.c.* and *N.c.*, the days are numbered for this elusive RAP. As technological advancements in cryo-EM continue to progress, structural resolution of this stalling mechanism is just around the corner.

Outlook

This work clarified that the postulated role of Dhh1 as a sensor for translational stalling on non-optimally coded mRNA was incorrect. Additionally, a novel eukaryotic ribosome hibernation complex was structurally characterised and contextualised with functional analysis. Finally, a system was optimised for the preparation of purified RNCs for structural analysis of the fungal AAP using both N.c. and S.c. cell free translation systems. Still, with this progress new questions have arisen to be addressed in subsequent analysis.

First, the question of assembly for the eukaryotic hibernation complex remains largely enigmatic. It is unclear at what point and by what mechanism Lso2/CCDC124 binding to the ribosome may occur. There are two primary theories for how this may occur. On the one hand, the factors may probe the intersubunit space in order to detect vacancy. This explanation could explain crosslinking data which finds Lso2/CCDC124 interacting with tRNAs, despite that their binding to the ribosome should be mutually exclusive. On the other hand, that Lso2 binding seems to stabilise the assembled 80S from subunit dissociation may imply these factors are capable of recruiting and assembling the 80S artificially, without initiation having to occur (Wang et al., 2018).

With regards to disassembly of the hibernation complex, the question of the fate for the Stm1-80S hibernation complex remains. Additionally, occupancy of eEF2 in the *H.s.* structure though not observed in the *S.c.* structure calls for more thorough species comparison to delineate the relevance of A site occupancy in these Stm1/SERPB1 hibernation complexes (Brown et al., 2018). In the case of the Lso2-80S complex, though ribosome recycling by Dom34 and ABCE1 (Rli1 in *S.c.*) has been clarified, further studies may seek to address how cells prevent futile cycling wherein, these complexes could continuously form and dissociate without additional regulation.

In the human system, the new evidence showing 80S ribosomes bound by CCDC124 in complex with ABCE1 and eRF1 in a new confirmation provides an exciting development and further validation for the findings on this study (Thoms et al., 2020). Still, whether these CCDC124-80S ribosomes are preferentially recycled by the activity

of eRF1 or Dom34 should be probed. Additionally, the incidence of the additional factor. EBP1 at the ribosome exit site requires a much more comprehensive analysis of the role for this biogenesis factor. More specifically, whether or not EBP1 binding is at all specific to ribosome hibernation or represents its own form of translational regulation entirely should be pursued in future work (Kowalinski et al., 2007; Liu et al., 2006).

Finally, subsequent work should certainly pursue the preliminary biochemistry presented herein, and perform a full structural analysis for AAP RNCs generated from *S.c.*. Given the mounting evidence to suggest that the stalling mechanism of the AAP is intrinsically linked to a large degree of structural flexibility for the NC, cross-species comparison may prove vital for accumulating and verifying structural findings with respect to the location of Arg moieties, the orientation of PTC bases, and observing mRNA-rRNA base stacking in the ribosomal A-site. Additionally, further attempts should be made to prepare AAP stalled RNCs in both *N.c.* and *S.c.* in the presence of an RGD tripeptide, known to induce translational stalling at similar concentrations where Arg dependent stalling is observed. The increased size of this tripeptide may well aid in stabilising the AAP NC for structural resolution, as well as provide more signal for the Arg binding pocket to be identified.

Appendix I

Final vector maps for cloning plasmids.

Plasmid 1, used for genomic tagging of endogenous *S.c. DHH1* at the C-terminus

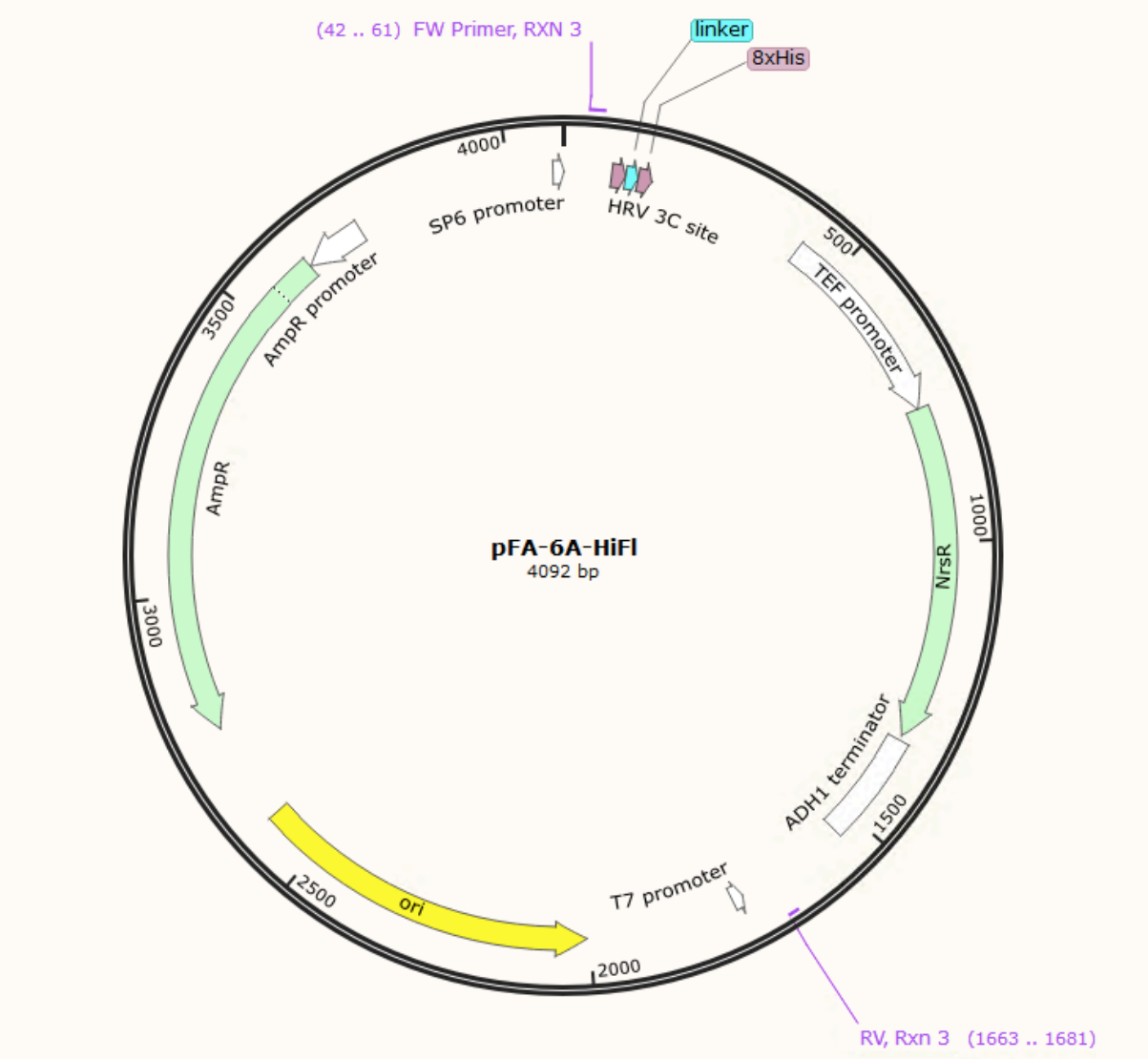

Plasmid 2, used for recombinant overexpression and purification of *S.c.* Lso2 from *E.c.*

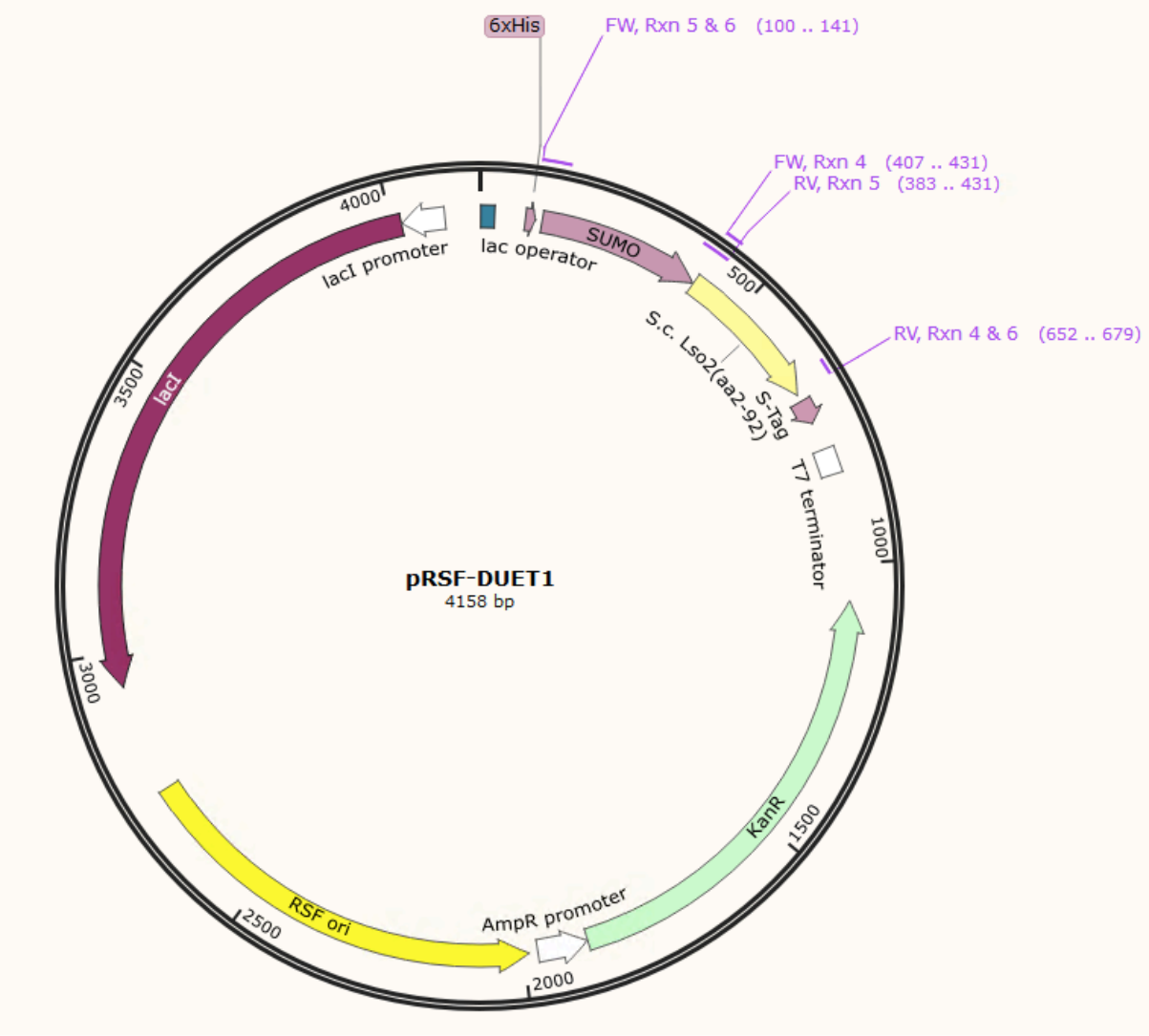

Plasmids 3-5, used for generating reporter mRNA for *in vitro* translation of the N.c. AAP for biochemical and structural analysis.

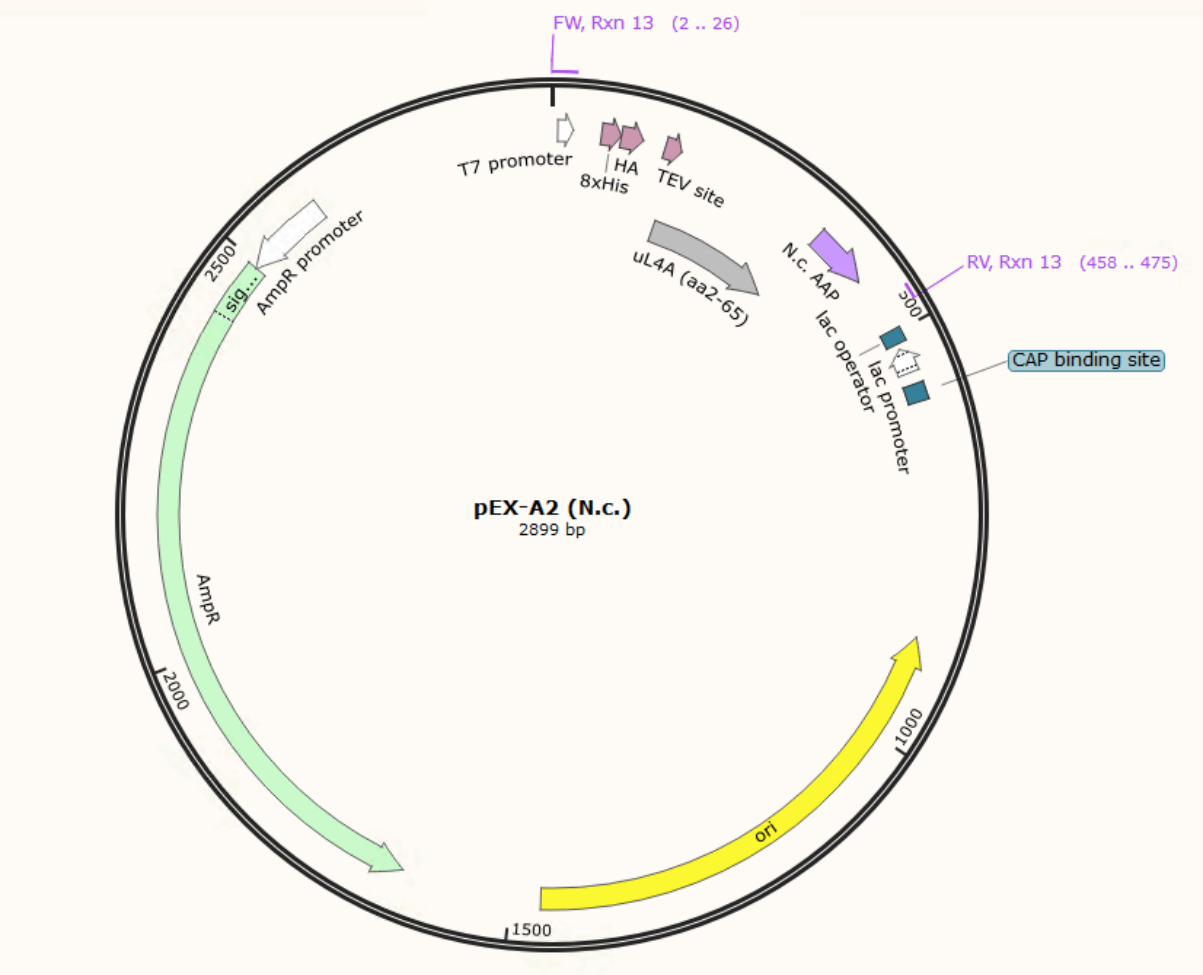

Plasmids 6-8, used for generating reporter mRNA for *in vitro* translation of the *S.c.* AAP for biochemical analysis.

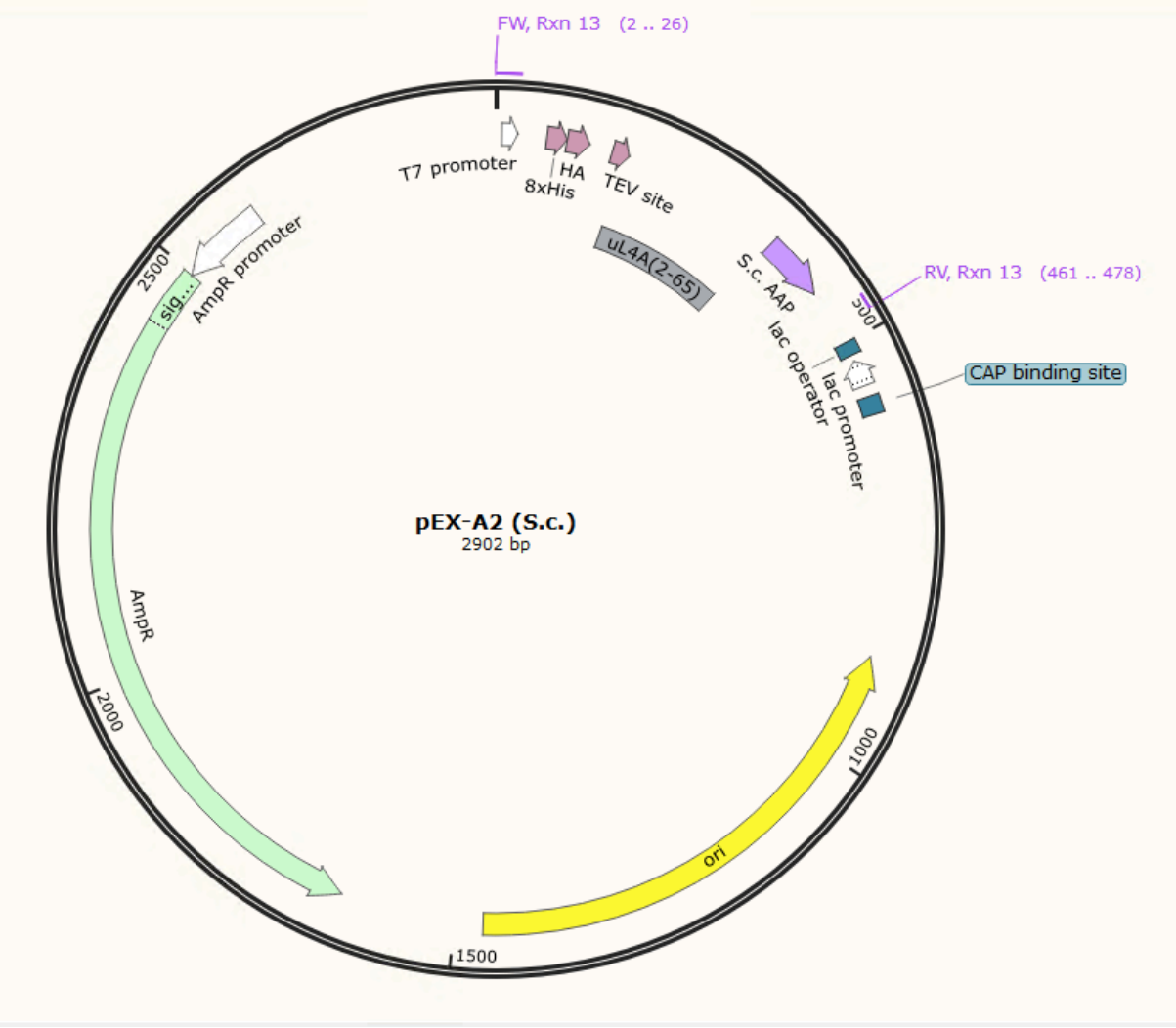

Appendix 2

Thermocycler settings used for PCR

Reaction 1

Step	Temp	Time (min)
heating	98°C	02:00
melting	98°C	00:10
annealing	51.7°C	00:15
elongation	72°C	00:30
	x 35	
elongation	72°C	05:00

Reaction 2

Step	Temp	Time (min)
heating	98°C	02:00
melting	98°C	00:10
annealing	54.7°C	00:15
elongation	68°C	03:45
	x 35	
Elongation	65°C	10 min

Reaction 3

Step	Temp	Time
heating	94°C	02:00
melting	98°C	00:10
annealing	40°C	00:30
elongation	68°C	03:00
	x 40	
Elongation	72°C	05:00

Reaction 4

Step	Temp	Time
heating	94°C	02:00
melting	98°C	00:10
annealing	57°C	00:30
elongation	74°C	00:30
	x 5	
melting	98°C	00:10
annealing	57°C	00:30
elongation	72°C	00:30
	x 30	
Elongation	72°C	05:00

Reaction 5

Step	Temp	Time
heating	94°C	02:00
melting	98°C	00:10
annealing	57°C	00:30
elongation	74°C	00:30
	x 5	
melting	98°C	00:10
annealing	57°C	00:30
elongation	72°C	00:30
	x 30	
Elongation	72°C	05:00

Reaction 6

Step	Temp	Time
heating	94°C	02:00
melting	98°C	00:10
annealing	57°C	00:30
elongation	72°C	00:45
	x 35	
Elongation	72°C	05:00

Reactions 7-12

Step	Temp	Time
heating	94°C	02:00
melting	98°C	00:10
annealing	57.7°C	00:30
elongation	72°C	01:30
	x 35	
Elongation	72°C	05:00

Reaction 13

Step	Temp	Time
heating	94°C	02:00
melting	98°C	00:05
annealing	60°C	00:10
elongation	72°C	00:30
	x 35	
Elongation	72°C	05:00

References

Abeyrathne, P.D., Koh, C.S., Grant, T., Grigorieff, N., and Korostelev, A.A. (2016). Ensemble cryo-EM uncovers inchworm-like translocation of a viral IRES through the ribosome. Elife 5.

Aitken, C.E., and Lorsch, J.R. (2012). A mechanistic overview of translation initiation in eukaryotes. Nat Struct Mol Biol 19, 568-576.

Allen, G.S., Zavialov, A., Gursky, R., Ehrenberg, M., and Frank, J. (2005). The cryo-EM structure of a translation initiation complex from Escherichia coli. Cell 121, 703-712.

Anger, A.M., Armache, J.P., Berninghausen, O., Habeck, M., Subklewe, M., Wilson, D.N., and Beckmann, R. (2013). Structures of the human and Drosophila 80S ribosome. Nature 497, 80-85.

Arenz, S., Meydan, S., Starosta, A.L., Berninghausen, O., Beckmann, R., Vazquez-Laslop, N., and Wilson, D.N. (2014a). Drug sensing by the ribosome induces translational arrest via active site perturbation. Mol Cell 56, 446-452.

Arenz, S., Ramu, H., Gupta, P., Berninghausen, O., Beckmann, R., Vazquez-Laslop, N., Mankin, A.S., and Wilson, D.N. (2014b). Molecular basis for erythromycin-dependent ribosome stalling during translation of the ErmBL leader peptide. Nat Commun 5, 3501.

Arthur, L.L., and Djuranovic, S. (2018). PolyA tracks, polybasic peptides, poly-translational hurdles. Wiley Interdiscip Rev RNA, e1486.

Ashe, M.P., Slaven, J.W., De Long, S.K., Ibrahimo, S., and Sachs, A.B. (2001). A novel eIF2B-dependent mechanism of translational control in yeast as a response to fusel alcohols. EMBO J 20, 6464-6474.

Baird, T.D., and Wek, R.C. (2012). Eukaryotic initiation factor 2 phosphorylation and translational control in metabolism. Adv Nutr 3, 307-321.

Balagopal, V., and Parker, R. (2011). Stm1 modulates translation after 80S formation in Saccharomyces cerevisiae. RNA 17, 835-842.

Ballesta, J.P., and Remacha, M. (1996). The large ribosomal subunit stalk as a regulatory element of the eukaryotic translational machinery. Prog Nucleic Acid Res Mol Biol 55, 157-193.

Ban, N., Beckmann, R., Cate, J.H., Dinman, J.D., Dragon, F., Ellis, S.R., Lafontaine, D.L., Lindahl, L., Liljas, A., Lipton, J.M., et al. (2014). A new system for naming ribosomal proteins. Curr Opin Struct Biol 24, 165-169.

Barrio-Garcia, C., Thoms, M., Flemming, D., Kater, L., Berninghausen, O., Bassler, J., Beckmann, R., and Hurt, E. (2016). Architecture of the Rix1-Rea1 checkpoint machinery during pre-60S-ribosome remodeling. Nat Struct Mol Biol 23, 37-44.

Basquin, J., Roudko, V.V., Rode, M., Basquin, C., Seraphin, B., and Conti, E. (2012). Architecture of the nuclease module of the yeast Ccr4-not complex: the Not1-Caf1-Ccr4 interaction. Mol Cell 48, 207-218.

Basu, A., and Yap, M.N. (2017). Disassembly of the Staphylococcus aureus hibernating 100S ribosome by an evolutionarily conserved GTPase. Proc Natl Acad Sci U S A 114, E8165-E8173.

Becker, T., Armache, J.-P., Jarasch, A., Anger, A.M., Villa, E., Sieber, H., Motaal, B.A., Mielke, T., Berninghausen, O., and Beckmann, R. (2011a). Structure of the no-go mRNA decay complex Dom34–Hbs1 bound to a stalled 80S ribosome. Nature Structural & Molecular Biology 18, 715-720.

Becker, T., Armache, J.P., Jarasch, A., Anger, A.M., Villa, E., Sieber, H., Motaal, B.A., Mielke, T., Berninghausen, O., and Beckmann, R. (2011b). Structure of the no-go mRNA decay complex Dom34-Hbs1 bound to a stalled 80S ribosome. Nat Struct Mol Biol 18, 715-720.

Becker, T., Franckenberg, S., Wickles, S., Shoemaker, C.J., Anger, A.M., Armache, J.P., Sieber, H., Ungewickell, C., Berninghausen, O., Daberkow, I., et al. (2012). Structural basis of highly conserved ribosome recycling in eukaryotes and archaea. Nature 482, 501-506.

Beckert, B., Abdelshahid, M., Schafer, H., Steinchen, W., Arenz, S., Berninghausen, O., Beckmann, R., Bange, G., Turgay, K., and Wilson, D.N. (2017). Structure of the Bacillus subtilis hibernating 100S ribosome reveals the basis for 70S dimerization. EMBO J 36, 2061-2072.

Beckert, B., Turk, M., Czech, A., Berninghausen, O., Beckmann, R., Ignatova, Z., Plitzko, J.M., and Wilson, D.N. (2018). Structure of a hibernating 100S ribosome reveals an inactive conformation of the ribosomal protein S1. Nat Microbiol 3, 1115-1121.

Beckmann, R., Bubeck, D., Grassucci, R., Penczek, P., Verschoor, A., Blobel, G., and Frank, J. (1997a). Alignment of conduits for the nascent polypeptide chain in the ribosome-Sec61 complex. Science 278, 2123-2126.

Beckmann, R., Bubeck, D., Grassucci, R.A., Penczek, P., Verschoor, A., Blobel, G., and Frank, J. (1997b). Alignment of Conduits for the Nascent Polypeptide Chain in the Ribosome-Sec61 Complex. Science 278, 2123-2126.

Beckmann, R., Spahn, C.M., Frank, J., and Blobel, G. (2001). The active 80S ribosome-Sec61 complex. Cold Spring Harb Symp Quant Biol 66, 543-554.

Ben-Shem, A., Garreau de Loubresse, N., Melnikov, S., Jenner, L., Yusupova, G., and Yusupov, M. (2011). The structure of the eukaryotic ribosome at 3.0 A resolution. Science 334, 1524-1529.

Bernstein, J.A., Khodursky, A.B., Lin, P.H., Lin-Chao, S., and Cohen, S.N. (2002). Global analysis of mRNA decay and abundance in Escherichia coli at single-gene resolution using two-color fluorescent DNA microarrays. Proc Natl Acad Sci U S A 99, 9697-9702.

Bertram, G., Bell, H.A., Ritchie, D.W., Fullerton, G., and Stansfield, I. (2000). Terminating eukaryote translation: domain 1 of release factor eRF1 functions in stop codon recognition. RNA 6, 1236-1247.

Boeck, R., Tarun, S., Jr., Rieger, M., Deardorff, J.A., Muller-Auer, S., and Sachs, A.B. (1996). The yeast Pan2 protein is required for poly(A)-binding protein-stimulated poly(A)-nuclease activity. J Biol Chem 271, 432-438.

Bradatsch, B., Leidig, C., Granneman, S., Gnadig, M., Tollervey, D., Bottcher, B., Beckmann, R., and Hurt, E. (2012). Structure of the pre-60S ribosomal subunit with nuclear export factor Arx1 bound at the exit tunnel. Nat Struct Mol Biol 19, 1234-1241.

Brandman, O., and Hegde, R.S. (2016). Ribosome-associated protein quality control. Nat Struct Mol Biol 23, 7-15.

Brown, A., Baird, M.R., Yip, M.C., Murray, J., and Shao, S. (2018a). Structures of translationally inactive mammalian ribosomes. Elife 7.

Brown, A., Baird, M.R., Yip, M.C., Murray, J., and Shao, S. (2018b). Structures of translationally inactive mammalian ribosomes. eLife 7, 1-18.

Brown, A., Long, F., Nicholls, R.A., Toots, J., Emsley, P., and Murshudov, G. (2015a). Tools for macromolecular model building and refinement into electron cryo-microscopy reconstructions. Acta Crystallogr D Biol Crystallogr 71, 136-153.

Brown, A., Shao, S., Murray, J., Hegde, R.S., and Ramakrishnan, V. (2015b). Structural basis for stop codon recognition in eukaryotes. Nature 524, 493-496.

Budkevich, T.V., Giesebrecht, J., Behrmann, E., Loerke, J., Ramrath, D.J., Mielke, T., Ismer, J., Hildebrand, P.W., Tung, C.S., Nierhaus, K.H., et al. (2014). Regulation of the mammalian elongation cycle by subunit rolling: a eukaryotic-specific ribosome rearrangement. Cell 158, 121-131.

Buschauer, R., Matsuo, Y., Sugiyama, T., Chen, Y.H., Alhusaini, N., Sweet, T., Ikeuchi, K., Cheng, J., Matsuki, Y., Nobuta, R., et al. (2020). The Ccr4-Not complex monitors the translating ribosome for codon optimality. Science 368.

Butcher, R.A., Bhullar, B.S., Perlstein, E.O., Marsischky, G., LaBaer, J., and Schreiber, S.L. (2006). Microarray-based method for monitoring yeast overexpression strains reveals small-molecule targets in TOR pathway. Nat Chem Biol 2, 103-109.

Carroll, J.S., Munchel, S.E., and Weis, K. (2011). The DExD/H box ATPase Dhh1 functions in translational repression, mRNA decay, and processing body dynamics. J Cell Biol 194, 527-537.

Castilho, B.A., Shanmugam, R., Silva, R.C., Ramesh, R., Himme, B.M., and Sattlegger, E. (2014). Keeping the eIF2 alpha kinase Gcn2 in check. Biochim Biophys Acta 1843, 1948-1968.

Chandrasekaran, V., Juszkiewicz, S., Choi, J., Puglisi, J.D., Brown, A., Shao, S., Ramakrishnan, V., and Hegde, R.S. (2019). Mechanism of ribosome stalling during translation of a poly(A) tail. Nat Struct Mol Biol 26, 1132-1140.

Chang, Y.F., Imam, J.S., and Wilkinson, M.F. (2007). The nonsense-mediated decay RNA surveillance pathway. Annu Rev Biochem 76, 51-74.

Chaveroux, C., Lambert-Langlais, S., Cherasse, Y., Averous, J., Parry, L., Carraro, V., Jousse, C., Maurin, A.C., Bruhat, A., and Fafournoux, P. (2010). Molecular mechanisms involved in the adaptation to amino acid limitation in mammals. Biochimie 92, 736-745.

Chen, Y., Boland, A., Kuzuoglu-Ozturk, D., Bawankar, P., Loh, B., Chang, C.T., Weichenrieder, O., and Izaurralde, E. (2014). A DDX6-CNOT1 complex and W-binding pockets in CNOT9 reveal direct links between miRNA target recognition and silencing. Mol Cell 54, 737-750.

Chiba, S., and Ito, K. (2012). Multisite ribosomal stalling: a unique mode of regulatory nascent chain action revealed for MifM. Mol Cell 47, 863-872.

Collart, M.A. (2016). The Ccr4-Not complex is a key regulator of eukaryotic gene expression. Wiley Interdiscip Rev RNA 7, 438-454.

Correia, H., Medina, R., Hernandez, A., Bustamante, E., Chakraburtty, K., and Herrera, F. (2004). Similarity between the association factor of ribosomal subunits and the protein Stm1p from Saccharomyces cerevisiae. Mem Inst Oswaldo Cruz 99, 733-737.

Crick, F. (1970). Central dogma of molecular biology. Nature 227, 561-563.
D'Orazio, K.N., Wu, C.C., Sinha, N., Loll-Krippleber, R., Brown, G.W., and Green, R. (2019).
The endonuclease Cue2 cleaves mRNAs at stalled ribosomes during No Go Decay. Elife 8.

De Leon, V., Johnson, A., and Bachvarova, R. (1983). Half-lives and relative amounts of stored and polysomal ribosomes and poly(A) + RNA in mouse oocytes. Dev Biol 98, 400-408.

Denis, C.L., and Chen, J. (2003). The CCR4-NOT complex plays diverse roles in mRNA metabolism. Prog Nucleic Acid Res Mol Biol 73, 221-250.

Dever, T.E., Yang, W., Astrom, S., Bystrom, A.S., and Hinnebusch, A.G. (1995). Modulation of tRNA(iMet), eIF-2, and eIF-2B expression shows that GCN4 translation is inversely coupled to the level of eIF-2.GTP.Met-tRNA(iMet) ternary complexes. Mol Cell Biol 15, 6351-6363.

Dimitrova, L.N., Kuroha, K., Tatematsu, T., and Inada, T. (2009). Nascent peptide-dependent translation arrest leads to Not4p-mediated protein degradation by the proteasome. J Biol Chem 284, 10343-10352.

Doma, M.K., and Parker, R. (2006). Endonucleolytic cleavage of eukaryotic mRNAs with stalls in translation elongation. Nature 440, 561-564.

Fang, P., Spevak, C.C., Wu, C., and Sachs, M.S. (2004). A nascent polypeptide domain that can regulate translation elongation. Proc Natl Acad Sci U S A 101, 4059-4064.

Fang, P., Wang, Z., and Sachs, M.S. (2000). Evolutionarily conserved features of the arginine attenuator peptide provide the necessary requirements for its function in translational regulation. J Biol Chem 275, 26710-26719.

Flygaard, R.K., Boegholm, N., Yusupov, M., and Jenner, L.B. (2018). Cryo-EM structure of the hibernating Thermus thermophilus 100S ribosome reveals a protein-mediated dimerization mechanism. Nat Commun 9, 4179.

Fox, G.E. (2010). Origin and evolution of the ribosome. Cold Spring Harb Perspect Biol 2, a003483.

Frank, J., Gao, H., Sengupta, J., Gao, N., and Taylor, D.J. (2007). The process of mRNA-tRNA translocation. Proc Natl Acad Sci U S A 104, 19671-19678.

Friedman, R.A., and Honig, B. (1995). A free energy analysis of nucleic acid base stacking in aqueous solution. Biophys J 69, 1528-1535.

Gaba, A., Jacobson, A., and Sachs, M.S. (2005). Ribosome occupancy of the yeast CPA1 upstream open reading frame termination codon modulates nonsense-mediated mRNA decay. Mol Cell 20, 449-460.

Gaba, A., Wang, Z., Krishnamoorthy, T., Hinnebusch, A.G., and Sachs, M.S. (2001). Physical evidence for distinct mechanisms of translational control by upstream open reading frames. EMBO J 20, 6453-6463.

Gamble, C.E., Brule, C.E., Dean, K.M., Fields, S., and Grayhack, E.J. (2016). Adjacent Codons Act in Concert to Modulate Translation Efficiency in Yeast. Cell 166, 679-690.

Graille, M., Chaillet, M., and van Tilbeurgh, H. (2008). Structure of yeast Dom34: a protein related to translation termination factor Erf1 and involved in No-Go decay. J Biol Chem 283, 7145-7154.

Greber, B.J., Gerhardy, S., Leitner, A., Leibundgut, M., Salem, M., Boehringer, D., Leulliot, N., Aebersold, R., Panse, V.G., and Ban, N. (2016). Insertion of the Biogenesis Factor Rei1 Probes the Ribosomal Tunnel during 60S Maturation. Cell 164, 91-102.

Guydosh, N.R., and Green, R. (2014). Dom34 rescues ribosomes in 3' untranslated regions. Cell 156, 950-962.

Halbach, F., Reichelt, P., Rode, M., and Conti, E. (2013). The yeast ski complex: crystal structure and RNA channeling to the exosome complex. Cell 154, 814-826.

Halic, M., Becker, T., Pool, M.R., Spahn, C.M., Grassucci, R.A., Frank, J., and Beckmann, R. (2004). Structure of the signal recognition particle interacting with the elongation-arrested ribosome. Nature 427, 808-814.

Halic, M., and Beckmann, R. (2005). The signal recognition particle and its interactions during protein targeting. Curr Opin Struct Biol 15, 116-125.

Halic, M., Blau, M., Becker, T., Mielke, T., Pool, M.R., Wild, K., Sinning, I., and Beckmann, R. (2006). Following the signal sequence from ribosomal tunnel exit to signal recognition particle. Nature 444, 507-511.

Han, A.P., Yu, C., Lu, L., Fujiwara, Y., Browne, C., Chin, G., Fleming, M., Leboulch, P., Orkin, S.H., and Chen, J.J. (2001). Heme-regulated eIF2alpha kinase (HRI) is required for translational regulation and survival of erythroid precursors in iron deficiency. EMBO J 20, 6909-6918.

Hanson, G., and Coller, J. (2018). Codon optimality, bias and usage in translation and mRNA decay. Nat Rev Mol Cell Biol 19, 20-30.

Harigaya, Y., and Parker, R. (2016). Codon optimality and mRNA decay. Cell Res 26, 1269-1270.

Hashimoto, S., Sugiyama, T., Yamazaki, R., Nobuta, R., and Inada, T. (2020). Identification of a novel trigger complex that facilitates ribosome-associated quality control in mammalian cells. Sci Rep 10, 3422.

Hayashi, H., Nagai, R., Abe, T., Wada, M., Ito, K., and Takeuchi-Tomita, N. (2018). Tight interaction of eEF2 in the presence of Stm1 on ribosome. J Biochem 163, 177-185.

Heuer, A., Gerovac, M., Schmidt, C., Trowitzsch, S., Preis, A., Kotter, P., Berninghausen, O., Becker, T., Beckmann, R., and Tampe, R. (2017). Structure of the 40S-ABCE1 post-splitting complex in ribosome recycling and translation initiation. Nat Struct Mol Biol 24, 453-460.

Hinnebusch, A.G. (2005). Translational regulation of GCN4 and the general amino acid control of yeast. Annu Rev Microbiol 59, 407-450.

Hinnebusch, A.G., and Lorsch, J.R. (2012). The mechanism of eukaryotic translation initiation: new insights and challenges. Cold Spring Harb Perspect Biol 4.

Ho, B., Baryshnikova, A., and Brown, G.W. (2018). Unification of Protein Abundance Datasets Yields a Quantitative Saccharomyces cerevisiae Proteome. Cell Syst 6, 192-205 e193.

Hood, H.M., Spevak, C.C., and Sachs, M.S. (2007). Evolutionary changes in the fungal carbamoyl-phosphate synthetase small subunit gene and its associated upstream open reading frame. Fungal Genet Biol 44, 93-104.

Hussain, T., Llacer, J.L., Fernandez, I.S., Munoz, A., Martin-Marcos, P., Savva, C.G., Lorsch, J.R., Hinnebusch, A.G., and Ramakrishnan, V. (2014). Structural changes enable start codon recognition by the eukaryotic translation initiation complex. Cell 159, 597-607.

Ikeuchi, K., Izawa, T., and Inada, T. (2018). Recent Progress on the Molecular Mechanism of Quality Controls Induced by Ribosome Stalling. Front Genet 9, 743.

Ikeuchi, K., Tesina, P., Matsuo, Y., Sugiyama, T., Cheng, J., Saeki, Y., Tanaka, K., Becker, T., Beckmann, R., and Inada, T. (2019). Collided ribosomes form a unique structural interface to induce Hel2-driven quality control pathways. EMBO J 38.

Inada, T., Winstall, E., Tarun, S.Z., Jr., Yates, J.R., 3rd, Schieltz, D., and Sachs, A.B. (2002). One-step affinity purification of the yeast ribosome and its associated proteins and mRNAs. RNA 8, 948-958.

Ingolia, N.T., Lareau, L.F., and Weissman, J.S. (2011). Ribosome profiling of mouse embryonic stem cells reveals the complexity and dynamics of mammalian proteomes. Cell 147, 789-802.

Ishimura, R., Nagy, G., Dotu, I., Zhou, H., Yang, X.L., Schimmel, P., Senju, S., Nishimura, Y., Chuang, J.H., and Ackerman, S.L. (2014). RNA function. Ribosome stalling induced by mutation of a CNS-specific tRNA causes neurodegeneration. Science 345, 455-459.
Ito, K., and Chiba, S. (2013). Arrest peptides: cis-acting modulators of translation. Annu Rev Biochem 82, 171-202.

Ivanov, P.V., Gehring, N.H., Kunz, J.B., Hentze, M.W., and Kulozik, A.E. (2008). Interactions between UPF1, eRFs, PABP and the exon junction complex suggest an integrated model for mammalian NMD pathways. EMBO J 27, 736-747.

Jackson, R.J., Hellen, C.U., and Pestova, T.V. (2010). The mechanism of eukaryotic translation initiation and principles of its regulation. Nat Rev Mol Cell Biol 11, 113-127.

Jenner, L., Melnikov, S., Garreau de Loubresse, N., Ben-Shem, A., Iskakova, M., Urzhumtsev, A., Meskauskas, A., Dinman, J., Yusupova, G., and Yusupov, M. (2012). Crystal structure of the 80S yeast ribosome. Curr Opin Struct Biol 22, 759-767.

Juszkiewicz, S., Chandrasekaran, V., Lin, Z., Kraatz, S., Ramakrishnan, V., and Hegde, R.S. (2018). ZNF598 Is a Quality Control Sensor of Collided Ribosomes. Mol Cell 72, 469-481 e467.

Kalambet, Y., Kozmin, Y., and Samokhin, A. (2018). Comparison of integration rules in the case of very narrow chromatographic peaks. Chemometrics and Intelligent Laboratory Systems 179, 22-30.

Kaminishi, T., Wilson, D.N., Takemoto, C., Harms, J.M., Kawazoe, M., Schluenzen, F., Hanawa-Suetsugu, K., Shirouzu, M., Fucini, P., and Yokoyama, S. (2007). A snapshot of the 30S ribosomal subunit capturing mRNA via the Shine-Dalgarno interaction. Structure 15, 289-297.

Karcher, A., Schele, A., and Hopfner, K.P. (2008). X-ray structure of the complete ABC enzyme ABCE1 from Pyrococcus abyssi. J Biol Chem 283, 7962-7971.

Kervestin, S., and Jacobson, A. (2012). NMD: a multifaceted response to premature translational termination. Nat Rev Mol Cell Biol 13, 700-712.

Kervestin, S., Li, C., Buckingham, R., and Jacobson, A. (2012). Testing the faux-UTR model for NMD: analysis of Upf1p and Pab1p competition for binding to eRF3/Sup35p. Biochimie 94, 1560-1571.

Komoda, T., Sato, N.S., Phelps, S.S., Namba, N., Joseph, S., and Suzuki, T. (2006). The A-site finger in 23 S rRNA acts as a functional attenuator for translocation. J Biol Chem 281, 32303-32309.

Kowalinski, E., Bange, G., Wild, K., and Sinning, I. (2007). Expression, purification, crystallization and preliminary crystallographic analysis of the proliferation-associated protein Ebp1. Acta Crystallogr Sect F Struct Biol Cryst Commun *63*, 768-770.

Krokowski, D., Gaccioli, F., Majumder, M., Mullins, M.R., Yuan, C.L., Papadopoulou, B., Merrick, W.C., Komar, A.A., Taylor, D., and Hatzoglou, M. (2011). Characterization of hibernating ribosomes in mammalian cells. Cell Cycle 10, 2691-2702.

Kuzuoglu-Ozturk, D., Bhandari, D., Huntzinger, E., Fauser, M., Helms, S., and Izaurralde, E. (2016). miRISC and the CCR4-NOT complex silence mRNA targets independently of 43S ribosomal scanning. EMBO J 35, 1186-1203.

Lagerkvist, U. (1978). "Two out of three": an alternative method for codon reading. Proc Natl Acad Sci U S A 75, 1759-1762.

Lee, H.H., Kim, Y.S., Kim, K.H., Heo, I., Kim, S.K., Kim, O., Kim, H.K., Yoon, J.Y., Kim, H.S., Kim, D.J., et al. (2007). Structural and functional insights into Dom34, a key component of no-go mRNA decay. Mol Cell 27, 938-950.

Li, W., Ward, F.R., McClure, K.F., Chang, S.T., Montabana, E., Liras, S., Dullea, R.G., and Cate, J.H.D. (2019). Structural basis for selective stalling of human ribosome nascent chain complexes by a drug-like molecule. Nat Struct Mol Biol 26, 501-509.

Lima, S.A., Chipman, L.B., Nicholson, A.L., Chen, Y.H., Yee, B.A., Yeo, G.W., Coller, J., and Pasquinelli, A.E. (2017). Short poly(A) tails are a conserved feature of highly expressed genes. Nat Struct Mol Biol 24, 1057-1063.

Ling, S.H., Qamra, R., and Song, H. (2011). Structural and functional insights into eukaryotic mRNA decapping. Wiley Interdiscip Rev RNA 2, 193-208.

Liu, Q., Greimann, J.C., and Lima, C.D. (2006). Reconstitution, activities, and structure of the eukaryotic RNA exosome. Cell 127, 1223-1237.

Liu, Z., Ahn, J.Y., Liu, X., and Ye, K. (2006). Ebp1 isoforms distinctively regulate cell survival and differentiation. Proc Natl Acad Sci U S A *103*, 10917-10922.

Loveland, A.B., Demo, G., Grigorieff, N., and Korostelev, A.A. (2017). Ensemble cryo-EM elucidates the mechanism of translation fidelity. Nature 546, 113-117.

Manners, J.M., and Nielsen, M.S. (1981). Magnesium flux during open heart surgery. The effect of St Thomas' Hospital cardioplegia solution. Anaesthesia 36, 157-166.

Matheisl, S., Berninghausen, O., Becker, T., and Beckmann, R. (2015). Structure of a human translation termination complex. Nucleic Acids Res 43, 8615-8626.

Matsuo, Y., Ikeuchi, K., Saeki, Y., Iwasaki, S., Schmidt, C., Udagawa, T., Sato, F., Tsuchiya, H., Becker, T., Tanaka, K., et al. (2017). Ubiquitination of stalled ribosome triggers ribosome-associated quality control. Nat Commun 8, 159.

Melnikov, S., Ben-Shem, A., Garreau de Loubresse, N., Jenner, L., Yusupova, G., and Yusupov, M. (2012). One core, two shells: bacterial and eukaryotic ribosomes. Nat Struct Mol Biol 19, 560-567.

Miller, J.E., Zhang, L., Jiang, H., Li, Y., Pugh, B.F., and Reese, J.C. (2018). Genome-Wide Mapping of Decay Factor-mRNA Interactions in Yeast Identifies Nutrient-Responsive Transcripts as Targets of the Deadenylase Ccr4. G3 (Bethesda) 8, 315-330.

Milon, P., and Rodnina, M.V. (2012). Kinetic control of translation initiation in bacteria. Crit Rev Biochem Mol Biol 47, 334-348.

Monod, J. (1949). The Growth of Bacterial Cultures. Annu Rev Microbiol 3, 371-394.
Montero-Lomeli, M., Morais, B.L., Figueiredo, D.L., Neto, D.C., Martins, J.R., and Masuda, C.A. (2002). The initiation factor eIF4A is involved in the response to lithium stress in Saccharomyces cerevisiae. J Biol Chem 277, 21542-21548.

Mugler, C.F., Hondele, M., Heinrich, S., Sachdev, R., Vallotton, P., Koek, A.Y., Chan, L.Y., and Weis, K. (2016). ATPase activity of the DEAD-box protein Dhh1 controls processing body formation. Elife 5.

Nika, J., Rippel, S., and Hannig, E.M. (2001). Biochemical analysis of the eIF2beta gamma complex reveals a structural function for eIF2alpha in catalyzed nucleotide exchange. J Biol Chem 276, 1051-1056.

Nissan, T., Rajyaguru, P., She, M., Song, H., and Parker, R. (2010). Decapping activators in Saccharomyces cerevisiae act by multiple mechanisms. Mol Cell 39, 773-783.

Ohno, H., Sakai, H., Washio, T., and Tomita, M. (2001). Preferential usage of some minor codons in bacteria. Gene 276, 107-115.

OpenStax, B. (2016). CC BY 4.0 OpenStax College, Concepts of Biology. OpenStax CNX. http://cnx.org/contents/b3c1e1d2-839c-42b0-a314-e119a8aafbdd@12.1.

Ortiz, J.O., Brandt, F., Matias, V.R., Sennels, L., Rappsilber, J., Scheres, S.H., Eibauer, M., Hartl, F.U., and Baumeister, W. (2010). Structure of hibernating ribosomes studied by cryoelectron tomography in vitro and in situ. J Cell Biol 190, 613-621.

Park, E.H., Walker, S.E., Zhou, F., Lee, J.M., Rajagopal, V., Lorsch, J.R., and Hinnebusch, A.G. (2013). Yeast eukaryotic initiation factor 4B (eIF4B) enhances complex assembly between eIF4A and eIF4G in vivo. J Biol Chem 288, 2340-2354.

Parker, R. (2012). RNA degradation in Saccharomyces cerevisae. Genetics 191, 671-702.

Petrov, A.N., Meskauskas, A., Roshwalb, S.C., and Dinman, J.D. (2008). Yeast ribosomal protein L10 helps coordinate tRNA movement through the large subunit. Nucleic Acids Res 36, 6187-6198.

Pisareva, V.P., Skabkin, M.A., Hellen, C.U., Pestova, T.V., and Pisarev, A.V. (2011). Dissociation by Pelota, Hbs1 and ABCE1 of mammalian vacant 80S ribosomes and stalled elongation complexes. EMBO J 30, 1804-1817.

Preis, A., Heuer, A., Barrio-Garcia, C., Hauser, A., Eyler, D.E., Berninghausen, O., Green, R., Becker, T., and Beckmann, R. (2014). Cryoelectron microscopic structures of eukaryotic translation termination complexes containing eRF1-eRF3 or eRF1-ABCE1. Cell Rep 8, 59-65.

Presnyak, V., Alhusaini, N., Chen, Y.H., Martin, S., Morris, N., Kline, N., Olson, S., Weinberg, D., Baker, K.E., Graveley, B.R., et al. (2015). Codon optimality is a major determinant of mRNA stability. Cell 160, 1111-1124.

Prossliner, T., Skovbo Winther, K., Sorensen, M.A., and Gerdes, K. (2018). Ribosome Hibernation. Annu Rev Genet 52, 321-348.

Radhakrishnan, A., Chen, Y.H., Martin, S., Alhusaini, N., Green, R., and Coller, J. (2016). The DEAD-Box Protein Dhh1p Couples mRNA Decay and Translation by Monitoring Codon Optimality. Cell 167, 122-132 e129.

Ramakrishnan, V. (1986). Distribution of protein and RNA in the 30S ribosomal subunit. Science 231, 1562-1564.

Ramakrishnan, V. (2002). Ribosome structure and the mechanism of translation. Cell 108, 557-572.

Richter, J.D., and Coller, J. (2015). Pausing on Polyribosomes: Make Way for Elongation in Translational Control. Cell 163, 292-300.

Rowlands, A.G., Panniers, R., and Henshaw, E.C. (1988). The catalytic mechanism of guanine nucleotide exchange factor action and competitive inhibition by phosphorylated eukaryotic initiation factor 2. J Biol Chem 263, 5526-5533.

Schmeing, T.M., Huang, K.S., Strobel, S.A., and Steitz, T.A. (2005). An induced-fit mechanism to promote peptide bond formation and exclude hydrolysis of peptidyl-tRNA. Nature 438, 520-524.

Schmeing, T.M., and Ramakrishnan, V. (2009). What recent ribosome structures have revealed about the mechanism of translation. Nature 461, 1234-1242.

Schmidt, C., Kowalinski, E., Shanmuganathan, V., Defenouillere, Q., Braunger, K., Heuer, A., Pech, M., Namane, A., Berninghausen, O., Fromont-Racine, M., et al. (2016). The cryo-EM structure of a ribosome-Ski2-Ski3-Ski8 helicase complex. Science 354, 1431-1433.

Schuette, J.C., Murphy, F.V.t., Kelley, A.C., Weir, J.R., Giesebrecht, J., Connell, S.R., Loerke, J., Mielke, T., Zhang, W., Penczek, P.A., et al. (2009). GTPase activation of elongation factor EF-Tu by the ribosome during decoding. EMBO J 28, 755-765.

Schuller, A.P., and Green, R. (2018). Roadblocks and resolutions in eukaryotic translation. Nat Rev Mol Cell Biol 19, 526-541.

Seidelt, B., Innis, C.A., Wilson, D.N., Gartmann, M., Armache, J.P., Villa, E., Trabuco, L.G., Becker, T., Mielke, T., Schulten, K., et al. (2009). Structural insight into nascent polypeptide chain-mediated translational stalling. Science 326, 1412-1415.

Serdar, L.D., Whiteside, D.L., and Baker, K.E. (2016). ATP hydrolysis by UPF1 is required for efficient translation termination at premature stop codons. Nat Commun 7, 14021.

Shanmuganathan, V., Schiller, N., Magoulopoulou, A., Cheng, J., Braunger, K., Cymer, F., Berninghausen, O., Beatrix, B., Kohno, K., von Heijne, G., et al. (2019). Structural and mutational analysis of the ribosome-arresting human XBP1u. Elife 8.

Shao, S., and Hegde, R.S. (2016). Target Selection during Protein Quality Control. Trends Biochem Sci 41, 124-137.

Sharif, H., Ozgur, S., Sharma, K., Basquin, C., Urlaub, H., and Conti, E. (2013). Structural analysis of the yeast Dhh1-Pat1 complex reveals how Dhh1 engages Pat1, Edc3 and RNA in mutually exclusive interactions. Nucleic Acids Res 41, 8377-8390.

Sharp, P.M., Tuohy, T.M., and Mosurski, K.R. (1986). Codon usage in yeast: cluster analysis clearly differentiates highly and lowly expressed genes. Nucleic Acids Res 14, 5125-5143.

Shen, P.S., Park, J., Qin, Y., Li, X., Parsawar, K., Larson, M.H., Cox, J., Cheng, Y., Lambowitz, A.M., Weissman, J.S., et al. (2015). Protein synthesis. Rqc2p and 60S ribosomal subunits mediate mRNA-independent elongation of nascent chains. Science 347, 75-78.

Shine, J., and Dalgarno, L. (1974). The 3'-terminal sequence of Escherichia coli 16S ribosomal RNA: complementarity to nonsense triplets and ribosome binding sites. Proc Natl Acad Sci U S A 71, 1342-1346.

Shoemaker, C.J., and Green, R. (2012). Translation drives mRNA quality control. Nat Struct Mol Biol 19, 594-601.

Simms, C.L., Hudson, B.H., Mosior, J.W., Rangwala, A.S., and Zaher, H.S. (2014). An active role for the ribosome in determining the fate of oxidized mRNA. Cell Rep 9, 1256-1264.

Simonovic, M., and Steitz, T.A. (2009). A structural view on the mechanism of the ribosome-catalyzed peptide bond formation. Biochim Biophys Acta 1789, 612-623.

Sohmen, D., Chiba, S., Shimokawa-Chiba, N., Innis, C.A., Berninghausen, O., Beckmann, R., Ito, K., and Wilson, D.N. (2015). Structure of the Bacillus subtilis 70S ribosome reveals the basis for species-specific stalling. Nat Commun 6, 6941.

Sonenberg, N., and Hinnebusch, A.G. (2009). Regulation of translation initiation in eukaryotes: mechanisms and biological targets. Cell 136, 731-745.

Sood, R., Porter, A.C., Olsen, D.A., Cavener, D.R., and Wek, R.C. (2000). A mammalian homologue of GCN2 protein kinase important for translational control by phosphorylation of eukaryotic initiation factor-2alpha. Genetics 154, 787-801.

Spahn, C.M., Beckmann, R., Eswar, N., Penczek, P.A., Sali, A., Blobel, G., and Frank, J. (2001). Structure of the 80S ribosome from Saccharomyces cerevisiae--tRNA-ribosome and subunit-subunit interactions. Cell 107, 373-386.

Spahn, C.M., Gomez-Lorenzo, M.G., Grassucci, R.A., Jorgensen, R., Andersen, G.R., Beckmann, R., Penczek, P.A., Ballesta, J.P., and Frank, J. (2004). Domain movements of elongation factor eEF2 and the eukaryotic 80S ribosome facilitate tRNA translocation. EMBO J 23, 1008-1019.

Spevak, C.C., Ivanov, I.P., and Sachs, M.S. (2010). Sequence requirements for ribosome stalling by the arginine attenuator peptide. J Biol Chem 285, 40933-40942.

Su, T., Cheng, J., Sohmen, D., Hedman, R., Berninghausen, O., von Heijne, G., Wilson, D.N., and Beckmann, R. (2017). The force-sensing peptide VemP employs extreme compaction and secondary structure formation to induce ribosomal stalling. Elife 6.

Su, T., Izawa, T., Thoms, M., Yamashita, Y., Cheng, J., Berninghausen, O., Hartl, F.U., Inada, T., Neupert, W., and Beckmann, R. (2019). Structure and function of Vms1 and Arb1 in RQC and mitochondrial proteome homeostasis. Nature 570, 538-542.

Svedberg, T. (1947). Molecular sedimentation in the ultracentrifuge. Endeavour 6, 89-95.
Sweet, T., Kovalak, C., and Coller, J. (2012). The DEAD-box protein Dhh1 promotes decapping by slowing ribosome movement. PLoS Biol 10, e1001342.

Tate, W.P., and Mannering, S.A. (1996). Three, four or more: the translational stop signal at length. Mol Microbiol 21, 213-219.

Taylor, D.J., Nilsson, J., Merrill, A.R., Andersen, G.R., Nissen, P., and Frank, J. (2007). Structures of modified eEF2 80S ribosome complexes reveal the role of GTP hydrolysis in translocation. EMBO J 26, 2421-2431.

Tesina, P., Heckel, E., Cheng, J., Fromont-Racine, M., Buschauer, R., Kater, L., Beatrix, B., Berninghausen, O., Jacquier, A., Becker, T., et al. (2019). Structure of the 80S ribosome-Xrn1 nuclease complex. Nat Struct Mol Biol 26, 275-280.

Tesina, P., Lessen, L.N., Buschauer, R., Cheng, J., Wu, C.C., Berninghausen, O., Buskirk, A.R., Becker, T., Beckmann, R., and Green, R. (2020). Molecular mechanism of translational stalling by inhibitory codon combinations and poly(A) tracts. EMBO J 39, e103365.

Thoms, M., Buschauer, R., Ameismeier, M., Koepke, L., Denk, T., Hirschenberger, M., Kratzat, H., Hayn, M., Mackens-Kiani, T., Cheng, J., et al. (2020). Structural basis for translational shutdown and immune evasion by the Nsp1 protein of SARS-CoV-2. https://doi.org/10.1101/2020.05.18.102467

Tsai, A., Kornberg, G., Johansson, M., Chen, J., and Puglisi, J.D. (2014). The dynamics of SecM-induced translational stalling. Cell Rep 7, 1521-1533.

Uesono, Y., and Toh, E.A. (2002). Transient inhibition of translation initiation by osmotic stress. J Biol Chem 277, 13848-13855.

Ueta, M., Ohniwa, R.L., Yoshida, H., Maki, Y., Wada, C., and Wada, A. (2008). Role of HPF (hibernation promoting factor) in translational activity in Escherichia coli. J Biochem 143, 425-433.

Ueta, M., Wada, C., Daifuku, T., Sako, Y., Bessho, Y., Kitamura, A., Ohniwa, R.L., Morikawa, K., Yoshida, H., Kato, T., et al. (2013). Conservation of two distinct types of 100S ribosome in bacteria. Genes Cells 18, 554-574.

Ueta, M., Yoshida, H., Wada, C., Baba, T., Mori, H., and Wada, A. (2005). Ribosome binding proteins YhbH and YfiA have opposite functions during 100S formation in the stationary phase of Escherichia coli. Genes Cells 10, 1103-1112.

Utsugi, T., Toh-e, A., and Kikuchi, Y. (1995). A high dose of the STM1 gene suppresses the temperature sensitivity of the tom1 and htr1 mutants in Saccharomyces cerevisiae. Biochim Biophys Acta 1263, 285-288.

van den Elzen, A.M., Schuller, A., Green, R., and Seraphin, B. (2014). Dom34-Hbs1 mediated dissociation of inactive 80S ribosomes promotes restart of translation after stress. EMBO J 33, 265-276.

Van Dyke, M.W., Nelson, L.D., Weilbaecher, R.G., and Mehta, D.V. (2004). Stm1p, a G4 quadruplex and purine motif triplex nucleic acid-binding protein, interacts with ribosomes and subtelomeric Y' DNA in Saccharomyces cerevisiae. J Biol Chem 279, 24323-24333.

Van Dyke, N., Baby, J., and Van Dyke, M.W. (2006). Stm1p, a ribosome-associated protein, is important for protein synthesis in Saccharomyces cerevisiae under nutritional stress conditions. J Mol Biol 358, 1023-1031.

Van Dyke, N., Chanchorn, E., and Van Dyke, M.W. (2013). The Saccharomyces cerevisiae protein Stm1p facilitates ribosome preservation during quiescence. Biochem Biophys Res Commun 430, 745-750.

Van Dyke, N., Pickering, B.F., and Van Dyke, M.W. (2009). Stm1p alters the ribosome association of eukaryotic elongation factor 3 and affects translation elongation. Nucleic Acids Res 37, 6116-6125.

van Hoof, A., Frischmeyer, P.A., Dietz, H.C., and Parker, R. (2002). Exosome-mediated recognition and degradation of mRNAs lacking a termination codon. Science 295, 2262-2264.

Verma, R., Reichermeier, K.M., Burroughs, A.M., Oania, R.S., Reitsma, J.M., Aravind, L., and Deshaies, R.J. (2018). Vms1 and ANKZF1 peptidyl-tRNA hydrolases release nascent chains from stalled ribosomes. Nature 557, 446-451.

Villa-Garcia, M.J., Choi, M.S., Hinz, F.I., Gaspar, M.L., Jesch, S.A., and Henry, S.A. (2011). Genome-wide screen for inositol auxotrophy in Saccharomyces cerevisiae implicates lipid metabolism in stress response signaling. Mol Genet Genomics 285, 125-149.

Voorhees, R.M., and Ramakrishnan, V. (2013). Structural basis of the translational elongation cycle. Annu Rev Biochem 82, 203-236.

Walter, P., and Ron, D. (2011). The unfolded protein response: from stress pathway to homeostatic regulation. Science 334, 1081-1086.

Wang, Y., Liu, C.L., Storey, J.D., Tibshirani, R.J., Herschlag, D., and Brown, P.O. (2002). Precision and functional specificity in mRNA decay. Proc Natl Acad Sci U S A 99, 5860-5865.

Wang, Y.J., Vaidyanathan, P.P., Rojas-Duran, M.F., Udeshi, N.D., Bartoli, K.M., Carr, S.A., and Gilbert, W.V. (2018). Lso2 is a conserved ribosome-bound protein required for translational recovery in yeast. PLoS Biol 16, e2005903.

Waters, M.G., and Blobel, G. (1986). Secretory protein translocation in a yeast cell-free system can occur posttranslationally and requires ATP hydrolysis. J Cell Biol 102, 1543-1550.

Webster, M.W., Chen, Y.H., Stowell, J.A.W., Alhusaini, N., Sweet, T., Graveley, B.R., Coller, J., and Passmore, L.A. (2018). mRNA Deadenylation Is Coupled to Translation Rates by the Differential Activities of Ccr4-Not Nucleases. Mol Cell 70, 1089-1100 e1088.

Wei, J., Wu, C., and Sachs, M.S. (2012). The arginine attenuator peptide interferes with the ribosome peptidyl transferase center. Mol Cell Biol 32, 2396-2406.

Weis, F., Giudice, E., Churcher, M., Jin, L., Hilcenko, C., Wong, C.C., Traynor, D., Kay, R.R., and Warren, A.J. (2015). Mechanism of eIF6 release from the nascent 60S ribosomal subunit. Nat Struct Mol Biol 22, 914-919.

Werner, M., Feller, A., Messenguy, F., and Pierard, A. (1987). The leader peptide of yeast gene CPA1 is essential for the translational repression of its expression. Cell 49, 805-813.

Weston, A., and Sommerville, J. (2006). Xp54 and related (DDX6-like) RNA helicases: roles in messenger RNP assembly, translation regulation and RNA degradation. Nucleic Acids Res 34, 3082-3094.

Whitford, P.C., Geggier, P., Altman, R.B., Blanchard, S.C., Onuchic, J.N., and Sanbonmatsu, K.Y. (2010). Accommodation of aminoacyl-tRNA into the ribosome involves reversible excursions along multiple pathways. RNA 16, 1196-1204.

Wilson, D.N., Arenz, S., and Beckmann, R. (2016). Translation regulation via nascent polypeptide-mediated ribosome stalling. Curr Opin Struct Biol 37, 123-133.

Wilson, D.N., and Beckmann, R. (2011). The ribosomal tunnel as a functional environment for nascent polypeptide folding and translational stalling. Curr Opin Struct Biol 21, 274-282.

Wohlgemuth, I., Brenner, S., Beringer, M., and Rodnina, M.V. (2008). Modulation of the rate of peptidyl transfer on the ribosome by the nature of substrates. J Biol Chem 283, 32229-32235.

Wu, C., Wei, J., Lin, P.J., Tu, L., Deutsch, C., Johnson, A.E., and Sachs, M.S. (2012). Arginine changes the conformation of the arginine attenuator peptide relative to the ribosome tunnel. J Mol Biol 416, 518-533.

Yang, E., van Nimwegen, E., Zavolan, M., Rajewsky, N., Schroeder, M., Magnasco, M., and Darnell, J.E., Jr. (2003). Decay rates of human mRNAs: correlation with functional characteristics and sequence attributes. Genome Res 13, 1863-1872.

Yip, M.C.J., Keszei, A.F.A., Feng, Q., Chu, V., McKenna, M.J., and Shao, S. (2019). Mechanism for recycling tRNAs on stalled ribosomes. Nat Struct Mol Biol 26, 343-349.

Yip, M.C.J., Savickas, S., Gygi, S.P., and Shao, S. (2020). ELAC1 Repairs tRNAs Cleaved during Ribosome-Associated Quality Control. Cell Rep 30, 2106-2114 e2105.

Yonath, A., Mussig, J., and Wittmann, H.G. (1982). Parameters for crystal growth of ribosomal subunits. J Cell Biochem 19, 145-155.

Yoshikawa, K., Tanaka, T., Ida, Y., Furusawa, C., Hirasawa, T., and Shimizu, H. (2011). Comprehensive phenotypic analysis of single-gene deletion and overexpression strains of Saccharomyces cerevisiae. Yeast 28, 349-361.

Zhang, K. (2016). Gctf: Real-time CTF determination and correction. J Struct Biol 193, 1-12.

Zhang, P., McGrath, B.C., Reinert, J., Olsen, D.S., Lei, L., Gill, S., Wek, S.A., Vattem, K.M., Wek, R.C., Kimball, S.R., et al. (2002). The GCN2 eIF2alpha kinase is required for adaptation to amino acid deprivation in mice. Mol Cell Biol 22, 6681-6688.

Zheng, S.Q., Palovcak, E., Armache, J.P., Verba, K.A., Cheng, Y., and Agard, D.A. (2017). MotionCor2: anisotropic correction of beam-induced motion for improved cryo-electron microscopy. Nat Methods 14, 331-332.

Zinoviev, A., Ayupov, R.K., Abaeva, I.S., Hellen, C.U.T., and Pestova, T.V. (2020). Extraction of mRNA from Stalled Ribosomes by the Ski Complex. Mol Cell.

Acknowledgements

Wow can you believe I did this all on my own? Haha just kidding. So, first, I will thank Prof. Dr. Dr. Roland Beckmann for the opportunity and funding to obtain my PhD. Thanks to those who have agreed to participate as members of my examination committee, Prof. Dr. Klaus Förstemann, Dr. Gregor Witte, Prof. Dr. Karl-Klaus Conzelmann, Prof Dr Johannes Stigler, and Prof Dr. Karl-Peter Hopfner. Thanks to the organisers of my graduate school, the international Max Planck graduate school for life science for organising the many workshops, seminars, retreats, and other social events I enjoyed taking part in. To the members of my thesis advisory committee Prof. Dr. Daniel Wilson and Prof. Dr. Klaus Förstemann for their guidance and support in helping me navigate the successful completion of these projects, and, the unsuccessful completion of many more. To Dr. Birgitta Beatrix, for her consistent teaching style and wealth of knowledge and Dr Thomas Becker for the unprecedented support, teaching, and guidance. Thomas without you this truly would have been impossible. To my collaborator Prof. Dr. Matt Sachs, for whose help and support I am incredibly grateful. Tech support! Dr Andre Heuer, Leslie Heinz, Wilmer Montenegro, Lukas Kater, Michael Ameismeier, and Katharina Best, for coding, maintaining, and moderating our pipeline and Terabytes of data. To Dr Otto Berninghausen and the ice queens Susanne Rieder and Charlotte Ungewickell, for cryo-EM sample preparation, data collection, systems maintenance. To our incredible technicians, Heidimarie Sieber, Andrea Gilmozzi, and Johanna Musial for immeasurable contributions to maintaining the lab so we could actually work as well as providing additional support whenever it was needed. To my first supervisor Dr. Christian Schmidt for helping me settle in and getting my work started. To Dr JingDong Cheng for his magic eye for molecular modelling, dependable guidance, and ultimately teaching me data processing along with the legends Ting Su and Robert Buschauer. To my other colleagues Vivek Shanmuganathan, Hanna Kratzat, Tsai-Hsuan Weng, Alexandra Knorr, and Timur Mackens-Kiani, for their company, support, and meaningful scientific discussions. To the incredible visiting scientific collaborators, Eva Pauwels and Dr Karole D'Orazio, who made Munich more alive, and always went to karaoke with me on Thursdays even though they paid for it on Fridays. To my FRIENDS for preserving my sanity and translating all my mail: Dr Anne Preis, who met me once a week for Anne day and art projects, and Petr Durik, if for nothing else, then for convincing me to give "that

English guy" my number. You guys are angels for real. To the teachers I've had who let me be myself and, in their understanding, were able to guide me to grow: Laura Flanagan, Joe Koger, and Dr. Mark Odell. To my parents, who have always helped me to thrive. I genuinely don't understand how you have been so supportive of me but, mum would say I never gave her a choice, and dad would say "it's genetics!" Thank you teaching me to have a sense of humour, it's been handy. To my grandparents whom I just love so much. Whom I could always call, and they'd always answer excited to hear from me. It made all the hard days easier. To my sister, for being better than me and keeping me humble. Finally, to myself.

And none for Gretchen Wieners. Bye.